LBL-37004
UC-400

Lawrence Berkeley Laboratory

UNIVERSITY OF CALIFORNIA

EARTH SCIENCES DIVISION

Degassing and Two-Phase Flow Pilot Hole Test Report

J.T. Geller and J. Jarsjö

March 1995

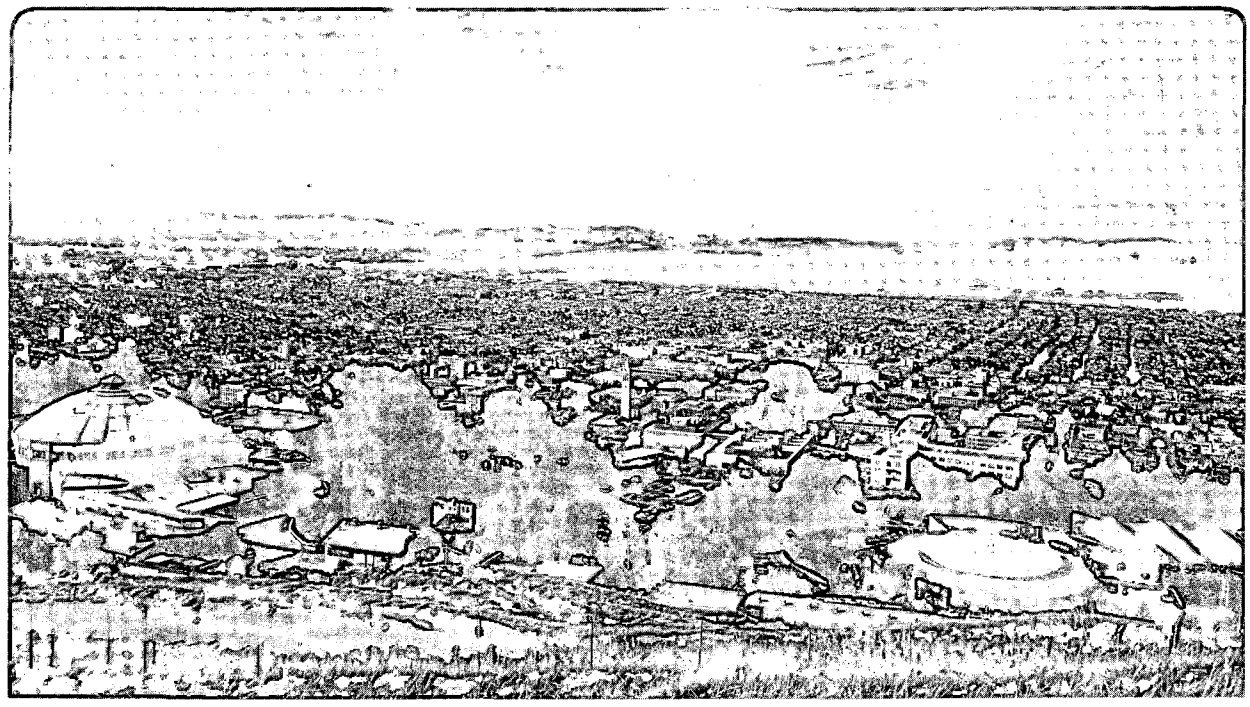

REFERENCE COPY
Does Not
Circulate
Bldg. 50 Library.
Copy 1
LBL-37004

Prepared for the U.S. Department of Energy under Contract Number DE-AC03-76SF00098

DISCLAIMER

This document was prepared as an account of work sponsored by the United States Government. While this document is believed to contain correct information, neither the United States Government nor any agency thereof, nor the Regents of the University of California, nor any of their employees, makes any warranty, express or implied, or assumes any legal responsibility for the accuracy, completeness, or usefulness of any information, apparatus, product, or process disclosed, or represents that its use would not infringe privately owned rights. Reference herein to any specific commercial product, process, or service by its trade name, trademark, manufacturer, or otherwise, does not necessarily constitute or imply its endorsement, recommendation, or favoring by the United States Government or any agency thereof, or the Regents of the University of California. The views and opinions of authors expressed herein do not necessarily state or reflect those of the United States Government or any agency thereof or the Regents of the University of California.

LBL-37004
UC-400

Degassing and Two-Phase Flow Pilot Hole Test Report

JIL T. GELLER

Earth Sciences Division
Lawrence Berkeley Laboratory
University of California
Berkeley, CA 94720

and

JERKER JARSJÖ

Water Resource Engineering
Royal Institute of Technology
S-100 44 Stockholm
Sweden

March 1995

This work was supported by the International Program in the Office of Civilian Radioactive Waste Management of the U.S. Department of Energy under Contract Number DE-AC03-76SF00098.

Revision 0.2

DEGASSING AND TWO-PHASE FLOW PILOT HOLE TEST REPORT

Jil T. Geller

Earth Sciences Division, Lawrence Berkeley Laboratory

Jerker Jarsjö

Water Resources Engineering, Royal Institute of Technology

March 17, 1995

Keywords: Degassing, Two-Phase Flow, Gas Measurement, Blasting, Transmissivity, Storativity, Fractured Rock, Hydrologic Testing

ABSTRACT

A pilot hole test was conducted to support the design of the Degassing of Groundwater and Two-Phase Flow experiments planned for the Hard Rock Laboratory, Äspö, Sweden. The test consisted of a sequence of constant pressure borehole inflow tests (CPTs) and pressure recovery tests (PRTs) in borehole KA2512A. The test sequence was designed to detect degassing effects from the change in transmissivity, or hydraulic conductivity, and storativity when the borehole pressure is lowered below the groundwater bubble pressure. A bubble pressure estimate of 300 kPa was calculated from earlier gas contents measurements in KA2511A and KA2598A. Borehole KA2512A was drilled while maintaining the borehole pressure greater than 1500 kPa to prevent the possible formation of a gas phase and ensure that single phase flow behavior could be well characterized. The entire 37.3m of the borehole section was tested without packers. Flow response to pressure changes in CPTs occurred rapidly. Flowrates fluctuated before attaining a steady trend, probably due to effective stress changes when borehole pressure was reduced for the first time. These factors decreased the sensitivity of type-curve fits to values of specific storage. The relationship between borehole pressure and steady-state flowrates was linear over borehole pressures of 1500 kPa (abs) down to 120 kPa (abs) during testing in December 1994, indicating that processes that may change hydraulic conductivity at low borehole pressures, such as degassing, calcite precipitation or turbulence, did not occur to a measurable degree. The gas contents of water from KA2512A, KA2598A, KA3010A and KA3067A were measured by two methods which indicated the volume of evolved gas per known volume of liquid. These methods indicated a gas contents in KA2512A on the order of 0.5% v/v, in which case it is possible that pressures below the groundwater bubble pressure were not attained in the formation. Samples from other boreholes had higher gas contents (ranging from 1 to 3% v/v). Test resultss during January and February of 1995 suggest that degassing may have occurred. The hydraulic conductivity measured at a borehole pressure equal to 120 kPa (abs) was 20% lower than the hydraulic conductivity measured at a borehole pressure of 1500 kPa (abs); the latter value was 10% lower than the hydraulic conductivity measured in December, 1994. The volumetric gas content measured during this time was 1% v/v. Pressures in monitoring well KA2511A responded to the testing in KA2512A. Step-changes in flowrates coincided with blasting at 3300-3400 m tunnel length. The magnitude of these changes was greater at the lower borehole pressures. Step increases in pressures in KA2511A also coincided with the blasts.

TABLE OF CONTENTS

ABSTRACT		**iii**
LIST OF FIGURES		**vii**
EXECUTIVE SUMMARY		**ix**
ACKNOWLEDGEMENTS		**xiii**
1.	**BACKGROUND AND OBJECTIVES**	**1**
2.	**PROCEDURES**	**5**
2.1	TEST SEQUENCE	5
2.2	BOREHOLE DESCRIPTION	7
2.3	EQUIPMENT DESCRIPTION AND METHODS	7
2.3.1	Pressure and flow regulation	7
2.3.2	Data acquisition	8
2.3.3	Gas contents	8
2.3.4	Glass accumulator	9
2.3.5	Tube trap	9
3.	**RESULTS**	**13**
3.1	TEST DATA AND AMBIENT CONDITIONS	13
3.1.1	Measurements in KA2512A	13
3.1.2	Response in monitoring wells	14
3.1.3	Blasting activities	15
3.1.4	Precipitation, barometric pressure and temperature	16
3.1.5	Gas contents	17
3.2	DATA ANALYSIS	20
3.2.1	Steady-state data (flowrate as a function of borehole pressure)	20
3.2.2	Constant pressure tests	22
3.2.3	Pressure recovery tests	26
3.2.4	Discussion	27
4.	**CONCLUSIONS AND RECOMMENDATIONS**	**31**
	REFERENCES	**35**
	APPENDIX I. Estimation of gas contents and bubble pressures	**37**
	APPENDIX II. Record of blasting activities during pilot hole test	**39**
	FIGURES	

LIST OF FIGURES

Page	Figure No	Description
	Figure 2-1 a	Pilot hole test sequence, phase 1-3.
	Figure 2-1 b	Pilot hole test sequence, phase 4.
	Figure 2-2	Plan view of the tunnel and the boreholes at the 300 - 460 m level.
	Figure 2-3	Experimental set-up for pressure- and flow regulation and installation of the tube trap for gas contents measurements.
	Figure 2-4	Glass accumulator for measurement of volumetric gas contents.
	Figures 2-5 a and b	Tube trap for measurement of volumetric gas contents. (a) Installation in boreholes. (b) Orientation to relieve pressures and measure evolved gas.
	Figure 3-1	Flowrates as a function of time from test start for constant pressure tests (CPTs) 1 to 3.
	Figure 3-2	Flowrates as a function of time from test start for CPTs 4 and 5.
	Figure 3-3	Flowrates as a function of time from test start for CPTs 6 to 8.
	Figure 3-4	Flowrates as a function of time from test start for CPTs 9 to CPT 11 (middle part only).
	Figure 3-4 a	Flowrates as a function of time from test start for last part of CPT 11.
	Figure 3-4 b	Flowrates as a function of time from test start for CPT 12.
	Figure 3-4 c	Borehole pressures during CPTs 11 and 12.
	Figure 3-5	Borehole pressures as a function of time for pressure recovery tests (PRTs) 1 and 2.
	Figure 3-6 a	Plan view of tunnel and selected boreholes.
	Figure 3-6 b	Section view of tunnel and selected boreholes
	Figure 3-7	Steady-state flowrates as a function of borehole pressure and flow fluctuations for CPTs 1 to 12.
	Figure 3-8	Steady-state flowrates as a function of borehole pressure with intercepts for CPTs 1 to 9.
	Figure 3-9	Pressures in KA2511A, section 1 to 4, at the times of tests in KA2512A.
	Figure 3-10	Pressures in KA2162B, section 1 to 4, at the times of tests in KA2512A.
	Figure 3-11	Pressures in KA1754A, section 1 and 2, at the times of tests in KA2512A.
	Figure 3-12	Pressures in HAS13, section 1 and 2, at the times of tests in KA2512A.
	Figure 3-12 a	Precipitation in Västervik and northern-most Öland at the times of tests in KA2512A.

Figure 3-13	Barometric pressure in the tunnel at KA2512A, at the times of tests in KA2512A.
Figure 3-14	Temperature of air in the ventilation shaft at the times of tests in KA2512A.
Figures 3-15 to 3-23a	Match of field data from CPTs 1-4 and 6-11 to analytical solutions for spherical flow geometry (n=3).
Figures 3-24 and 3-25	Match of field data from CPTs 2 and 6 to analytical solutions for radial flow geometry (n=2).
Figure 3-25a	Lin-log plot of pressures versus time for data from PRTs 1 and 2.
Figures 3-25b and 3-25c	Plot of $\Delta h/q$ versus $\log(t_1 + t)/t$ for field data from PRTs 1 and 2 and analytical solution for radial flow geometry (n=2).
Figures 3-26 and 3-27	Match of field data from PRTs 1 and 2 to analytical solutions for spherical flow geometry (n=3).

EXECUTIVE SUMMARY

This report describes a pilot hole test to support the design of the Degassing of Groundwater and Two-Phase Flow experiments planned for the Hard Rock Laboratory, Äspö, Sweden. These experiments will investigate the development of two-phase flow conditions in the near-drift region and their effect on hydraulic test interpretation. One hypothesis is that liquid flow rates are reduced due to the evolution of two phase flow conditions that evolve as a result of groundwater degassing upon pressure reduction. This will be tested by measuring the inflow to a single borehole as a function of borehole pressure. This relationship is linear for single liquid phase conditions; deviations from linearity at low borehole pressures may indicate the presence of a gas phase. The first tests at borehole pressures above the partial pressure of the dissolved gases (or bubble pressure) establish the linear trend between borehole pressure and flowrates; however, there is concern that depressurization of the borehole during drilling and packer installation may irreversibly disturb the initial conditions of the flow system by allowing the formation of a gas phase.

Equipment exists to drill a borehole while maintaining formation pressure; however, the development and construction of a packer system that could be installed without depressurization would be costly and its performance uncertain. To assess the need for such a packer system, a pilot hole test was conducted in borehole KA2512A. This borehole was drilled while maintaining water pressure above the estimated partial pressure of the dissolved gases. The entire 37.3 m of the borehole section was tested without packers. One water-flowing fracture occurred at the end of the borehole. The pilot hole test provided the opportunity to test the degassing hypothesis and investigate whether other mechanisms at low borehole pressures could cause a change in transmissivity, including effective stress changes, calcite precipitation and turbulence.

The pilot hole test sequence had four phases: (1) characterize the flow system for single-phase conditions by a series of tests at borehole pressures above the estimated bubble pressure; (2) allow two-phase flow conditions to develop by reducing the borehole pressure to atmospheric pressure and measure the change in transmissivity; (3) repeat tests of the first phase to observe any hysteresis as the flow system returned to single liquid phase conditions and measure the time required for resaturation; and (4) a long-term test at atmospheric borehole pressures to observe any time-dependence in degassing effects.

In test phases (1) through (3), the relationship between borehole pressure and inflow rate was linear over borehole pressures ranging from 1500 kPa (abs) down to 120 kPa (abs). The low gas contents measured in KA2512A (0.5% v/v) indicate that during phase (2), water pressures below the bubble pressure may not have been achieved with the equipment configuration used. The results show no evidence of other processes that might reduce transmissivity at low borehole pressures, such as calcite precipitation, increase in effective stress or turbulence. An analysis of the transient CPT data by type-curve matching for spherical flow geometry gave a hydraulic conductivity value of 1.2×10^{-6} m/s which did not vary significantly with borehole pressure. The specific storage was approximately 10^{-4} 1/m, however the sensitivity of the type-curve matching to the specific storage was low.

In phase (4), which began 25 days following phase (3), the hydraulic conductivity meausred at a borehole pressure of 1500 kPa (abs) was 10%, or one standard deviation, below the mean hydraulic conductivity measured in phases (1) through (3). At a borehole pressure of 120 kPa (abs) the hydraulic conductivity decreased by another 20%. Gas contents measured at the beginning of phase (4) were twice as high as previously measured (1% v/v), suggesting that degassing may have caused the flow reduction. On the other hand, not enough testing was done above the bubble pressure to exclude the possibility that the observed flow reduction was caused by other changes in the system.

Step changes in flowrates coincided with blasts occurring at the 420 to 450 m levels below the test site. The magnitude of the changes was larger at lower borehole pressures. Pressure increases in monitoring well KA2511A also coincided with the blasts. Possible mechanisms of blasting effects on the flow system include changes in boundary conditions, effective stresses or deformation of fracture-lining materials. The flow fluctuations were not large enough to affect the hydraulic conductivity estimates; however, they illustrate how tunnel activities can affect the flow system and complicate the interpretation of test results.

Volumetric gas contents measured in other boreholes were variable and higher than in KA2512A, ranging from 1 to 3% v/v. More information regarding the composition of the dissolved gases in the groundwater at Äspö is required to understand the observed variability, however there is evidence from other researchers that biological activity in the near borehole region in the SELECT project borehole has increased following drilling. Water samples from KA2512A, KA2511A, and SELECT project boreholes KA3010A, 3067A and 3105A were obtained for gas composition analysis at Lawrence Berkeley Laboratory. The results will be reported in a separate document.

We recommend that the pilot hole test be repeated in a borehole with higher gas contents and that the equipement configuration ensure that the groundwater pressure can be reduced to values below the bubble pressure. The sampling for gas content measurement must be cognizant of the spatial and temporal variation indicated by the data in this report. Ideally, the dissolved gas contents in a potential test hole should approach the values measured at Stripa. In addition, air injection tests should be considered to demonstrate the occurrence of flow reduction when a known gas phase is present. Single-hole and cross-hole air injection-resaturation tests are recommended to continue the study of two-phase flow effects on hydrologic characterization from drifts and the performance of the repository following closure.

ACKNOWLEDGEMENTS

This work was carried out under U. S. Department of Energy Contract No. DE-AC03-76SF00098, for the Director, Office of Civilian Radioactive Waste Management, Office of External Relations, administered by the Nevada Operations Office and under the Swedish Nuclear Fuel and Waste Management Company (SKB) Contract No 268070. We would like to gratefully acknowledge the assistance provided by the staff at the Äspö Hard Rock Laboratory Site Office. Olle Olsson of SKB, Gia Destouni of KTH, Kent Hansson of Geosigma and Jane Long, Christine Doughty and Stefan Finsterle of LBL contributed to the design of the pilot hole test and thoughtfully reviewed this report.

1. BACKGROUND AND OBJECTIVES

The investigation of potential underground nuclear waste repositories relies upon hydrologic testing from excavations, which provide access to the subsurface with the purpose of characterizing flow systems in undisturbed rock. Effects of the excavation on the hydrologic response of the system must be understood so that the measured behavior can be extrapolated to the rock away from the drift. Evidence from an investigation of excavation effects in the Stripa Mine in Sweden, a regionally saturated granitic rock formation, suggests that two-phase flow conditions evolved in the region of the drift, reducing flowrates by an order of magnitude compared to pre-excavation conditions (Olsson, 1992; Long *et al.*, 1992). The observation of gas bubbles in the water at Stripa led to the hypothesis that two-phase flow conditions can develop due to the depressurization of formation water, causing the dissolved gases to come out of solution.

A test plan entitled "The Degassing of Groundwater and Two-Phase Flow" was developed to investigate the occurrence of two-phase flow conditions in the near-drift region and their effects on hydrologic characterization. The test plan proposes a series of single hole, constant pressure, inflow tests to be performed at the Hard Rock Laboratory in Äspö, Sweden. For single phase conditions, Darcy's Law predicts that the inflow rate should be directly proportional to borehole pressure. A reduction in measured transmissivity at lower borehole pressures would indicate two-phase flow conditions. The presence of a gas phase may also cause flow fluctuations, hysteresis during pressure cycling and changes in compressibility. Because the magnitude of flow changes due to groundwater degassing is anticipated to be a function of fracture aperture, the test borehole will be packed off into as many as five sections to isolate fractures of varying transmissivities.

Equipment exists to drill a borehole while maintaining formation pressure. However, the development and construction of a packer system that could be installed without depressurization would be costly and its performance uncertain. It was decided to conduct a pilot hole test in a cased borehole drilled under pressure, without packers, which would eliminate uncertainty regarding the existence of single phase conditions when measuring the baseline flow tests above the bubble pressure. Hysteresis following borehole depressurization could then be examined and the need for the design and deployment of a packer system to be installed under pressure could be assessed. The pilot hole test also provided the opportunity to address other issues identified below before proceeding with the design and

implementation of the Degassing of Groundwater and Two-Phase Flow Experiments.

The objectives of the pilot hole test were as follows:

- Test whether degassing causes measurable changes in transmissivity and storativity at atmospheric borehole pressures.

- Evaluate the occurrences of hysteresis caused by borehole depressurization which would interfere with the interpretation of the degassing and two-phase flow tests.

- If gas evolves during depressurization, demonstrate whether the formation is resaturated when background pressure is restored and what is the time required for resaturation.

- Obtain measurements of gas contents of the water to estimate bubble pressure.

- Determine whether two-phase flow effects can be distinguished from other possible causes of flow reduction at low borehole pressures such as effective stress changes, calcite precipitation and turbulence.

A series of constant pressure tests as a function of borehole pressure and pressure recovery tests were designed to meet the pilot hole test objectives. The test sequence and its rationale are described in the following section. The approach in these tests is to detect degassing effects from changes in transmissivity (T), or hydraulic conductivity (K), and storativity (S), or specific storage (S_s) at lower borehole pressures. Hydraulic conductivity should decrease and specific storage should increase in the presence of two-phase flow conditions. Calcite precipitation, the increase in effective stress, or turbulence may also cause a reduction in hydraulic conductivity at lower borehole pressures, however these effects may be distinguished from degassing effects because they should also cause a decrease in storativity. Hysteresis is evaluated by seeing if K and S_S values at higher borehole pressures are restored when the borehole is repressurized. One cause of hysteresis would be the slow dissolution of evolved gas when the borehole pressure is increased. Another cause is a change in the initial set of the fractures when the borehole is depressurized for the first time. These effects may be differentiated on the basis of changes in S_S. An increase in compressibility due to the presence of gas greatly increases the time for flowrates and pressures to reach a steady trend which may also be used to indicate degassing effects and hysteresis. Determination of S_S is inherently unreliable, however relative changes may be significant and useful even if the absolute value is unknown. Because changes in K and S_S, as opposed to their absolute values, will be used to indicate degassing effects, a thorough

characterization of the system above the estimated bubble pressure is essential.

2. PROCEDURES

2.1 TEST SEQUENCE

The pilot hole test sequence consists of the following four phases:

(1) characterize the flow system for single-phase conditions by a series of tests at borehole pressures above the estimated bubble pressure;

(2) allow two-phase flow conditions to develop by reducing the borehole pressure to atmospheric pressure and measure the change in transmissivity;

(3) repeat tests to observe any hysteresis as the flow system returned to single liquid phase conditions and measure the time required for resaturation;

(4) a long-term test at atmospheric borehole pressure to see if degassing effects evolve over time as water farther away from the borehole is sampled.

The timelines for borehole pressures and inflow rates for phases (1) through (3) are depicted in Figure 2-1a. Constant pressure tests (CPTs) and pressure recovery tests (PRTs) were conducted within each phase of the sequence. The bubble pressure is indicated by the heavy dashed line in the upper figure. Appendix I describes how the bubble pressure was estimated using previous gas content measurements in KA2511A and KA2598A. The fine dashed lines indicate the anticipated behavior for two-phase flow conditions. In the CPTs below the bubble pressure, flowrates are expected to drop off as the gas phase evolves and the time to reach steady-state conditions is expected to be much greater compared to single-phase conditions. The time to reach background pressure in a PRT is also expected to increase when a gas phase is present. If the formation does not completely resaturate following well shut-in, flowrates during the subsequent CPTs of phase (3) may be lower than in phase (1).

Because the best evidence of two-phase flow conditions is in the deviation from single-phase behavior, it is critical to obtain the best characterization as practically possible above the bubble pressure. The test sequence was designed to allow the use of analytical solutions (type curves) to estimate values for hydraulic conductivity and storativity from both PRTs and CPTs. The PRTs were scheduled to provide quiescent conditions before a CPT to

allow use of the Jacob and Lohman (1952) solution to interpret the CPT. A long-term CPT was conducted before a PRT to establish a constant flowrate which is assumed in the Horner solution used to interpret the PRT. Other considerations in the design of the test sequence were to minimize the number of perturbations to the system, allow time for flowrates to achieve a recognizable trend and to complete the test cycle within the 2.5 week period available for testing.

Phase (4) was added to the test sequence upon the completion of phase (2), because no significant change in hydraulic conductivity had been observed and there was concern that two-phase flow effects might take a longer time to develop than the test schedule allowed for.

The test sequence for phase (4) is shown in Figure 2-1b. Because of the need to use the borehole test equipment for other purposes, phase (4) was conducted 25 days after CPT 9, during which time the well was shut in. CPT 10 was conducted at a borehole pressure of 1500 kPa (abs) for comparison with phase (1) and (3) because there was concern that the system's response may change over the shut in period. The well was shut in for 8 days between CPT 11 and 12 to obtain water samples under pressure. The test numbers and their schedule are listed in Table 2-1.

Table 2-1. Tests performed in KA2512A. CPT indicates constant pressure test, PRT indicates pressure recovery test. CPT 1 began after the well was shut-in overnight. Well was shut-in between CPT 9 and CPT 10, and between CPT 11 and CPT 12.

Test Phase	Test Number	Borehole Pressure (kPa abs)	Start Date and Time	Test Duration (min)
(1)	**CPT 1**	1500	12/01/94 15:59	1800
	PRT 1	n.a.	12/02/94 20:58	1700
	CPT 2	1000	12/03/94 23:54	1300
	CPT 3	500	12/04/94 20:27	1500
(2)	**CPT 4**	120	12/05/94 23:30	4905
	CPT 5	300	12/09/94 10:51	1549
	PRT 2	n.a.	12/10/94 12:42	1239
(3)	**CPT 6**	1500	12/11/94 09:21	1547
	CPT 7	1000	12/12/94 11:11	1425
	CPT 8	500	12/13/94 11:36	1887

	CPT 9	120	12/14/94	19:43	725
(4)	**CPT 10**	1500	01/09/95	19:03	819
	CPT 11*	120	01/10/95	08:42	11865
	CPT 12	120	01/24/95	16:05	19980

*Data only available from 01/10/95 13:58.

2.2 BOREHOLE DESCRIPTION

Borehole KA2512A is located at 2512 m linear distance along the tunnel and extends in a direction 264° from North, outward from the tunnel spiral, dipping at a 2° angle from the horizontal. The map in Figure 2-2 shows the plan view of the tunnel and the orientation of KA2512A. The plan view indicates locations of fracture zones, which should be interpreted as indicating general trends, rather than precise locations because they were mapped using surface borehole data. The 85 mm diameter borehole was drilled while maintaining formation pressure above 1500 kPa. The borehole was drilled to a length of 37.27 m, when an inflow rate of 10.6 L/min was obtained at a borehole pressure of 1580 kPa. Almost all of the flow into the borehole occurred over the last 4 to 5 cm of drilling and the core log revealed an undulating, calcite-coated fracture at this location. During drilling, a pressure response was observed in all four packed-off sections along the approximately 300 m length of the nearby monitoring borehole KA2511A. Figure 2-2 shows that KA2511A crosses the line indicating the trend of NNW fractures. These observations suggest that the fracture encountered in KA2512A is hydraulically connected to a larger network of fractures. Water from borehole KA2598A was used for drilling. This water was dyed with uranine which was flushed from the borehole before testing. Detailed descriptions of the borehole drilling and the core log are provided in Rundquist et al. (1995) and Gass et al. (1995), respectively. Tests were conducted in the cased borehole without packers.

2.3 EQUIPMENT DESCRIPTION AND METHODS

2.3.1 Pressure and flow regulation

The experimental set-up is shown schematically in Figure 2-3. A Druck PTX 510-00 50 bar absolute pressure transducer monitored the borehole pressure and was connected to a back pressure controller (PC). A motor-driven pressure regulating valve was used to control the borehole pressure. The time required for stabilizing borehole pressures at the set pressure was approximately 15 seconds. The regulating valve controlled pressures to

within ± 2 kPa for pressures, down to a minimum pressure of 200 kPa (abs). The minimum borehole pressure achievable was 120 kPa (abs) due to head losses in valves and lines dowstream of the casing. The pressure regulating valve was set to 120 kPa (abs) for these tests, however it could not actually regulate at this low pressure as the valve was completely open. A flowmeter (Fischer and Porter COPA-X D10D1165 volumetric flowmeter with a maximum range of 0 to 100L/min and a minimum range of 0 to 5 L/min) was installed upstream the pressure control valve. The accuracy of the flowmeter is ±1% of the real value. A Druck PTX 510-00 12 bar absolute pressure transducer was used to measure the barometric pressure. Figure 2-3 also shows the installation of the tube trap for gas content measurements described in section 2.3.3.

2.3.2 Data acquisition

The flowrate, the borehole pressure and the barometric pressure were continuously logged using BORRE datalogger version 2.2. During the first 30 seconds of the tests, data was logged each 4 seconds. During the subsequent two hours, sample rates decreased incrementally until they reached a rate of once every 15 minutes which was maintained throughout the rest of the test.

Data from the logger was transferred to a laptop PC every one to three days using the menu-driven SHELL program in WP-Lib, which is a part of the Äspö Hydro Monitoring System (see, e.g., Gentzschein, 1993). The SHELL program was also used to enter the calibration constants and transform the hexadecimal data to decimal format.

2.3.3 Gas contents

Volumetric gas contents were measured by two methods: (1) trapping evolved gas over several liters of flowing water in a glass vessel at atmospheric pressure (referred to as a glass accumulator) and (2) measuring the evolved gas upon depressurization of a known volume of water sampled under pressure in a stainless steel tube (referred to as a tube trap). Boreholes KA2512A, KA2598A, KA3010A and KA3067A were sampled by these methods which are described in more detail in the following paragraphs. Neither of these methods are suitable for obtaining gas samples for chemical composition analysis; however, they are useful for immediate estimations of gas contents of sampled water. Measurements by these methods should be interpretated as indications of relative values because they have not been calibrated for known gas contens. Samples for gas contents and chemical and isotopic composition were obtained from boreholes KA2511A, KA2512A, KA3010A, KA3067A and KA3105A and

will be analyzed at LBL. These samples are acquired under pressure in a copper tubing which is clamped to effectively cold-weld the tubing and maintain the sample under pressure until analysis. The clamped seal is leak-proof to helium.

2.3.4 Glass accumulator

A sketch of the glass accumulator is shown in Figure 2-4. The inflow tube of the accumulator is connected downstream of a shutoff valve from the borehole and the outflow tube is directed to a 2 L graduated cylinder. The accumulator is filled with water until the meniscus reaches a gradation mark near the top of the cylindrical portion of the vessel, i.e. below the conical section. The shutoff valve is adjusted to achieve a flowrate of approximately 100 mL/min and the change in the level of the meniscus and the volume of water collected in the graduated cylinder are recorded with time. The gradation marks in the accumulator occur every 5 mL, so a minimum of 10 mL of gas must be collected to obtain a reliable reading. The gas contents are calculated as the percent volume of gas accumulated per volume of water collected in the graduated cylinder. In borehole KA2512A, the water is sampled upstream of the pressure control valve so that samples are obtained at several pressures (see Figure 2-3).

One limitation of this method is that the residence time of the water in the accumulator may be too short for all of the dissolved gas to come out solution. Bubbles were generally observed in the graduated cylinder downstream of the accumulator. Another problem is that dissolved gas may come out of solution in the tubing between the shut-off valve and the accumulator and become trapped upstream of the accumulator. For low gas contents, this could be a significant fraction of the evolved gas. Before taking a reading, the tubing was tapped to release any trapped gas. We observed that the amount of gas accumulated in the vessel was sensitive to flowrate and that approximately 100 mL/min was the optimum value. At significantly lower flowrates the volume of trapped gas decreased, perhaps because there was insufficient energy for gas nucleation. At much higher flowrates the volume of trapped gas decreased, presumably due to inadequate residence time.

2.3.5 Tube trap

The tube trap is shown in Figure 2-5 a and b. It consists of a section of stainless steel tube that has a volume of 187 mL and a section of nylon tubing that has a volume of 31 mL. In borehole KA2512A the tube trap is installed upstream of the pressure control valve to allow sampling at the set pressure (see Figure 2-3). The tube is installed with valves a and d closed.

Valves a, b, c and d are then opened and valve e is partially closed to drive flow through the sample tube. The tube trap is flushed for 15 minutes, during which time the tube is tapped and the translucent tubing checked to ensure that no gas bubbles are present. After flushing, valves a, b, c and d are closed, valve e is fully opened and the tube trap is removed by disconnecting the swagelok fittings between valves a and b and between valves c and d.

The installation of the tube trap for the other boreholes is shown in Figure 2-5 a. The trap is flushed by fully opening valves a, b and c and adjusting the flowrate with valve d. Then valve d is almost closed to maintain pressure in the tube trap while allowing a small outflow to continue flushing the tube. When approximately 2 L of water have been flushed through the tube, valve d is closed first to allow the pressure to build up in the tube, then valves c, b and a are closed, in that order, and the trap is removed by disconnecting the swagelok fittings between valves a and b.

The pressure in the tube trap is relieved by hanging it vertically, as shown in Figure 2-5 b. Valves b and c are initially closed. A water-saturated filter is connected to the end of valve c and submerged in water. The filter allows the outflow of water only, while trapping the evolved gas. Valve c is slowly opened to relieve pressure. After an equilibration period of 2 to 24 hours, the stainless steel tube is tapped to allow the gas to accumulate in the nylon tube section. The gas volume is calculated from the length of the trapped gas bubble multiplied by the cross-sectional area of the nylon tube.

The uncertainties of this method have to do with the potential for gas diffusion through the nylon tubing. Approximately 85% of the trapped water is held in the impermeable stainless steel tubing, although gas diffusion could affect the remaining 15% of water contained in the nylon tube. The manufacturer's specifications list the following values of gas permeability through the nylon tubing:

Table 2- 1 Gas permeability through nylon tubing

Gas	Permeability at 25°C {cm^3-mm/(s-cm^2-cm Hg)}x 10^{-10}
CO_2	9.1–20
H_2	19
O_2	2.0–5.4
N_2	0.2–1.1

No data is available for some of the other gases that might be in the water, such as methane. The amount of gas diffusion through the tube will depend upon the gas composition and the difference between the partial pressures of the gases in the tube and in the atmosphere. A sample calculation for worst case conditions assumes that after relieving tube pressure, the trapped gas phase consists of the most permeable gas, either H_2 or CO_2, using the high permeability value, and neglects the partial pressure of these gases in the atmosphere. This would result in a loss of 0.03 cm^3/hr through the nylon tubing, or a total of 0.8 cm^3 loss over 24 hours, which is equivalent to 0.33% v/v gas at STP per volume of water in the tube trap. Previous analyses of gas composition indicate that most of the gas volume is nitrogen. Because the atmosphere contains 79% nitrogen, there would be little driving force for diffusion of nitrogen through the tubing.

3. RESULTS

3.1 TEST DATA AND AMBIENT CONDITIONS

3.1.1 Measurements in KA2512A

The measured flowrates as a function of time for CPT 1 throughout CPT 12 are shown in Figures 3-1 to 3-4 b. CPTs 1-9 correspond to phases (1)-(3) of the pilot hole test sequence; CPTs 1-3 are conducted above the bubble pressure (Figure 3-1), CPTs 4 and 5 correspond to the conditions below the bubble pressure (Figure 3-2) and CPTs 6-9 are repeat tests (Figure 3-3). CPTs 10-12 (Figures 3-4 to 3-4 b) correspond to phase (4) of the pilot hole test sequence. CPTs 10 through 12 were conducted in January 1995, after the well had been shut-in for 25 days. Two pressure recovery tests were performed (Figure 3-5): PRT 1 followed a constant pressure test of 1500 kPa (abs) and PRT 2 followed a constant pressure test of 300 kPa (abs). The data for the last part of CPT 11 and the whole CPT 12 are shown in separate figures (3-4 a and 3-4 b) since the data was not available electronically at the time of this writing.

Flowrates responded quickly to changes in borehole pressure; however, significant fluctuations in the flowrate occurred, as seen in CPTs 3 and 4 (Figures 3-1 and 3-2). Flowrates over the first 400 minutes of CPT 3 and over the first 500 minutes of CPT 4 have a "sawtooth" pattern, consisting of a series of sloping declines and step increases. The behavior also occured in the first hour of CPTs 1 and 2, although it is not discernable in the scale of the plots. Such fluctuations did not occur in CPTs 6 through 8.

Some step changes in flowrates coincide with blasts at tunnel length 3370-3505 m (see section 3.1.2). The direction of change appears to be random. The times of the blasts are indicated with vertical arrows in the plots of the flowrates versus time (Figures 3-1 to 3-4). Blasting activities in the tunnel also affected the flowrates of repeat tests CPT 7 and 8, although to a lesser extent. There were no blasts during CPT 1, 2, 5 and 6. The cause of the step-increase in flowrate during CPT 8 at $t = 1420$ minutes is unknown. In CPT 3 a flowrate decline proceeds a blast, at $t = 1160$ minutes by approximately 40 minutes. Similarly, a flow rate decline proceeds the blast at $t = 600$ minutes by 80 minutes in CPT 4. These time intervals are longer than possible discrepancies between the data-logger clock and the blasting records. Flowrates during CPT 11 (Figure III-1 and 2) are quite constant with the exception of blast-correlated step changes. However, the first 27 hours of data were lost. During CPT 12, the frequency of blasting was two

to three times a day, which was much higher than in the other tests. Not all of the flowrate fluctuations in CPT 12 coincide with blasts and not all the blasts caused a response in flowrate. Figure 3-4 c shows that the borehole pressures during CPTs 11 and 12 fluctuate in a pattern similar to the flowrates. Borehole pressures during CPT 11 are slightly less than 120 kPa (abs), while during CPT 12 they are slightly higher than 120 kPa (abs). Disregarding the effect of the blasts on the CPT-curves and the initial perturbations seen in CPT 3 and 4, flowrates seem to stabilize within the first hour of the test. Beyond this time, flowrates decline very slowly.

The data for the pressure recovery tests are shown in Figures 3-5 and 3-6. Pressures went up to 99% of the background pressure within the first few seconds of the test, and then it took about 8 hours to reach the full background pressure. Subsequent changes in pressure trends appear to be in response to changing far-field conditions. In the second half of PRT 1 (Figure 3-5) pressures leveled off and then declined slightly. In PRT 2 (Figure 3-6), pressures did not level off as they did in PRT 1, probably due to the increase in background pressure observed in other boreholes (see section 3.1.2).

3.1.2 Response in monitoring wells

Pressures in borehole KA2511A (location shown in Figure 3-6 a and b) responded to the tests in borehole KA2512A, indicating hydraulic communication between the two boreholes. KA2511A is divided into four sections with packers separating each section. Figure 3-9 shows the pressures in KA2511A, sections 1-4, at the time of the hydraulic testing of KA2512A. The linear distance along the borehole from the drift wall for each section are as follows: section 4 extends 6 to 30 m, section 3 extends 31 to 80 m, section 2 extends 81 to 170 m and section 1 extends 171 to 293 m. Pressure changes in sections 1-4 correlate well with the the start times of the hydraulic tests (indicated with horizontal arrows in Figure 3-9). Section 4 of KA2511A (i.e., the section next to the tunnel) is spatially closer to KA2512A as compared with section 1, due to differences in dip of the two boreholes. The pressures in section 4 (squares in Figure 3-9) also show a bigger response to the test sequence compared to section 1 (circles in Figure 3-9). The incremental increase in pressure in each section reflects the regional water table drawdown caused by the presence of the drift.

A trend of pressure increase occurs in KA2511A in addition to the response to the testing in KA2512A. Pressures in KA2511A, section 4, increase by almost 65 kPa over the seven days between the end of PRT 1 and the end of PRT 2. This is in agreement with the observed difference of 62 kPa between the pressures in KA2512A measured at the end PRT 1 and PRT 2. Figure 3-9 shows that this pressure increase begins at the end of CPT 3 and

continues while the pressure in KA2512A is constant at 120 kPa during CPT 4. The times of blasts at tunnel length 3370-3505 m (Appendix II) are indicated with vertical arrows in Figure 3-9 and coincide with step increases in background pressure.

The pressure record of KA2162B (see Figure 3-6 a and b for the locations of boreholes), is shown in Figure 3-10. There is no obvious influence of the hydraulic tests in KA2512A on the pressures in KA2162B, but the step increases in pressures that were observed in KA2511A, starting at the end of CPT 3 (12/05/94, 5 p.m.), is also very pronounced in the first section (circles in Figure 3-10) of KA2162B. In sections 2 (+) and 3 (x) the pressure increase is less pronounced but still visible, and in section 4 (squares) there is practically no pressure increase.

In KA1754A (Figure 3-11), the general pressure increase starting at about 5 p.m. 12/05/94 coincides with increases in KA2511A and KA2562B. Although these boreholes show similar responses, pressure records from other boreholes show that this is not a general behavior. For instance, in KA2555A (no figure shown) a pressure increase can be observed during this period, but the changes in pressure with time are different. Furthermore, there was precipitation during this period of time which also could affect pressures in these boreholes. Nevertheless, there are some indications that the blasts at the end of CPT 3 and throughout CPT 4 affected the fracture system, changing the pressure conditions in several boreholes at various depths.

3.1.3 Blasting activities

Blasting occurred at the 430 to 450 m level of the laboratory during the course of the experiment. A record of the times and locations of the blasts appear in Table II-1 of Appendix II. The times of blasts are also indicated in the plots of the CPTs in section 3.1.1 and in Appendix III.

An accelerometer was installed in the KA2512A niche to get a measure of stress changes resulting from the blasts. The results are summarized in Table 3-1. Each blast contained about 175-180 kg of explosives, but only 5 to 6 kg are detonated at the same time. The distance to the blast is 145 m. The results indicate a dominating frequency of about 300 Hz.

A rough estimate of the stress change due to the blasts can be obtained from the measurements in Table 3-1 where

stress = elastic modulus x ground velocity / wave velocity. (3-1)

A compressional wave velocity of 6 km s^{-1} gives a dilatational stress of about 30 kPa. Uncertainties in the type of stress would change this estimate by no more than a factor of 2. Only the first of the blasts for which ground motion measurement was made occurred during a CPT (CPT 11). The other two measurements were made during the time KA2512A was shut-in. The blasts in January were shot further down the tunnel than the blasts in December and the first blast in Table 3-1 did not cause a measurable flowrate change during CPT 11. Other blasts did occur during CPT 11 and CPT 12 which caused step changes in flowrates, although not all blasts resulted in a response. Without ground motion measurements that coincide with the December blasts, or with a significant flowrate change during the measurements of ground motion, it is difficult to arrive at any conclusions regarding the effect of the blasts. However, the observed pressure and flow response to the blasts suggest that the blasts changed conditions in the formation, including perhaps far-field boundary conditions, effective stresses, or deformation of softer fracture-lining materials. The blasts may open or close hydraulic connections to different parts of the system which could change both boundary conditions and water chemistry.

Table 3-1. Vibration monitoring of rounds at level 450m (UVS 1201 Vibration Monitor, Nitro Consult UVS standard geophone vertical orientation)

Date	Time	Velocity (mm/s)	Acceleration (g)	Displacement (microns)
01/17/95	09:59	2.6	0.55	2
01/17/95	19:47	3.9	0.78	2
01/18/95	10:45	2.8	0.61	1

3.1.4 Precipitation, barometric pressure and temperature

The water level in one of the vertical percussion boreholes located on the Äspö island (HAS13:2) rose 6.8 meters (Figure 3-12) between 5pm 12/05/94 and 12/07/94, i.e., the same time period as the observed pressure increase in boreholes KA2511A, KA2562B and KA1754A. It has previously been observed that rain may cause a large and rapid increase of the water level in this borehole (SKB PR 25-94-23). Typically, the water levels in HAS13:2 fluctuated between 0.5 and 10 meters below the surface level during the Autumn of 1994. If the fracture intersecting KA2512A is connected to a larger fracture network, this could explain the correlation

between pressure changes in KA2512A with pressure changes in more distant boreholes, and even surface boreholes.

Precipitation appears to have caused the observed increase in background pressures. Figure 3-12a shows precipitation data for the time period 12/01/94 to 12/15/94, obtained from the SMHI weather stations located in Västervik (light bars in Figure 3-12a) and northern-most Öland (dark bars). The precipitation events during this period begin just before the water level increase in HA213 and in background pressures in boreholes described above.

The measured barometric pressure in the tunnel at KA2512A (Figure 3-13) was also lower during the period when precipitation occurred. During the first 5 days of the test sequence, the pressure continuously decreased from 106.5 kPa to 103 kPa, and thereafter the pressure fluctuated between a lowest value of 102 kPa and a highest value of 104 kPa. The discontinuities of the curve for $6000 < t < 8000$ and $t = 13500$ can be explained by the switching of data loggers at these times.

The temperature of the air in the ventilation shaft at the 70 m tunnel length is shown in Figure 3-14 and varied between +5°C and +12°C during the time of the test sequence.

3.1.5 Gas contents

Gas content measurements using the methods described in Section 2.3.3 are summarized in Table 3-2. Previous measurements by Arvidsson (1994) and Lif (1993) are listed in the table for comparison. Gas contents in KA2512A range from 0.1 to 0.5%, while values in the other boreholes range from 1 to 3%. The exception to the low values in borehole KA2512A is the January measurement, which is greater than 1%. One explanation for the increase of gas content in KA2512A is that dissolved gas concentrations may be higher in the water near the borehole, compared to water farther into the formation. December measurements in KA2512A were made after eight days of constant pressure flow tests, so one may assume that formation water originating at some distance from the borehole was sampled. The January measurement, however, was made 3 hours after CPT 10 had begun; previous to CPT 10, the well had been shut-in for 25 days. The other boreholes were only opened for sampling, and although they were flushed beforehand, the water sampled must have been from the near-borehole region.

In KA2512A, gas contents were sampled at different borehole pressures. Gas contents are generally greater at the higher borehole pressures, with the exception of the low gas contents measured at 1000 kPa. This raises the

possibility that some of the dissolved gas comes out of solution and becomes trapped in the formation at low borehole pressures. KA2598A, which was used as a supply of drilling water for KA2512A, was sampled at the end of a line near KA2512A. All the other boreholes were sampled at the cover of the casing. All measurements in KA2598A are less than the previously reported values of 3.9%. Higher gas contents were obtained in the tube sampler compared to the glass accumulator in KA2512A and in KA2598A, but this was not observed in KA3010A. The highest gas content was measured in KA3067A. Pressure and flow oscillations during the drilling of KA3067A, which was drilled at a small overpressure, but lower than in KA2512A, suggested the presence of a significant amount of gas.

Equilibration times for reading gas contents in the tube trap varied from 2 to 24 hours. If gas was lost through the nylon tubing, one would expect much lower gas contents for longer equilibration times and significantly higher gas contents compared to the gas accumulator. In KA2511A, longer equilibration times were used, and gas contents were comparable between the two methods. In KA2598A, gas contents measured with the tube trap with a 2-hour equilibration time were twice as high as measured in the accumulator. This was also true in KA3010A. It appears that some gas was lost through the tubing during the longer equilibration times; however, the calculation in section 2.3.3 indicates that the loss would not be more than 0.33% of the total gas contents. Given the uncertainties in the sampling method, there may be some error in the absolute values of the gas contents reported here. Nonetheless, conclusions can be made regarding the relative values of the measurements.

The variability in gas contents raises interesting questions regarding the origin of the gas and why gas contents in KA2512A would be lower than in the other boreholes and why they differ from earlier measurements in KA2511A, which is hydraulically connected to KA2512A. Earlier gas composition analysis of water from KA2598A, KA2511A and surface boreholes show that over 75% of the gas is nitrogen, with the next largest component being CO_2, then either O_2 or CH_4. Because the deep groundwater is anaerobic, the presence of O_2 indicates contamination during sampling. In some of the surface boreholes, helium and hydrogen made up as much as 5 to 50% of the total gas content. It is anticipated that the gas composition analysis of samples taken in January, as well as the water chemistry analysis, will provide some insight into the origin of the dissolved gas and reasons for measured spatial and temporal variablity. Pedersen (1995) has detected the presence of sulphate and sulphur-reducing bacteria as well as methane producing bacteria in groundwater extracted from the SELECT boreholes. They hypothesize that the these bacteria are indigenous and that their metabolic activity was increased following drilling. The occurrence of elevated dissolved gas concentrations in the borehole region due to biological activity is consistent with observations in

this report. This would account for the differences in measured gas contents between wells that are in hydraulic communication, such as KA2511A and KA2512A, as well as observations of temporal variability.

The boreholes sampled were drilled with different methods, which may impact the near-borehole, biologically-produced gas. KA2598A and KA2511A were drilled with standard techniques. To minimize contamination in the SELECT boreholes, the drilling equipment was washed before use.

Table 3-2. Summary of volumetric gas contents measurements

Borehole	Date and Time Sampled	Borehole Pressure (kPa abs)	Gas Content (% v/v STP)	Method	Comments
KA2511A	03/23/94	3000	3.2	*	(Arvidsson, 1994)
KA2512A	12/08/94 08:30	120	0.07	glass accum.	Q=220 mL/min
	12/12/94 09:17	1500	0.46	tube trap	equilib. 25 hours
	12/12/94 09:50	1500	0.23	glass accum.	Q=120 mL/min
	12/13/94 10:41	1000	0.06	tube trap	equilib. 22 hours
	12/14/94 09:21	500	0.07	glass accum.	Q=200 mL/min
	01/09/95 22:59	1500	1.19	tube trap	equilib. 10 hours
KA2598A	12/07/94 10:54	3000	0.93	glass accum.	Q=50 mL/min
	12/13/94 14:21	3000	1.18	glass accum.	Q=142 mL/min
	12/14/94 10:17	3000	2.19	tube trap	equilib. 2.3 hours
	12/07/93	n.a.	3.8	*	(Lif, 1993)
	03/23/94	n.a.	3.96	*	(Arvidsson, 1994)
KA3010A	12/14/94 13:30		1.58	glass accum.	Q=68 mL/min
	12/14/94 19:58		1.06	tube trap	equilib. 12 hours
	12/14/94 20:30		1.72	glass accum.	Q=127 mL/min
	01/09/95 20:04		1.06	tube trap	equilib. 2 hours
KA3067A	12/14/94 12:35		2.82	glass accum.	Q=98 mL/min

*Samples were obtained under pressure. Information regarding sampling device unavailable at this time.

3.2 DATA ANALYSIS

3.2.1 Steady-state data (flowrates as a function of borehole pressure)

The final steady-state flowrates as a function of borehole pressure for CPT 1 through CPT 12 are plotted in Figure 3-7, indicated by open circles. The number next to each data point refers to the CPT and an asterisk indicates that blasting occurred during that CPT. Flowrate fluctuations are indicated by maximum and minimum values for the specific CPT. The data for CPT 1 through CPT 9 are linear over the entire range of borehole pressures. There is a slight shift in the points of phase 3 (CPT 6 through CPT 9) compared to the points of phase 1 and 2 (CPT 1 through CPT 5), which may be related to the change in background pressure (See section 3.1.2); however, the change in slope is insignificant. The trend indicated by phase 4, (CPT 10 through CPT 12 which began after the well was shut in for 25 days) is unclear. The steady-state flowrate for CPT 11 is 30% lower than in phases 1 through 3; however, the value for CPT 12 approaches the trend exhibited by the previous phases. Most of the significant flow fluctuations occurred at the times of blasting (see CPT data in section 3.1.1) and the magnitude of the fluctuations is greater at the lower borehole pressures.

Several processes may induce changes in transmissivity at low borehole pressures in addition to groundwater degassing; however, effects of these processes were not observed in the results of CPT 1 through CPT 9. The groundwater has been reported to be super-saturated with respect to calcite (ref?). Calcite precipitation can occur quickly upon depressurization, with a subsequently slow dissolution upon pressure increase. Precipitation of calcite could block flow paths and decrease transmissivity at the lower borehole pressures. The actual degree of supersaturation in KA2512A will be computed when the water chemistry data is available; however, the fact that the flowrates increased from CPT 11 to CPT 12 is inconsistent with the occurrence of calcite precipitation. The increase of effective stress as a result of decreasing borehole pressure did not appear to affect transmissivity, although the flow fluctuations observed in the first part of the tests in phase 1 and 2 discussed in the previous section may indeed be related to effective stress changes. Effects of turbulence causing flow reductions at the higher flowrates were also not observed.

In Figure 3-8, the steady-state flowrates for test phases 1, 2 and 3 are plotted as a function of borehole pressure and transmissivity is determined from the slope of the data, using the following equation for steady-state radial flow conditions:.

$$Q = -\frac{2\pi T}{\rho g}\ln\left(\frac{r}{R_w}\right)\left[P_{borehole} - P(r)\right] \tag{3-2}$$

where Q is the inflow rate to the borehole, ρ is the density of water, g is the acceleration of gravity, r is radial distance away from the center of the borehole, R_w is the radius of the borehole and $P(r)$ is the formation pressure distance r away from the borehole. Transmissivity is then equal to

$$T = m\left[\frac{\mathrm{m^3/s}}{\mathrm{kPa}}\right]\ln(R_w/r)\frac{\rho g}{2\pi}\left[\frac{\mathrm{Pa}}{\mathrm{m}}\right]\mathrm{x}10^{-3}\left[\frac{\mathrm{kPa}}{\mathrm{Pa}}\right] \tag{3-3}$$

where m is the slope computed from the regression, listed in Table 3-2. The x intercepts at zero flow, shown in Figure 3-8, represent the background pressure at the end of the test phase and are included in the regression. A separate regression was done for CPT 1 through CPT 5 and for CPT 6 through CPT 9. Table 3-2 lists the regression results and the computed transmissivity for r=150 m.

Table 3-2. Linear regression results for CPT 1 through CPT 9 and transmissivity for steady-state radial flow.

	CPT 1 through 5	**CPT 6 through 9**
slope ($\Delta Q/\Delta P_b$) ($m^3\ s^{-1}\ kPa^{-1}$)	-5.8×10^{-8}	-6.3×10^{-8}
Y intercept ($m^3\ s^{-1}$)	1.8×10^{-4}	$2. \times 10^{-4}$
r^2	0.994	0.987
Predicted background pressure (kPa)	3066	3166
T ($m^2\ s^{-1}$)	7.81×10^{-7}	8.51×10^{-7}

The r^2 values on the order of 0.99 indicate that the flowrate is indeed linear with borehole pressure over the tested range and the fit with the x intercept at background pressure is good. The difference in transmissivities between the two test phases is insignificant.

3.2.2 Constant pressure tests (CPTs)

The theory for interpretation of single-well constant rate flow tests (e.g. Theis, 1935; Earlougher, 1977 and Barker, 1988) can be extended to develop diagnostic methods and interpretative equations for analyzing constant-head test data. We will in the following consider the conceptual flow models that have been developed for linear ($n = 1$), radial ($n = 2$) and spherical ($n = 3$) flow geometries. The expressions yielding the flow response for the periods of time at which outer boundary effects do not influence the system, are (Carslaw and Jaeger, 1959; Jacob and Loman, 1952):

$$\frac{\Delta H}{q(t)} = \frac{1}{A}\sqrt{\frac{\pi t}{K S_s}} \qquad \text{for } n = 1 \qquad (3\text{-}4)$$

$$\frac{\Delta H}{q(t)} = \frac{1}{4\pi K b}\ln\left(\frac{9}{16}\frac{t}{t_{diff}}\right) \qquad \text{for } n = 2 \qquad (3\text{-}5)$$

$$\frac{\Delta H}{q(t)} = \frac{1}{4\pi K r_w\left(1+\sqrt{\frac{4}{\pi}\cdot\frac{t_{diff}}{t}}\right)} \qquad \text{for } n = 3 \qquad (3\text{-}6)$$

where the diffusion time t_{diff} [T] is defined as:

$$t_{diff} = \frac{r_w^2 S_s}{4K} \qquad (3\text{-}7)$$

and ΔH is the drawdown head at the well [L], $q(t)$ is the flow response [L^3/T] as a function time, A is the linear well area [L^2] which equals $2bw_a$ wherew_a is the aperture width, K is the hydraulic conductivity [L/T], S_s is the specific storage [1/L], t is the time [T], b is the height of the cross-sectional area perpendicular to the flow direction [L] , w_a is the fracture aperture width and r_w is the radius of the borehole [L]. For radial flow geometry, the transmissivity T equals Kb, and the storativity S equals $S_s b$.

Equation (3-5) is a long-term approximation of the exact solution. However, for times relevant to the present set of data, this approximation coincided with the exact solution.

Field data is typically matched with the analytical solutions (3-4 through 3-6), for $\Delta H/q(t)$ in order to determine the flow geometry of the system and estimate the values of K and S_s. In Figures 3-15 to 3-25, flow data from the constant pressure tests (CPTs 1-4 and 6-11) are matched with analytical solutions for radial and spherical flow geometries. (Data for CPT 12 was not available in electronic form at the time of this writing.) CPT 5 was preceded by a CPT at a lower borehole pressure and is therefore excluded from the comparison. The drawdown head ΔH was calculated as $\left(P_f - P_w\right)/g\rho$, i.e. the formation (or background) pressure minus the constant pressure maintained in the well (or the borehole pressure). A P_f value of 3010 kPa (abs) was used for CPTs 1-4, and for CPTs 6-11, a P_f value of 3070 kPa (abs) was used. Curve matching was done on an Excel spreadsheet after Doughty (1995), adjusting values of K and S_s until the best match was obtained.

The match of the CPT data to the type curves representing spherical flow geometry is shown in Figures 3-15 to 3-23a. Flow perturbations during the first hours of CPTs 1-4 (note the logarithmic time-scale of the plot) makes it hard to match the data with the type curve, despite the fact that for CPT 1 and 2, these perturbations were small enough not to be visible in the plots of flow versus (normal) time (Figure 3-1). These fluctuations might be due to changes in rock stresses (due to the lowering of water pressures) causing plastic deformation of the rock and affecting the hydraulic properties of the fracture, a hypothesis which is supported by the fact these flow fluctuations were greater during CPT 3, when also the borehole pressure was lower in comparison with CPT 2. In addition, these early flow fluctuations cannot be observed at all during the repeat tests (CPT 6 to 10), which fit better to the type curves.

Changes in specific storage shift the plots in the x-direction, and therefore, the determination of S_s requires a bend in the curves. Because of the flatness of the field data curves, the match between the type curves and the field data is not very sensitive to S_s, whereas hydraulic conductivities can be more precisely determined because changes in K shift the curves in the y-direction. However, the first parts of the curves for CPT 6 through 10, corresponding to early time data, are not as flat as for CPT 1 through 4, which result in relatively good fit of data to the type curves, and presumably also a better accuracy in the storativity values obtained from the fit.

Equations 3-1 to 3-3 were developed under the assumption that the constant pressure period is preceded by a period of no-flow conditions. This was only the case for CPT 1, which was performed after a well shut-in

overnight, and CPT 2 and 6, which were preceded by PRTs 1 and 2, respectively. A strict analysis of the other CPTs would require that the flow perturbations induced by previous constant pressure tests be superimposed on the solution for the flow versus time, as in Mishra (1992). However, the data shown in Figures 3-15 to 3-23 suggest that for the present flow conditions, these perturbations do not significantly change the goodness of fit of the field data to the type curves, nor the result of the fit in terms of obtained K and S_s values.

The match of two representative CPTs (number 2 and 6) to the type curves for radial flow geometry is shown in Figures 3-24 to 3-25. The fit is not as good as for the spherical case, suggesting that the flow field around the borehole show more similarities with the spherical geometry rather than the radial. A match between the field data and the $n = 2$ curves based upon the first part of the field data curves results in a bad fit for the last part. For $n = 1$ (linear flow geometry), no agreement at all can be observed between the $n = 1$ curve and the field data.

Table 3-4. Values of K and S_S obtained through matching field data with $n = 2$ and $n = 3$ type curves.

CPT #	n	K * (m/s)	S_s (1/m)	Comments
1	3	$1.2 \cdot 10^{-6}$	Indeterminate	Fit not sensitive to S_s
2	3	$1.1 \cdot 10^{-6}$	Indeterminate	Fit not sensitive to S_s
3	3	$1.1 \cdot 10^{-6}$	Indeterminate	Fit not sensitive to S_s
4	3	$1.0 \cdot 10^{-6}$	Indeterminate	Fit not sensitive to S_s
6	3	$1.4 \cdot 10^{-6}$	$3.0 \cdot 10^{-4}$	Relatively good fit; better accuracy in S_s value.
7	3	$1.2 \cdot 10^{-6}$	$3.0 \cdot 10^{-4}$	Relatively good fit. First data point was not accounted for in fit
8	3	$1.1 \cdot 10^{-6}$	$6.0 \cdot 10^{-5}$	Relatively good fit. The lower Ss-value is due to differences in the two first data points as compared to CPT 6,7 & 9
9	3	$1.2 \cdot 10^{-6}$	$1.0 \cdot 10^{-4}$	Relatively good fit. First data point was not accounted for in fit
10	3	$1.05 \cdot 10^{-6}$	$3.0 \cdot 10^{-4}$	Relatively good fit
11	3	$0.80 \cdot 10^{-6}$	Indeterminate	Fit not sensitive to S_s due to lack of data for the first 36 hrs.
2	2	$1.1 \cdot 10^{-6}$	$1.0 \cdot 10^{-7}$	Poor fit
6	2	$0.90 \cdot 10^{-6}$	$1.0 \cdot 10^{-7}$	Poor fit

*) Tabulated K-values for $n = 2$ were obtained with $b = 1$, and are thus identical to corresponding T-values.

The K and S_s values derived from the type curve fits are tabulated in Table 3-4. The K values do not show any significant changes for CPTs at different borehole pressures. The mean value and standard deviation of the K values obtained in CPTs 1 - 9 for n=3 was $1.15 \cdot 10^{-6} \pm 0.12 \cdot 10^{-6}$ m/s. The K value for CPT 10 is within one standard deviation of the mean hydraulic conductivity measured for CPTs 1 through 9. In CPT 11, K is three standard deviations, or about 30%, lower than the mean. This decrease in K

might be due to degassing but could also be due to changes in the system during the period in which the well was shut in between CPT 9 and CPT 10, however the decrease in K between CPT 10 and CPT 11 is consistent with the occurrence of degassing effects.

The relatively good fits obtained for $n=3$ suggest S_s values around 10^{-4} m^{-1}. This value is higher than the relatively few values that have been reported for bulk crystalline rock (Almén et al, 1986), and may indicate the presence of a fracture zone. Almén et al. report values of S_s in the range of 10^{-6} to 10^{-10} m^{-1} for bulk rock in single-hole tests, and values ranging from 10^{-4} to 10^{-6} m^{-1} for fracture zones in cross-hole tests .

3.2.3 Pressure recovery tests (PRTs)

Applying the method of Horner (1951), the pressure head as a function of time when the well is shut in after a time period t_1 of constant flow, can be derived by superimposing the effects of a well flowing at a rate q for time $(t_1 + t)$ and a well flowing at rate $-q$ for time t, where t is the time from the well shut-in. The long-term solution for radial flow and the general solution for spherical flow yield:

$$\frac{\Delta h(t)}{q} = \frac{1}{4\pi Kb} \ln\left(\frac{t_1 + t}{t}\right) \qquad \text{for } n=2 \qquad (3\text{-}8)$$

$$\frac{\Delta h(t)}{q} = \frac{1}{4\pi K r_w}\left(\operatorname{erfc}\left(\sqrt{\frac{t_{diff}}{t+t_1}}\right) - \operatorname{erfc}\left(\sqrt{\frac{t_{diff}}{t}}\right)\right) \qquad \text{for } n=3 \qquad (3\text{-}9)$$

where Δh is the drawdown head in the well, q is the flow rate during t_1, and the rest of the parameters are as in equations (3-3) through (3-6). For the times relevant to the present set of data, equation (3-8) coincides with the exact solution.

Generally, the field data did not match the type-curves very well. Equation (3-8) predicts that for n=2, $\Delta h/q$ vs. $(t_1 + t)/t$ should be linear when plotted on a lin-log scale. The linearity of the field data in Figure 3-25a indicates a closer match to the n=2 Horner solution (equation 3-8) rather than the n=3 solution (equation 3-9). The bend of the early-time part of the curve for

PRT 1 could be due to skin effects and / or well borehole storage. However, the first part of PRT 2 shows no signs of such effects. The analysis of skin effects is not within the scope of this report. The bend of the late-time portion of the PRT 1 curve reflects the decrease in background pressure. Figure 3-25 b and c shows plots of $\Delta h/q$ versus $\log((t_1 + t)/t)$ for PRT 1 and 2, where K can be determined from the slope of the linear parts of the field data curves. The type curve for n=2 is also included in the plots and it can be seen that $\Delta h/q$ should go to zero as $(t_1 + t)/t$ goes to one, i.e. as time approaches infinity. The data for PRT 1 deviate from the type-curve at later times due to the increase in background pressures, therefore this part of the curve is disregarded. The obtained K values for n=2 were $3.0 \cdot 10^{-5}$ m/s for PRT 1 and $3.5 \cdot 10^{-5}$ m/s for PRT 2. These values are one order of magnitude higher than the K values obtained from the CPTs. The reported K value for PRT 2 corresponds to the slope of the later-time data, but the result changes by less than a factor two when other parts of the curve are used for determining K. Note that S_s cannot be evaluated assuming n=2 since this parameter is not included in equation (3-8).

Figures 3-26 and 3-27 show the fit of data from PRT 1 and PRT 2 to the Horner curve representing spherical flow geometry ($n=3$) using corresponding values of K and S_s obtained from the constant pressure tests. It can be seen from Figure 3-27 that the field data from PRT 2 crosses the type-curve using the K and S_S values obtained from the curve match with CPT 8. Similar results are obtained using the K and S_S pairs that were determined from CPT 6,7 and 9. The best fit for PRT 1 to the n=3 type curve was obtained for K=$1.2 \cdot 10^{-6}$ m/s and S_S=$1.0 \cdot 10^{-3}$ (1/m), as can be seen in Figure 3-26. Adopting average values of K and S_S from the best fits of CPT 6 to 9 shifts the field data to the right in Figure 3-26.

3.2.4 Discussion

In test phases (1) through (3), the relationship between borehole pressure and inflow rate was linear over borehole pressures ranging from 1500 kPa (abs) down to 120 kPa (abs), and a mean hydraulic conductivity of $1.15 \cdot 10^{-6} \pm 0.12 \cdot 10^{-6}$ m/s was obtained through fitting constant pressure test data to n=3 type curves. The results show no measurable effects of other processes that might reduce transmissivity at low borehole pressures, such as calcite precipitation, increase in effective stress or turbulence. The low gas contents measured in KA2512A (0.5% v/v STP) indicate that during phase (2), water pressures below the bubble pressure may not have been achieved with the equipment configuration used. The estimated bubble pressure for these gas contents, assuming that the gas is nitrogen and a Henry's Law constant of $8.14 \cdot 10^6$ kPa/(mole fraction), is 134 kPa (abs). From the 2° dip of the borehole, the end of the borehole where the water-flowing fracture was intersected is approximately 1.3 m below the elevation of the borehole

casing where pressure was measured. During phase (2), the borehole pressure was 120 kPa (abs), resulting in a pressure at the end of the borehole of approximately 133 kPa (abs).

In phase (4), the hydraulic conductivity decreased from a value of $1.05 \cdot 10^{-6}$ m/s at a borehole pressure of 1500 kPa (abs) to a value of $0.8 \cdot 10^{-6}$ m/s. Gas contents measured at the beginning of phase (4) were twice as high as previously measured (1% v/v), which gives an estimated bubble pressure of 167 kPa (abs). In this case, the groundwater pressure in the formation may have been less than the bubble pressure, suggesting that degassing may have caused the flow reduction. This suggestion must be qualified by the fact that not enough testing was done above the bubble pressure to exclude the possibility that the observed flow reduction was caused by a change in boundary conditions or blast-induced effects.

CPT 1-4 did not match the type curves as well as the CPT 6-10 mainly because of irregularities in the curves, which might have been caused by changes in rock stresses during the initial lowering of water pressure, which then can affect the hydraulic properties of the fracture. Before starting the test cycle, it would thus be preferable to lower the pressure as much as possible and possibly also cycle pressures up and down, in order to observe if effective stress changes cause hysteresis, particularly in the first cycle.

The response of the system was fast, and only the very first part of the curves showed an inclined shape that could be matched with the type curves. This particularly decreased the sensitivity of the analysis with respect to S_s values. More frequent data sampling during the first 20-30 seconds, preferably several times per second, might provide better sets of data for fractures with this yield; however, questions can be raised on whether this early time data reflects the hydraulic conditions of the borehole rather than the fracture itself. In addition, the backpressure controller can not ensure constant pressures during the first 15 seconds of the test.

The field CPT data fitted best to the type curves with spherical flow geometry, while the flat shape of the field PRT data made them more similar to radial flow geometry. The occurrence of these idealized flow geometries in fractured rock is questionable. For instance, a borehole intersecting a fracture zone might represent a geometry that, in reality, is in between radial and spherical, so that neither the conditions for n=2 nor the conditions for n=3 are fulfilled. Thus, a fit of field data to a curve representing n=3 does not necessarily imply that the flow field is spherical but rather that the flow field under certain conditions shows similarities to the spherical flow case.

Increasing amounts of gas phase in the borehole would be observed as an apparent increase in the specific storage obtained through matching field

data to equations 3-2, 3-3 and 3-6, since S_s is linearly proportional to the fluid compressibility, which increases by several orders of magnitude when a gas phase is present. Furthermore, a higher gas phase saturation in the fracture could reduce the hydraulic conductivity due to two-phase flow effects. The solutions for constant pressure tests are a function of the ratio of hydraulic conductivity and specific storage. Two-phase conditions should cause a decrease in hydraulic conductivity and an increase in specific storage, resulting in a large overall decrease in the ratio of the two terms. Consequently, the change in these parameters relative to single-phase conditions should be readily detectable, even if an absolute value of storativity cannot be measured with confidence. Studies have shown that absolute values of K and S_s might differ by orders of magnitude depending on which test method is chosen (e.g. Almén et al.); therefore, it is important to conduct similar tests to evaluate changes in K and S_s. No decrease in K was measured throughout the test sequence in KA2512A, and it is likely that changes in S_s. would have been much more obvious if degassing had been significant compared to those resulting from uncertainty in the type curve matching.

4. CONCLUSIONS AND RECOMMENDATIONS

The pilot hole experiment tested the application of borehole inflow tests to measure the effects of groundwater degassing on hydraulic parameters when pressure is reduced. The test sequence was designed to detect degassing effects by comparing flow behavior above the bubble pressure where single-liquid-phase conditions definitely exist with borehole inflow below the bubble pressure where two-phase flow conditions may evolve.

The hydraulic conductivity measured in borehole KA2512A was constant for borehole pressures ranging from 1500 kPa (abs) to 120 kPa (abs) during tests conducted in December, 1994. The low gas contents measured in KA2512A during these tests (0.5% v/v STP) indicate that water pressures below the bubble pressure may not have been achieved with the equipment configuration used. The estimated bubble pressure at this gas content is about 130 kPa (abs), which is close to the estimated minimum pressure attained at the end of the borehole where the flowing fracture occurred. Previous values of gas contents measured in other boreholes at Äspö were around 4%, which are within the range of values measured at Stripa where groundwater degasssing effects were thought to have occurred.

Hydraulic conductivity measured in January, 1995, decreased 20% with a reduction in borehole pressure from 1500 kPa (abs) to 120 kPa (abs). The gas contents measured at this time were about twice as high (1% v/v) as in December, suggesting that degassing may have caused the flow reduction. Although not enough testing was done above the bubble pressure to exclude the possibility that the observed flow reduction was caused by a change in boundary conditions, the decrease in hydraulic conductivity is approximately two times the standard deviation of measurements made in December. These tests ran about ten times longer than the tests conducted in December 1994, however there was no net decrease in flowrate associated with time.

The findings of this experiment have important implications for further testing. Testing a borehole with low gas contents provided a fortuitous opportunity to assess other factors that might cause borehole inflow rates to decrease at lower borehole pressures. Calcite precipitation, turbulence and the increase of effective stress could all cause a decrease in flowrates at lower borehole pressures. It would be difficult to distinguish which low-pressure effect is significant because they all cause a reduction in transmissivity. As no decrease in flowrate was observed at low borehole pressures, we can conclude that these three effects did not occur to any

measurable degree. This should aid in the interpretation of future borehole inflow tests.

Hydraulic conductivity / transmissivity and specific storage / storativity were estimated with transient test data using type-curve matching and with steady-state data. For the evaluation of hydraulic conductivity, type curve matching produced consistent results between tests. The evaluation of specific storage was indeterminate due to the generally flat shape of the curves, which resulted in poor resolution when matching in the horizontal direction. The solutions for constant-pressure tests are a function of the ratio of hydraulic conductivity and storativity. Two-phase conditions should cause a decrease in hydraulic conductivity and an increase in specific storage, resulting in a large overall decrease in the ratio of the two terms. Consequently, the change in these parameters relative to single-phase conditions should be readily detectable even if an absolute value of storativity cannot be measured with confidence. The requirement to use changes in the storativity and hydraulic conductivity to detect two-phase conditions reinforces the need of a thorough characterization of single-phase flow conditions before reducing borehole pressure below the bubble pressure.

A gas sampling tube was developed for measuring the volume of evolved gas from groundwater samples acquired under pressure. This device is connected to a valve on the borehole casing with a valve on the other end to maintain pressure. Once the sample is obtained, the pressure is relieved and the volume of gas evolving is measured from the length of the gas bubble in the translucent portion of the tube. In the continued use of this sampler, evolved gas volumes should be measured at 15-minute intervals to determine the optimum time required for the dissolved gas to come out of solution. Our experience indicates that a 2-hour equilibration time is adequate, however further calibration of this device is recommended.

Future degassing tests should be conducted in a borehole with significantly higher gas contents than in KA2512A. Experimental results by Geller et al. (in preparation) indicate that fracture geometry has a first order effect on flow reduction due to degassing and that gas content is a second order effect. However, the relationship between degassing effects and such low gas contents measured in KA2512A has not been tested and it is possible that flowrate changes cannot be detected at such low values. In order to test the degassing hypothesis with greater confidence, gas contents should be closer to the values measured at Stripa, where degassing is hypothesized to have caused the observed flow reductions.

A series of consistent gas content measurements should be performed in order to increase the understanding of the significant spatial and temporal variability of gas contents indicated by measurements in the pilot hole and

in other boreholes. The test series should include repeated volumetric gas content measurements and chemical analysis in several boreholes as a function of borehole inflow volume to detect changes with time and location. One hypothesis consistent with measurements reported here is that elevated dissolved gases are produced in the near-borehole region as a result of biological activity stimulated by drilling and that the gas content of the formation water away from the borehole is lower. If this is the case, then gas contents in water sampled from a borehole that has been shut-in for a long time should be higher than in water sampled from a flowing borehole, as indicated by the data in this report. This is a site-specific hypothesis in that dissolved gases have different origins, many of which are not biogenic, as in the case of Stripa (Andres, et al., 1989).

The experience of the pilot hole test has shown that for low gas contents and with a standard borehole configuration, the groundwater pressure in the fracture may not be reduced to below the bubble pressure. The order-of-magnitude flow reductions measured at Stripa were for water flowing into the drift where the fractures were directly subjected to atmospheric pressure, allowing pressures below the bubble pressure to exist in the formation. Due to the dip of KA2512A and frictional losses during flow, the pressure at the fracture intersection with the borehole was greater than atmospheric pressure. The test equipment should be configured to ensure that pressures below the bubble pressure of the groundwater are obtained in the formation. Lower borehole pressures can be achieved by maintaining a water-filled drain line and extending it to an elevation significantly lower than the test borehole.

Another consideration in borehole selection is the transmissivity of the fracture and its characteristic geometry. Degassing is most likely to cause measurable effects in rough, relatively tight fractures where gas can be trapped, as compared to smooth, highly transmissive fractures that do not provide conditions for gas trapping and subsequent flow reduction.

In addition to the degassing problem, there are compelling reasons to continue the investigation of two-phase flow effects at Äspö. Groundwater degassing may be important at other sites. Other two-phase flow effects can interfere with the interpretation of hydrologic tests from excavations, such as ventilation and air invasion. Two-phase flow studies are also relevant to the prediction of repository performance following closure in terms of resaturation rates and the fate of waste-generated gas.

Air injection-resaturation tests should be considered to demonstrate the occurrence of flow reduction in the presence of a known or controlled gas-phase saturation. Changes in hydrologic properties of the test region are then measured for controlled boundary conditions due to the presence of the gas phase and as resaturation occurs. The tests could be conducted from a

single hole, or as a dipole test, where two wells intersect the same fracture. Much greater flexibility in test design and control of boundary conditions would exist for the dipole test configuration.

REFERENCES

Almén, K.E., Andersson, J.E., Carlsson, L, Hansson K. and Larsson N.Ä., 1986. Hydraulic testing in crystalline rock. A comparative study of single-hole test methods. SKB Technical Report 86-27, Stockholm.

Andres, J.N., Hussain, N. and Youngman, M.J., 1989. Atmospheric and radiogenic gases in groundwaters from the Stripa granite. Geochemica et Cosmochimica Acta, Vol 53, pp 1831-1841.

Arvidsson, L., Eldraftteknik VU-EP, Vettenfall utveckling, report no. 219-224.94, Project no 34002, March 23, 1994.

Barker, J.A., 1988. A general radial flow model for hydraulic tests in fractured rock. Water Resour. Res, Vol 10, pp 1796-1804.

Carslaw, H.S. and Jaeger, J.C., 1959. Conduction of heat in solids. Oxford University Press, 2nd edition, pp 54 and 257.

Doughty, C., 1995. Personal comminucation. Earth Sciences Division, Lawrence Berkeley Laboratory, Berkeley, California.

Earlougher, R.C., Jr., 1977. Advances in well test analysis. Soc. Pet. Engr. Monograph Series, Vol 5, SPE, Dallas.

Gass et al., (core logging report for KA2512A) (1995).

Geller, J.T., Doughty C., Glass R.J. and Long, J.C.S., 1995. Disturbed zone effects: Two-phase flow, report to the international program under the cooperative - Agreement between SKB and U.S. DOE Radioactive Waste Management (LBL no. _____) (in preparation)

Gentzschein, B., 1993. Frontborre: mätning och handhavande. In: Nyberg, G., Manual för Hydro Monitoring System (HMS), del 1:1. SKB Tekniskt PM nr 25-94-014, Äspölaboratoriet.

Horner, D.R., 1951. Pressure buildup in wells. Proc. Third World Pet. Cong., The Hague, Sect II, pp 503-523.

Jacob, C.E., and Loman, S.W., 1952. Nonsteady flow to a well of constant drawdown in an extensive aquifer. Trans., Am. Geophys. Union, Vol 33, pp 559-569.

Lif, M., Elkraftteknik VU-EP, Vattenfall utveckling, report no. 1113.93, project no. 33116, December 7, 1993.

Long, J.C.S., Olsson, O., Martel, S. and Black, J., 1992. Effects of excavation on water inflow to a drift. Proceedings of the U. S. Rock Mechanics Meeting, Lake Tahoe, CA..

Mishra, S., 1992. Methods for analyzing single- and multi-well hydraulic test data. In: Vomvoris, S. and Frieg, B. (eds), Interpretation of crosshole.hydraulic tests and a pilot fluid logging test for selected boreholes within the BK-site. NAGRA Technical Report 91-09.

Olsson, O., ed, 1992. Site characterization and validation - final report, Stripa Project Technical Report 92-22, Swedish Nuclear Fueld and Waste Management Co., Stockholm, Sweden, 364 pp.

Pedersen, K., 1995. Personal communication.

Rundquist et al., 1995. (drilling report for KA2512A) (1995).

SKB PR 25-94-23, pp 40.

SKB-TR 90-05 (get complete reference)

Theis, C.V., 1935. The relation between the lowering of the piezometric surface and the rate and duration of discharge of a well using ground-water storage. Am. Geophys. Union Trans. 16, pp 519-524.

APPENDIX I

Estimation of gas contents and bubble pressure

Henry's Law describes the equilibrium of a species between the gas and liquid phases as follows:

$$P_g = Hx_g$$

where P_g is the partial pressure (absolute) of species g in the gas phase, H is Henry's Law constant, and x_g is the mole fraction of species g in the liquid phase.

At Stripa, gas bubbles were observed in the borehole after the pressure was decreased from 800 to 270 kPa(abs). Assuming nitrogen is the main component of the gas and H equals 6.77 x 10^6 kPa (mole fraction)$^{-1}$ at 10°C, Henry's Law predicts a gas contents of 3.4 to 5.9% v/v STP if the gas evolves at 270 to 400 kPa(abs) respectively. Measurements of dissolved gas concentrations reported by Andrews et al. (1989) ranged from 3.0 to 4.4%. Most of the gas is nitrogen and the $^{15}N/^{14}N$ ratio indicates that it is of atmospheric origin. Dissolved nitrogen concentrations of atmospheric origin in groundwater can be higher than surface water equilibrated with the atmosphere because of the dissolution of residual air in the formation at higher pressures. Andrews et al. (1989) did not report any values for CO_2, O_2 or CH_4.

At HRL, Pedersen (1993) reports a value of 3.8% gas contents in borehole KA2598A; 74% of the gas was N_2, 12% was CO_2, 4% was H_2+He, 2% was O_2, 0.3% was CH_4 and the rest unidentified. Gas contents measured in surface boreholes at depths of 200 to 400m range from 3.9 to 5.4% (SKB-TR-90-5), where N_2 is the major component of the gas. The estimates of the bubble pressure of the dissolved gas in KA2512A are bracketed for gas contents of 3.5 to 5% using Henry's Law constants for nitrogen in both pure water and water with 15% chlorinity. The values are summarized in Table I-1 :

Table I- 1. Estimate of bubble pressure in borehole KA2512A

Percent Chlorinity	*H* (kPa/mole fraction, 10°C)	Bubble Pressure (kPa, abs) 3.5% gas v/v STP	5.0% gas v/v STP
0	6.77×10^6	292	373
15	8.14×10^6	330	428

APPENDIX II

Table II-1. Record of blasting activities during pilot hole test

Date	Time	Tunnel Length (m)	Comments
11/30/94	11:14	3370	niche, 4 m
11/30/94	14:30	3370	ceiling
11/30/94	20:05	3370	niche, ~4 m
12/01/94	10:43	3370	niche, ~3 m
12/05/94	16:30	3450/3490	floor
12/05/94	19:45	3450/3490	reblast
12/06/94	11:17	3503/3505	broadening
12/06/94	19:55	3503/3505	broadening
12/07/94	14:05	3503/3505	broadening
12/08/94	16:15	3503/3505	broadening
12/12/94	12:38	?	?
12/13/94	19:53	3500	left niche
12/14/94	15:13	3500	left niche

Appendix II

Table II-1 (cont'd)

ÄSPÖ - HRL, Sprängsalvor 9 jan. - 6 febr. 1995

no head data	950109	09:40	salva #215	
	950110	12:52	" #216	
	950110	21:25	" B2	Bomsalva
	950111	13:11	" B2	Omskjutning
	950112	01:35	" Z1	Z = ZEDEX
	950112	12:54	" #218	
	950112	13:03	" Z1	Omskjutning
	950112	23:40	" Z2	
	950113	12:25	" #219	
	950113	12:19	" Z2	Omskjutning
	950114	01:55	" Z3	
	950115	22:00	" Z4	
	950116	11:55	" Z4	Omskjutning
	950116	13:15	" #220	
	950116	21:50	" Z5	
	950117	10:05	" #221	
	950117	19:48	" #222	
	950117	19:52	" Z6	
	950118	10:45	" #223	
	950118	12:15	" Z6	Omskjutning
Start in	950118	20:18	" #224	
	950119	10:19	" #225	
	950120	08:30	" #226	
	950123	11:16	" #227	
	950124	10:48	" #228	
	950124	20:30	" #229	
	950125	11:09	" #230	
	950125	20:50	" #231	
	950126	09:45	" #226	
	950126	19:50	" #233	
	950126	21:03	" Z7	
	950127	10:50	" #234	
	950127	22:20	" Z8	
	950128	10:30	" Z8	Omskjutning
	950128	23:10	" Z9	
	950130	17:36	" #235	
	950201	12:15	" #236	
	950201	16:00	" #237	Trappschakt
	950201	22:00	" #238	"
	950202	07:30	" #239	"
	950202	10:10	" #240	"
	950202	13:20	" #241	"
	950202	17:00	" #242	
	950204	15:03	" #243	
	950205	15:10	" #244	
	950206	09:00	" #245	

Z* = Sprängningar i "ZEDEX - tunneln"

bgz/950214

Figures

TEST SEQUENCE: Phases (1) - (3)

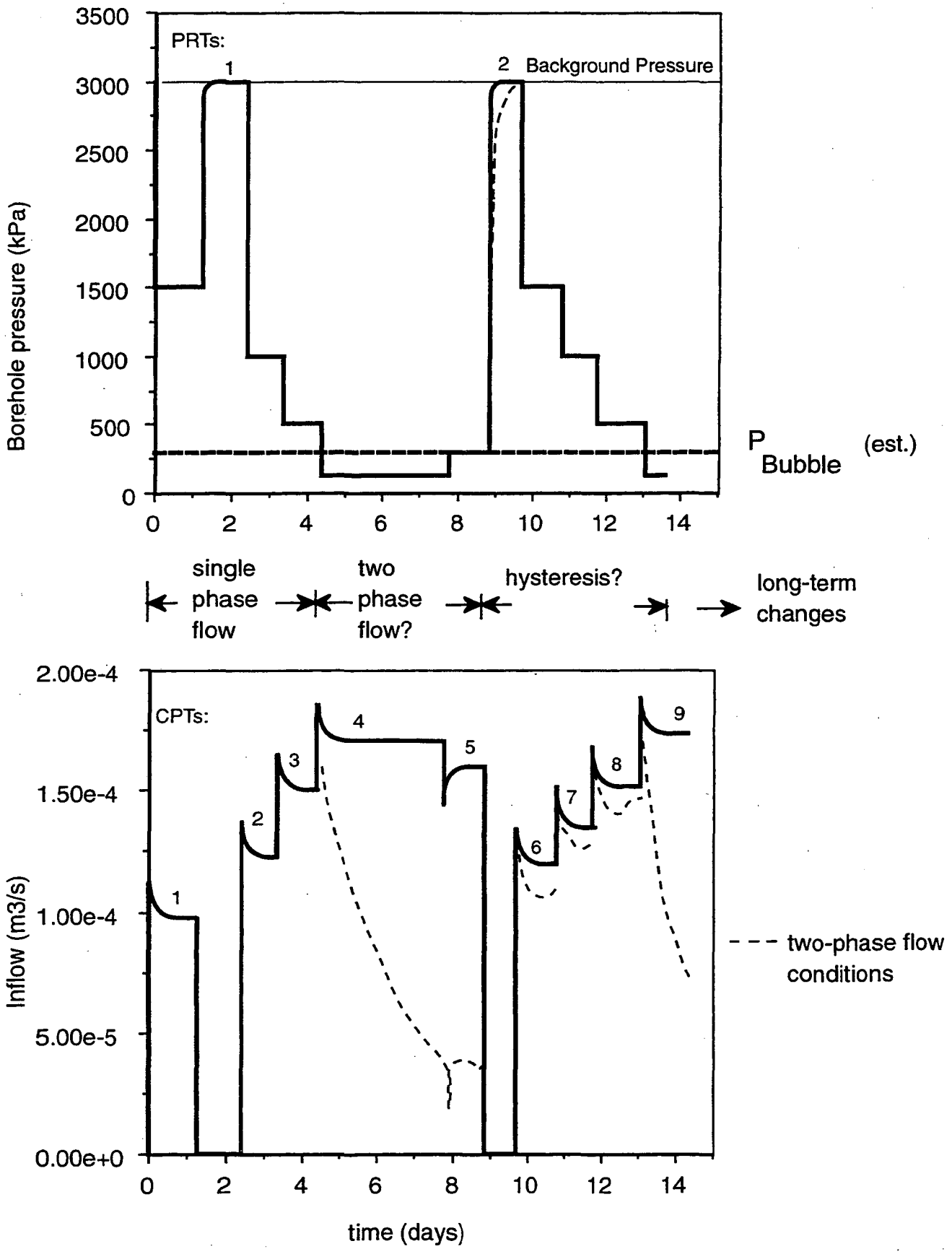

TEST SEQUENCE: Phase (4)

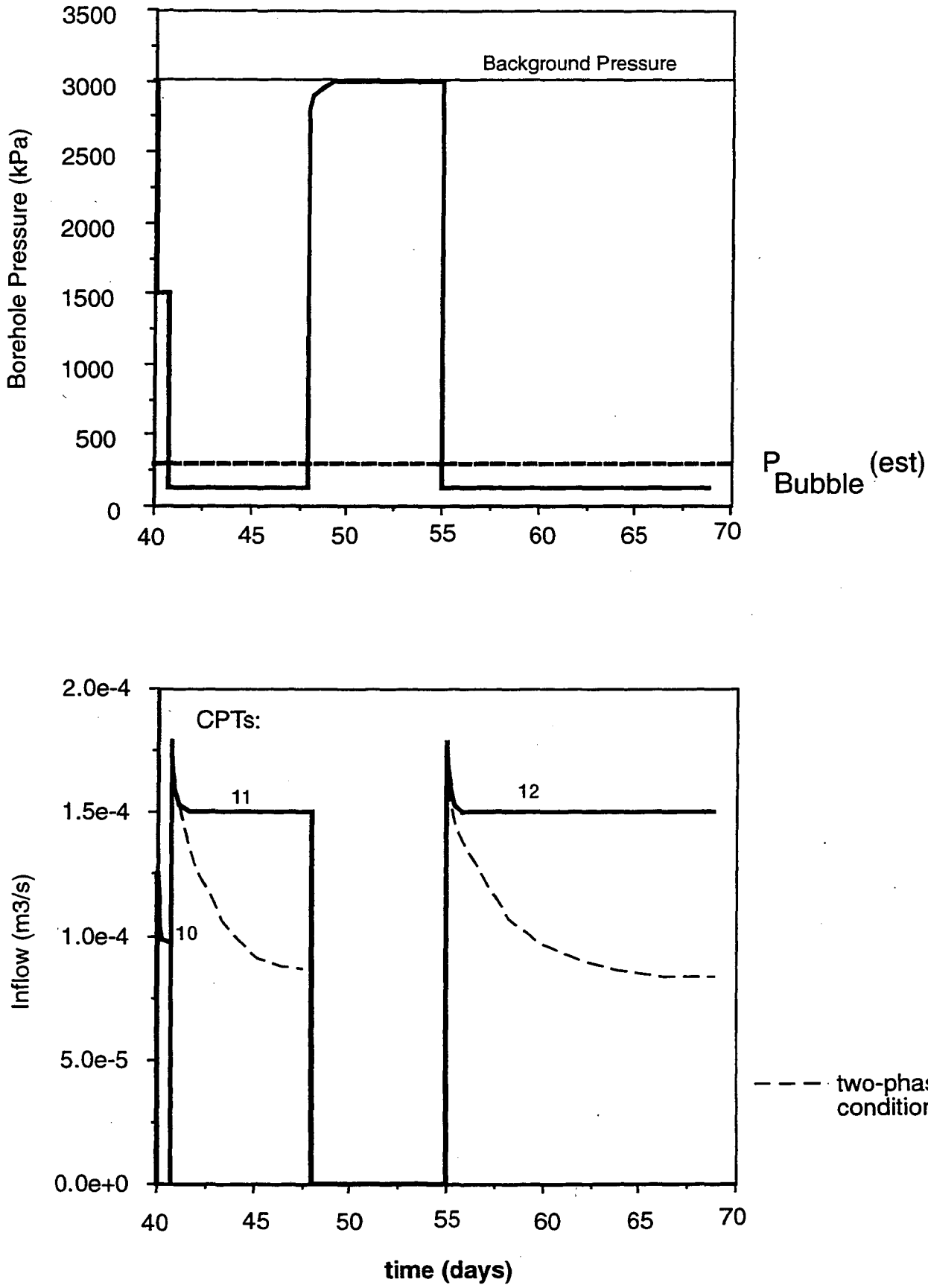

Fig 2-1 b

Äspö Hard Rock Laboratory - 300-460 m level

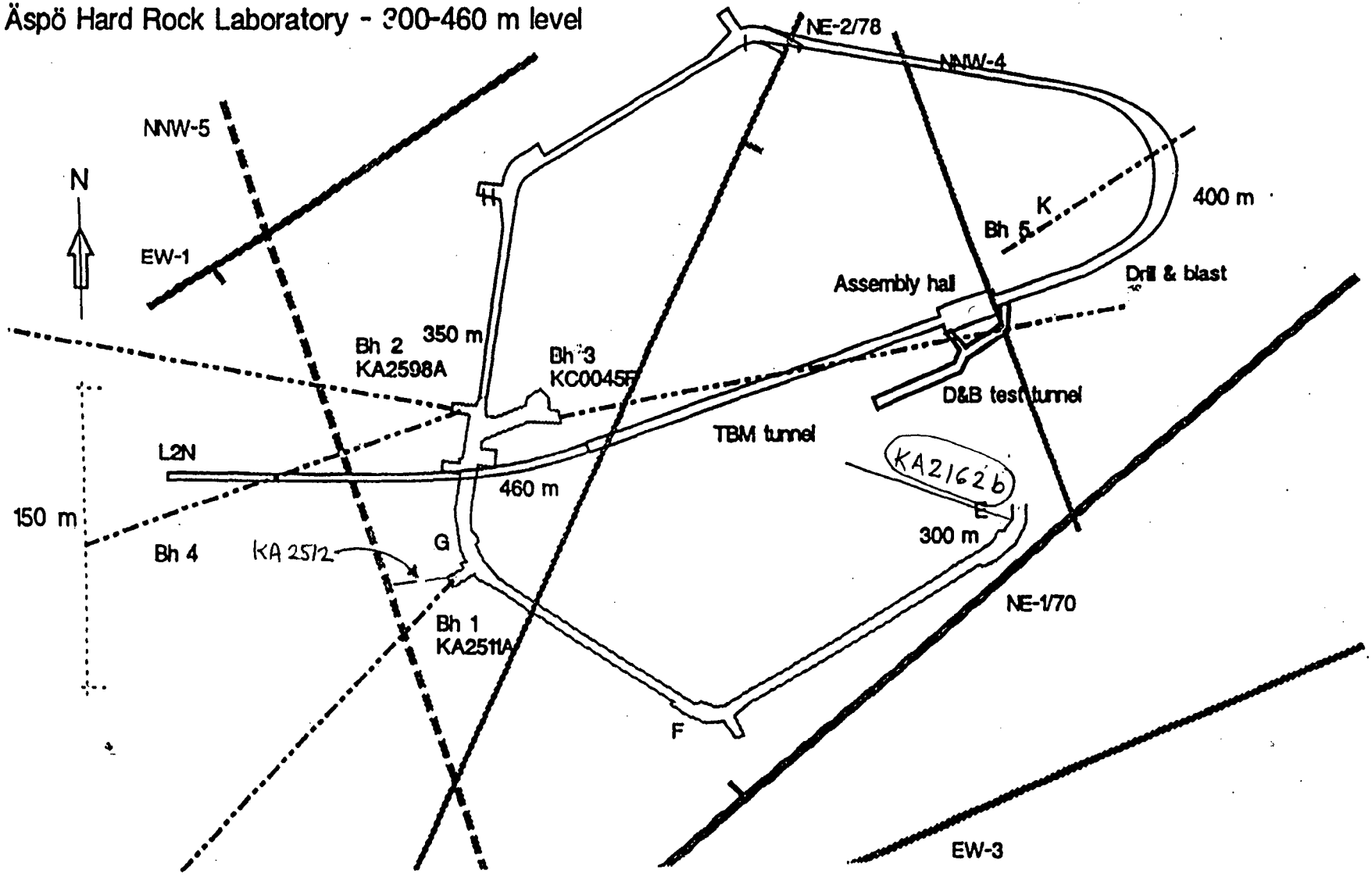

Fig 2-2

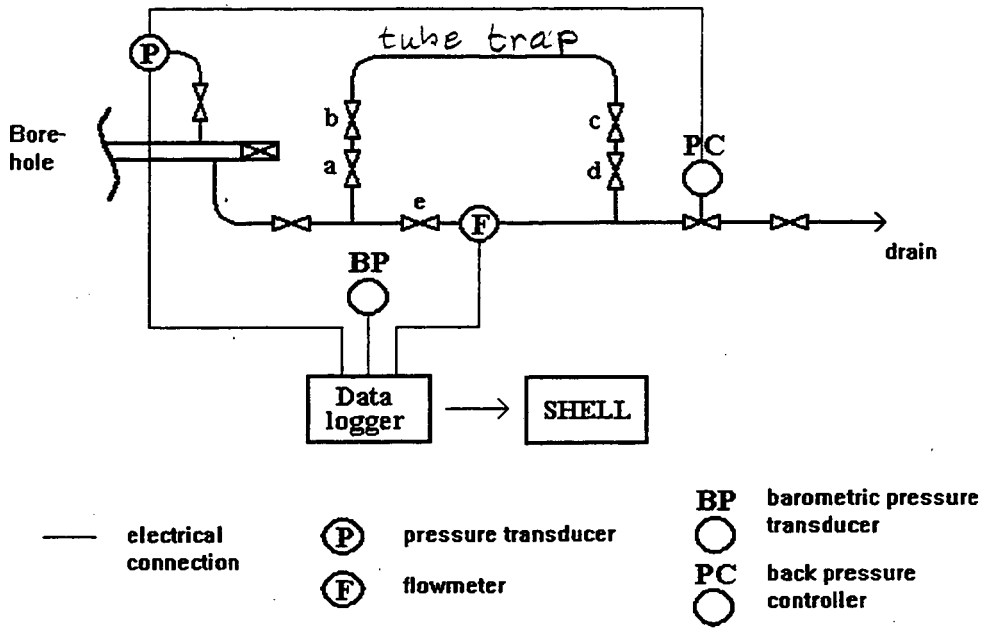
tube trap
P
Bore-
hole
b
a
c
d
e
F
PC
drain
BP
Data
logger
SHELL
electrical
connection
pressure transducer
flowmeter
BP
barometric pressure
transducer
PC
back pressure
controller

Fig 2-3

Glass Accumulator for Measurement of Volumetric Gas Contents

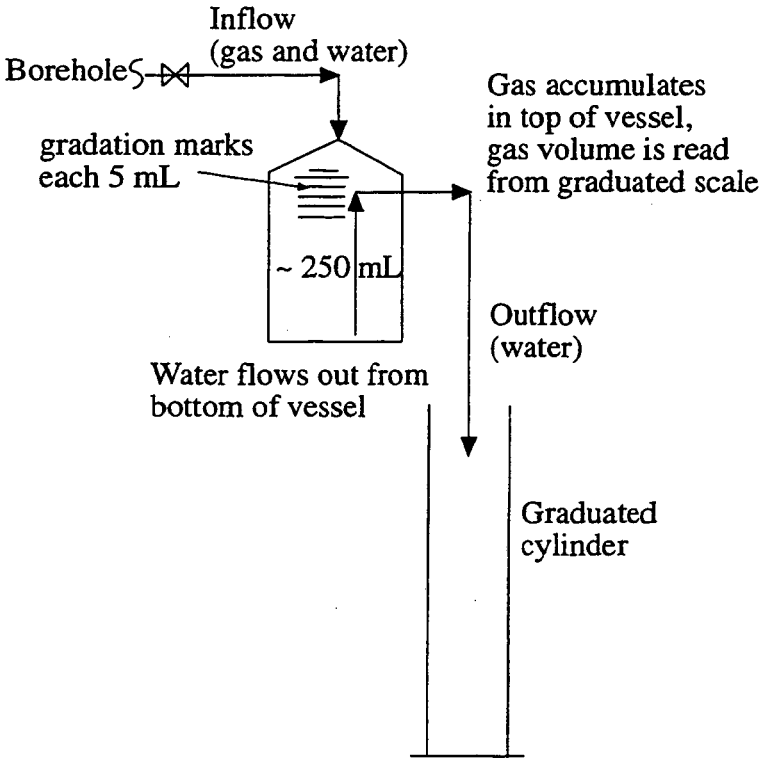

Fig 2-4

Tube Trap for Measurement of Volumetric Gas Contents

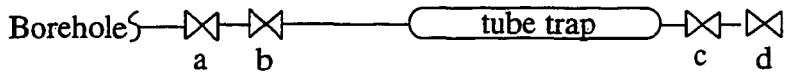

a. Tube trap installation

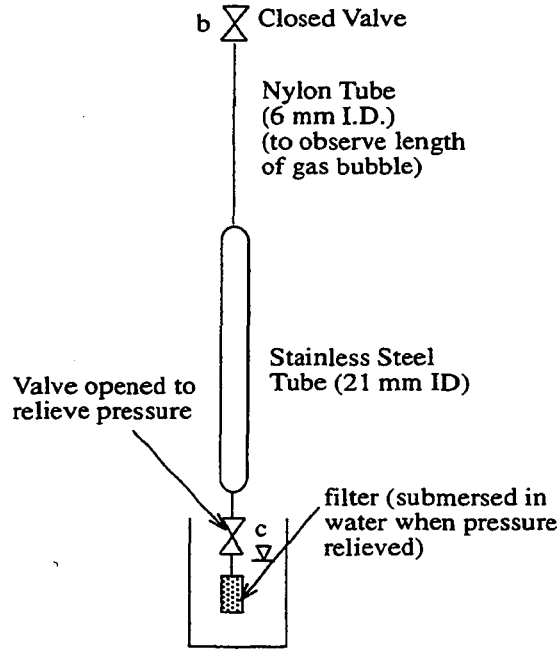

b ~~c~~. Orientation to relieve pressure and measure evolved gas

Fig 2-5

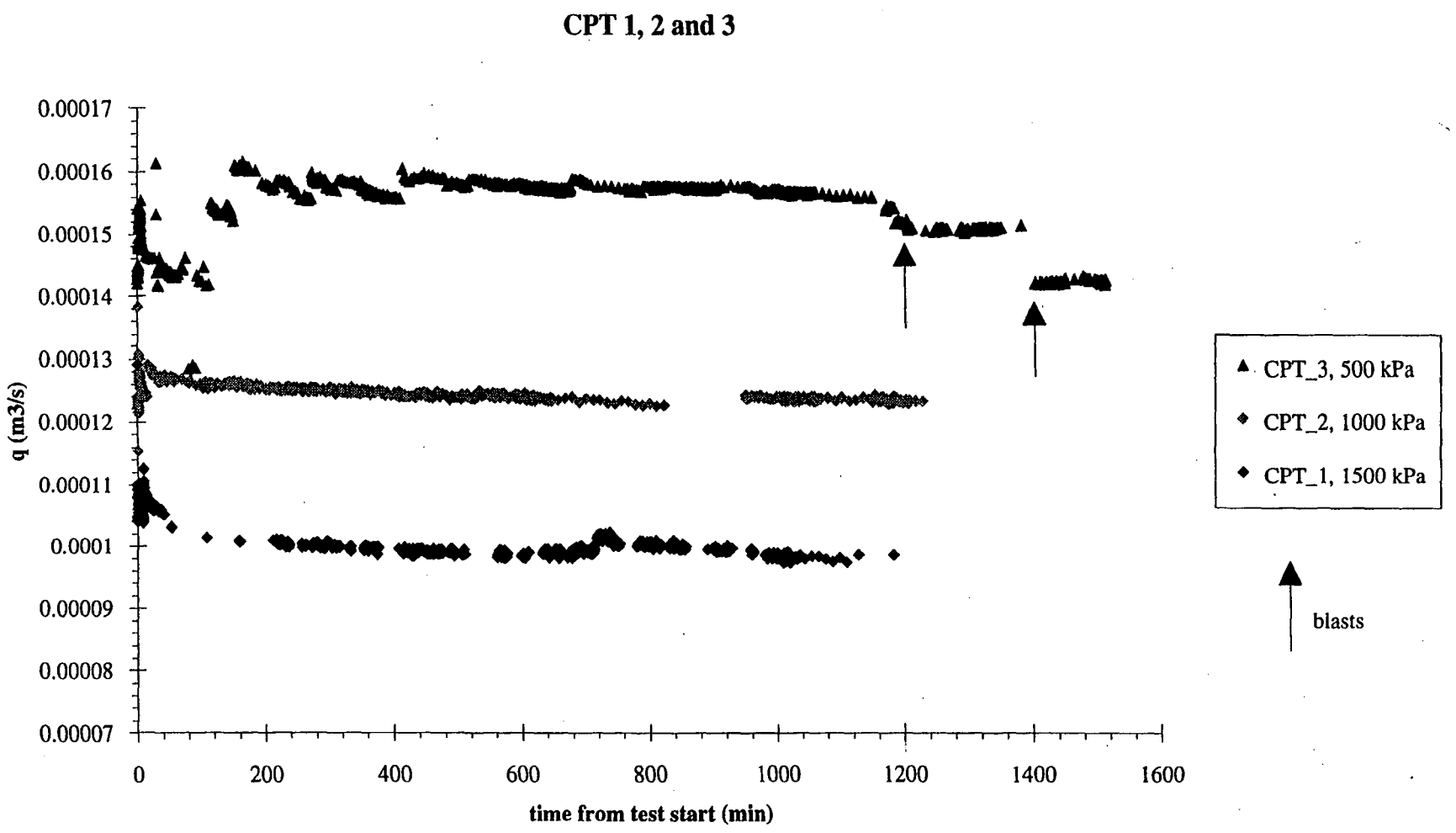
CPT 1, 2 and 3
0.00017
0.00016
0.00015
0.00014
0.00013
0.00012
0.00011
0.0001
0.00009
0.00008
0.00007
q (m3/s)
0
200
400
600
800
1000
1200
1400
1600
time from test start (min)
CPT_3, 500 kPa
CPT_2, 1000 kPa
CPT_1, 1500 kPa
blasts

Fig 3-1

Fig 3-2

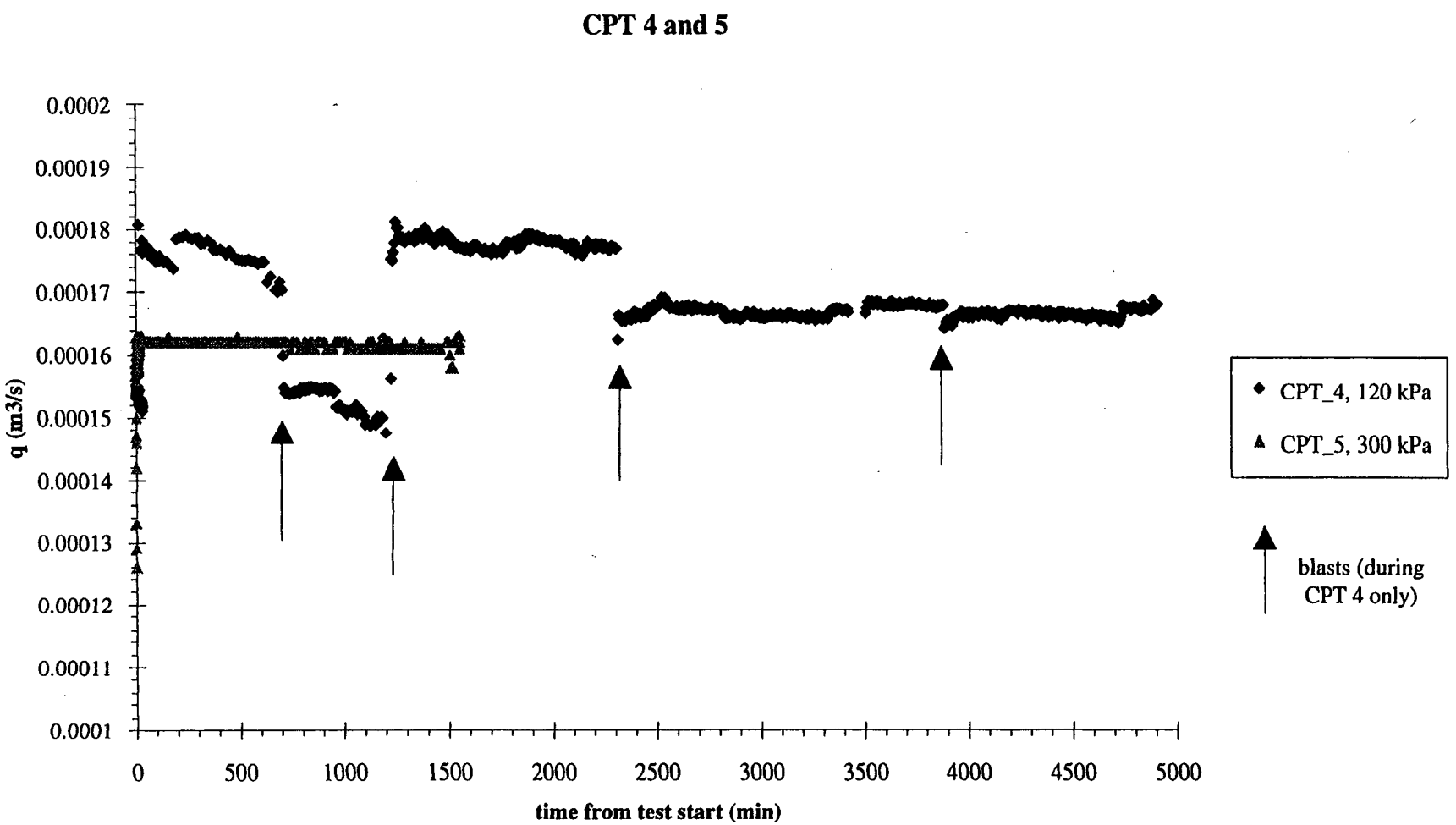
CPT 4 and 5
0.0002
0.00019
0.00018
0.00017
0.00016
0.00015
0.00014
0.00013
0.00012
0.00011
0.0001
q (m3/s)
0
500
1000
1500
2000
2500
3000
3500
4000
4500
5000
time from test start (min)
CPT_4, 120 kPa
CPT_5, 300 kPa
blasts (during CPT 4 only)

Fig 3-2

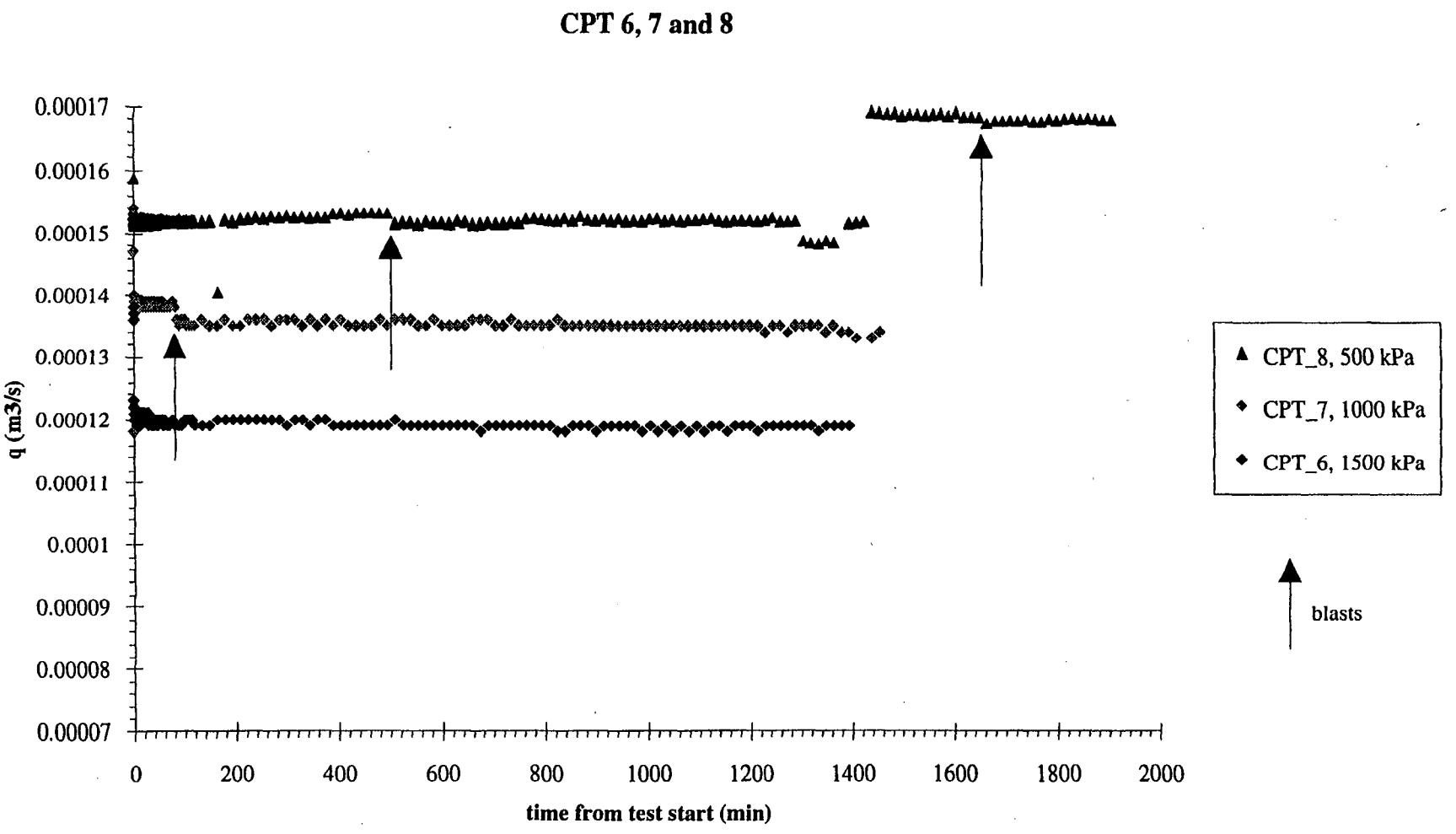
CPT 6, 7 and 8
0.00017
0.00016
0.00015
0.00014
0.00013
0.00012
0.00011
0.0001
0.00009
0.00008
0.00007
q (m3/s)
0
200
400
600
800
1000
1200
1400
1600
1800
2000
time from test start (min)
CPT_8, 500 kPa
CPT_7, 1000 kPa
CPT_6, 1500 kPa
blasts

Fig 3-3

Fig 3-4

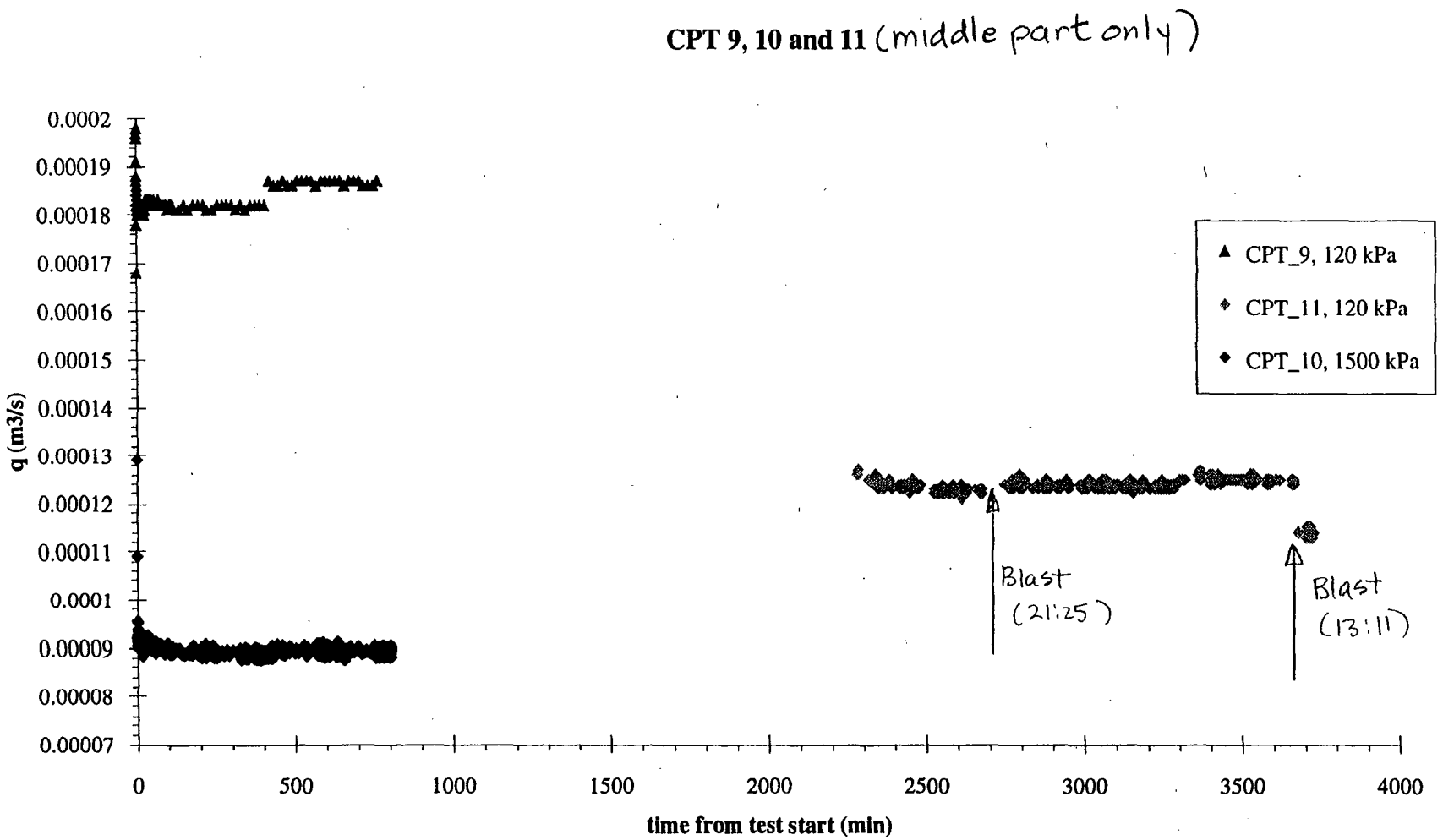
CPT 9, 10 and 11 (middle part only)
0.0002
0.00019
0.00018
0.00017
0.00016
0.00015
0.00014
0.00013
0.00012
0.00011
0.0001
0.00009
0.00008
0.00007
q (m3/s)
0
500
1000
1500
2000
2500
3000
3500
4000
time from test start (min)
CPT_9, 120 kPa
CPT_11, 120 kPa
CPT_10, 1500 kPa
Blast (21:25)
Blast (13:11)

Fig 3-4

CPT – 11

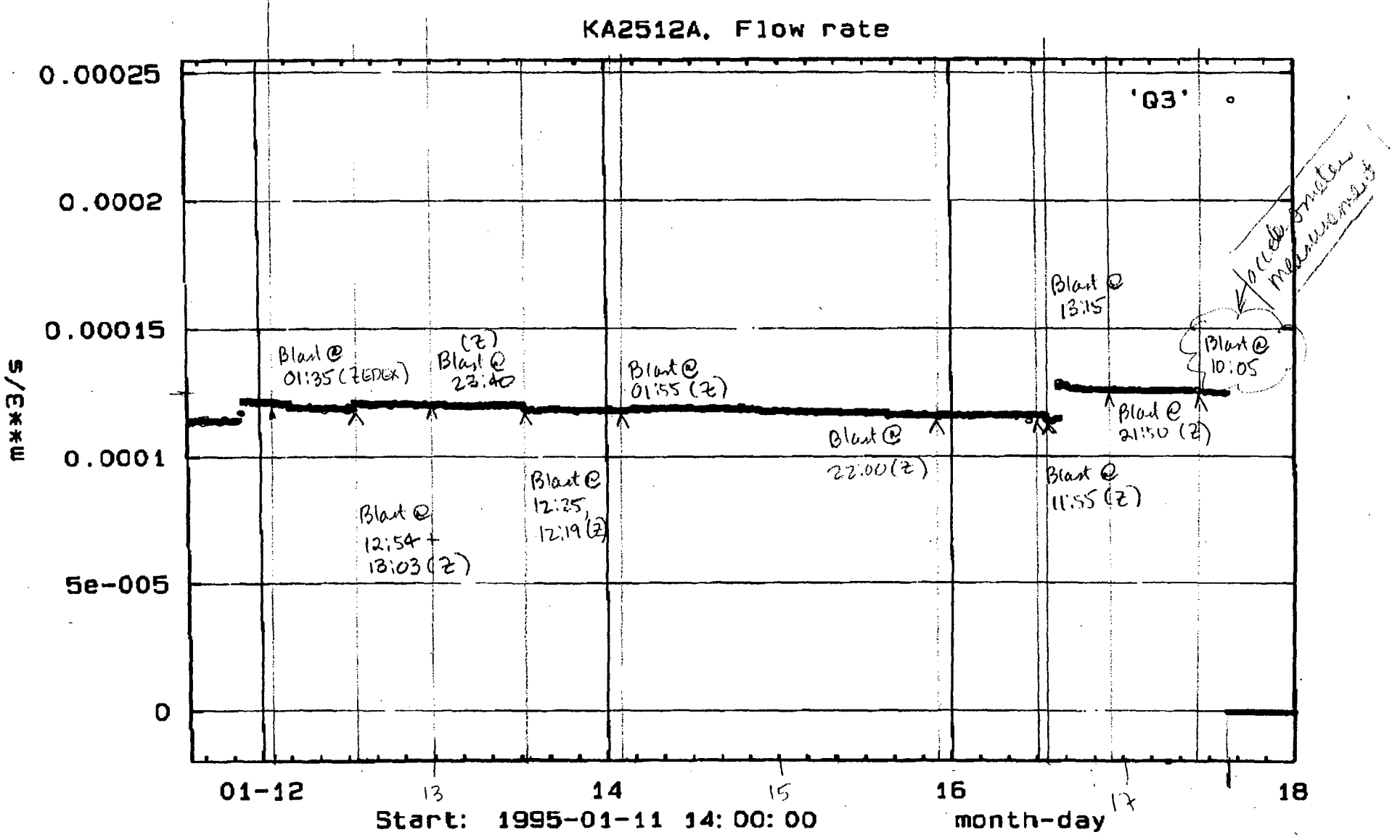

Fig 3-4a

Fig 3-4a

CPT-12

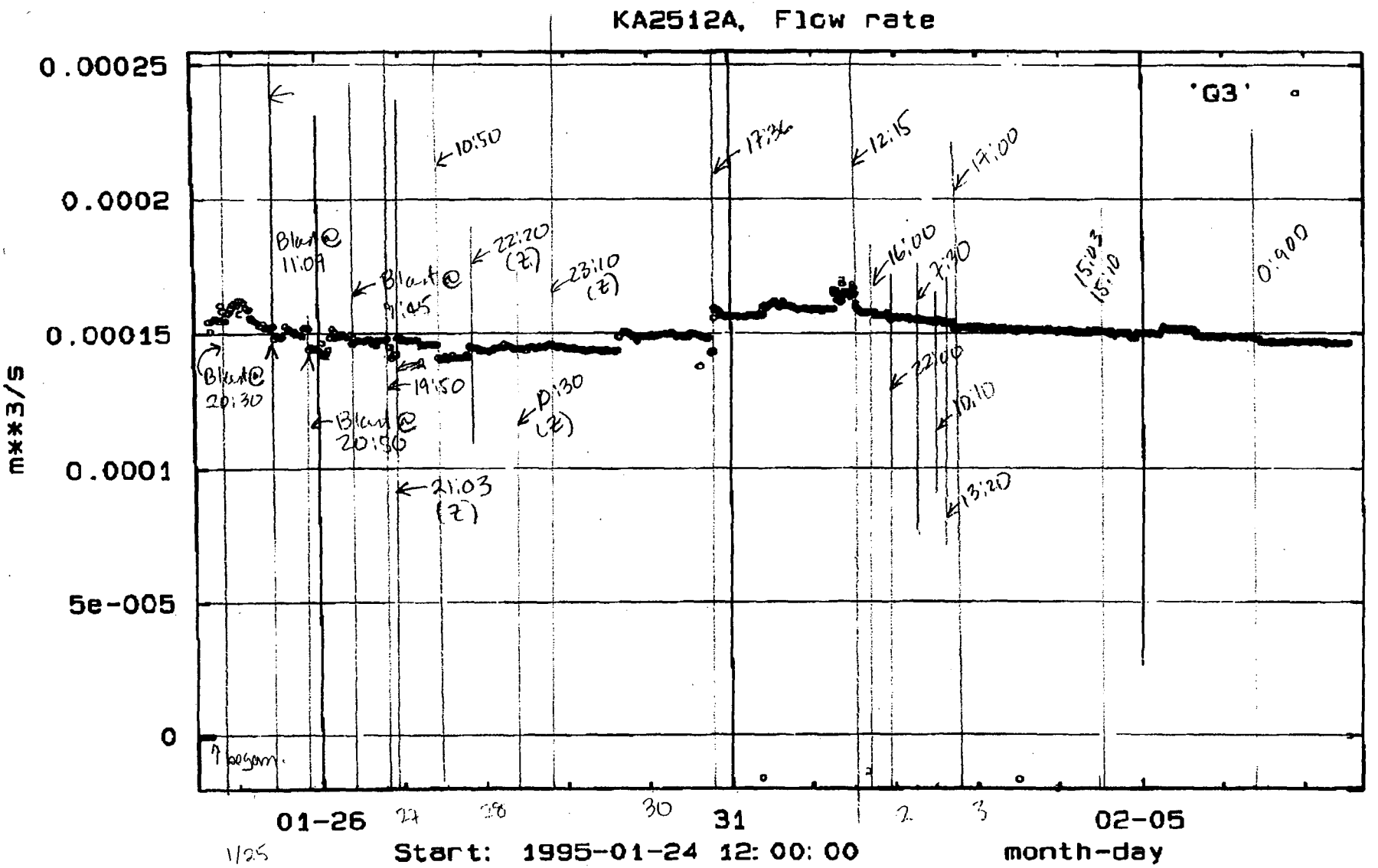

Fig 3-4 b

Fig 3-4 b

15-FEB. 95(ONS) 19:24 ASPOLA TEL:0407431 06000

Fig 3-4c

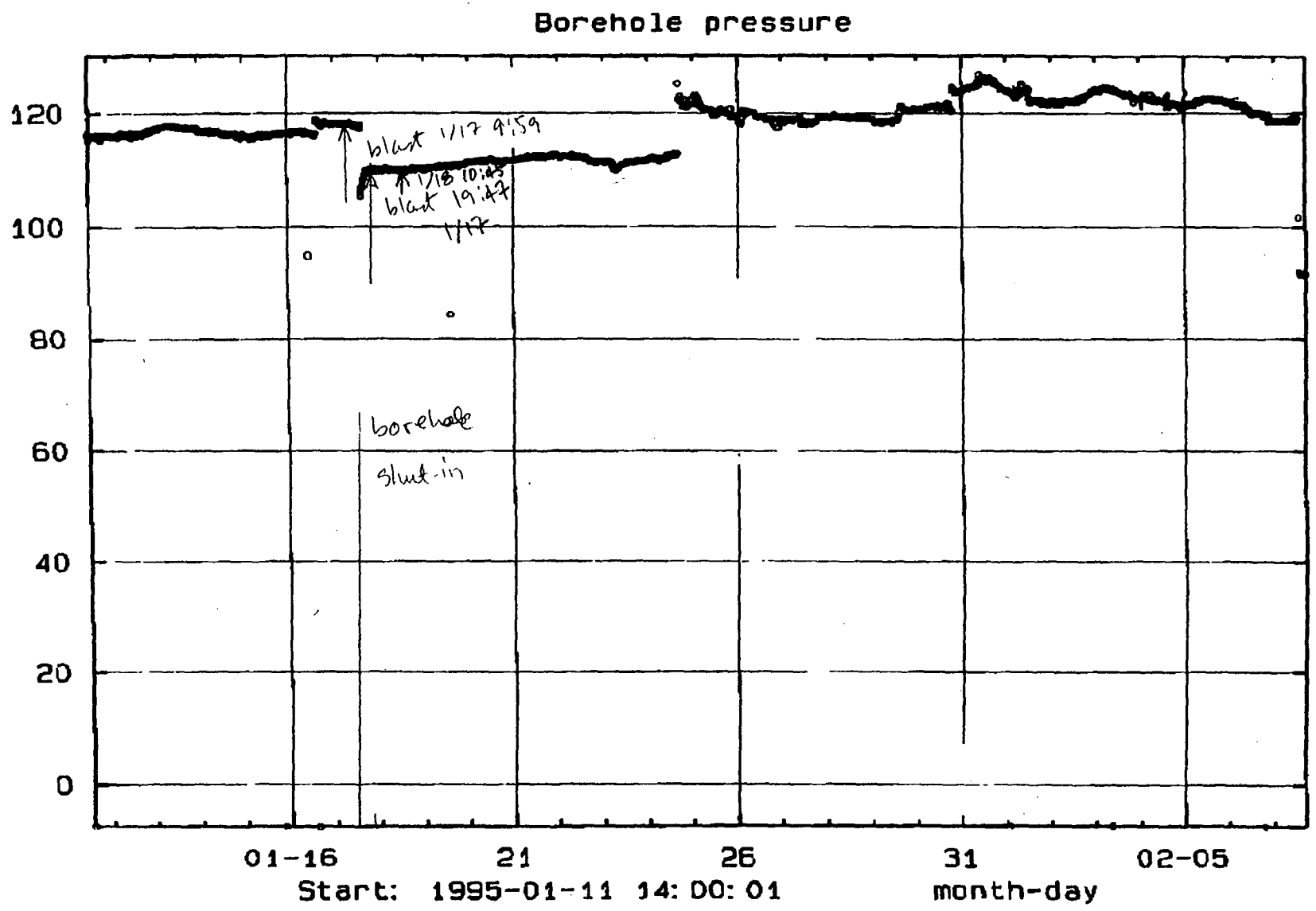

Fig 3-4c

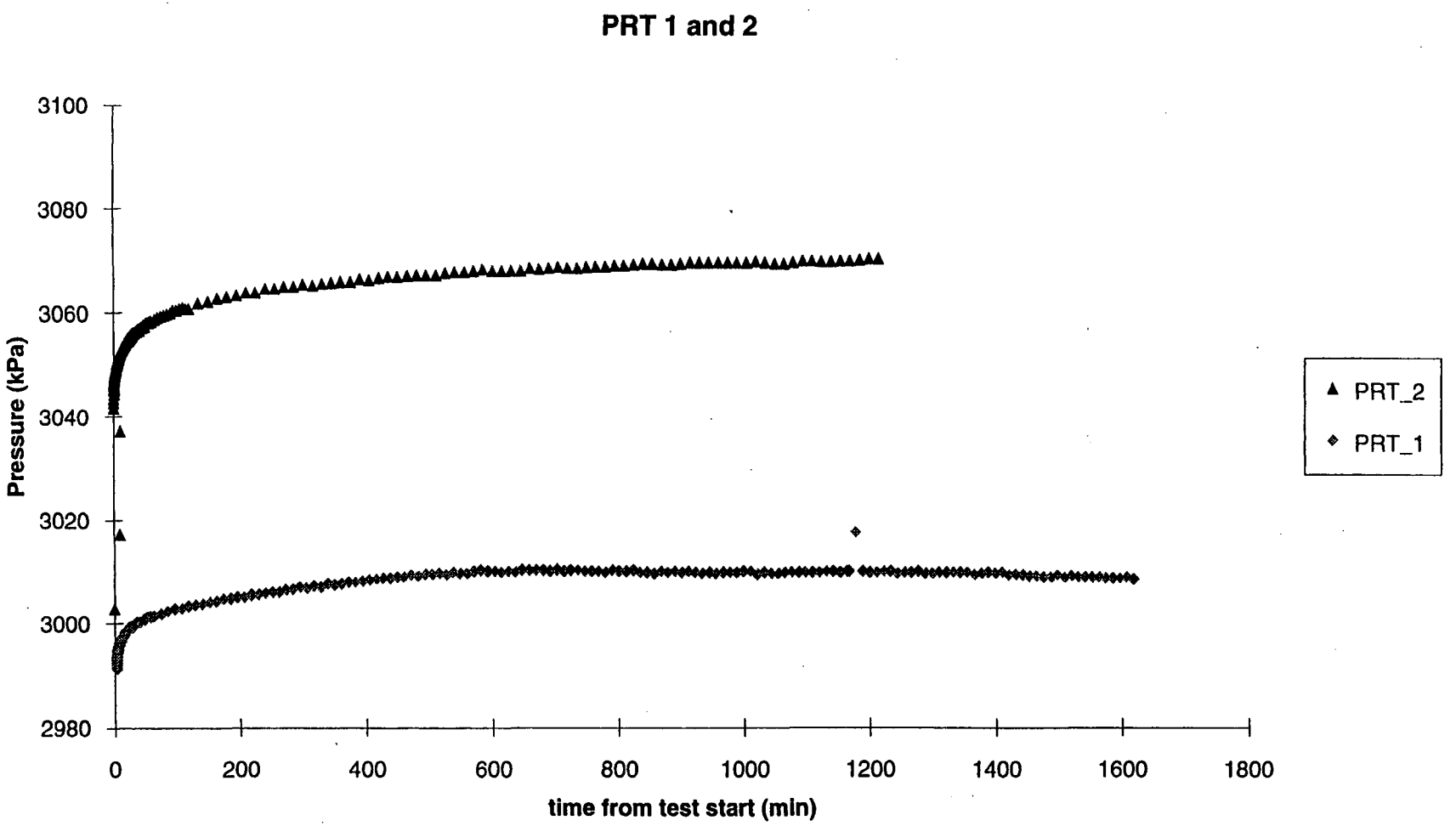
PRT 1 and 2
Pressure (kPa)
3100
3080
3060
3040
3020
3000
2980
0
200
400
600
800
1000
1200
1400
1600
1800
time from test start (min)
PRT_2
PRT_1

Fig 3-5

Fig 3-5

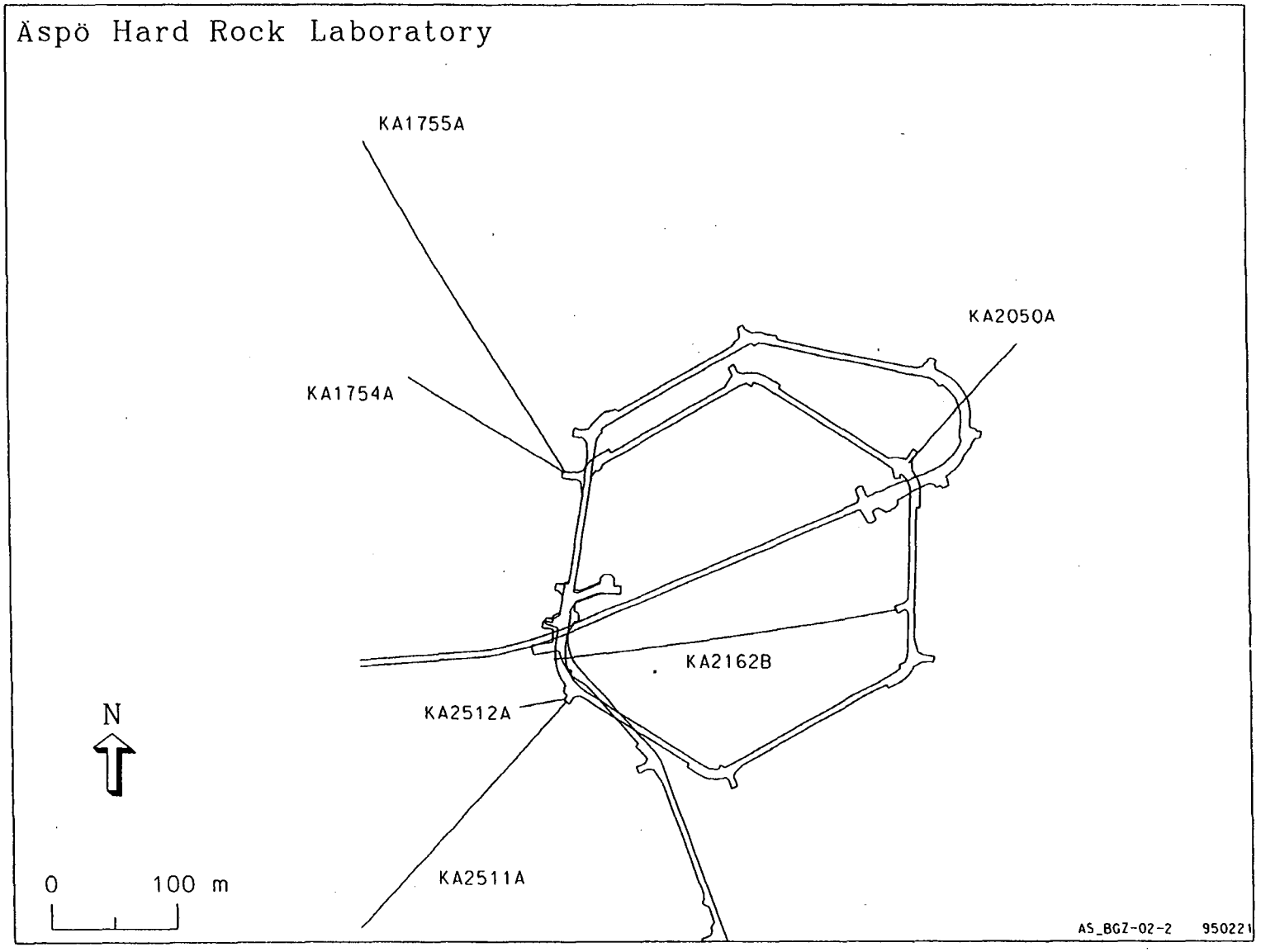

Fig 3-6a

Fig 3-6a

Äspö Hard Rock Laboratory

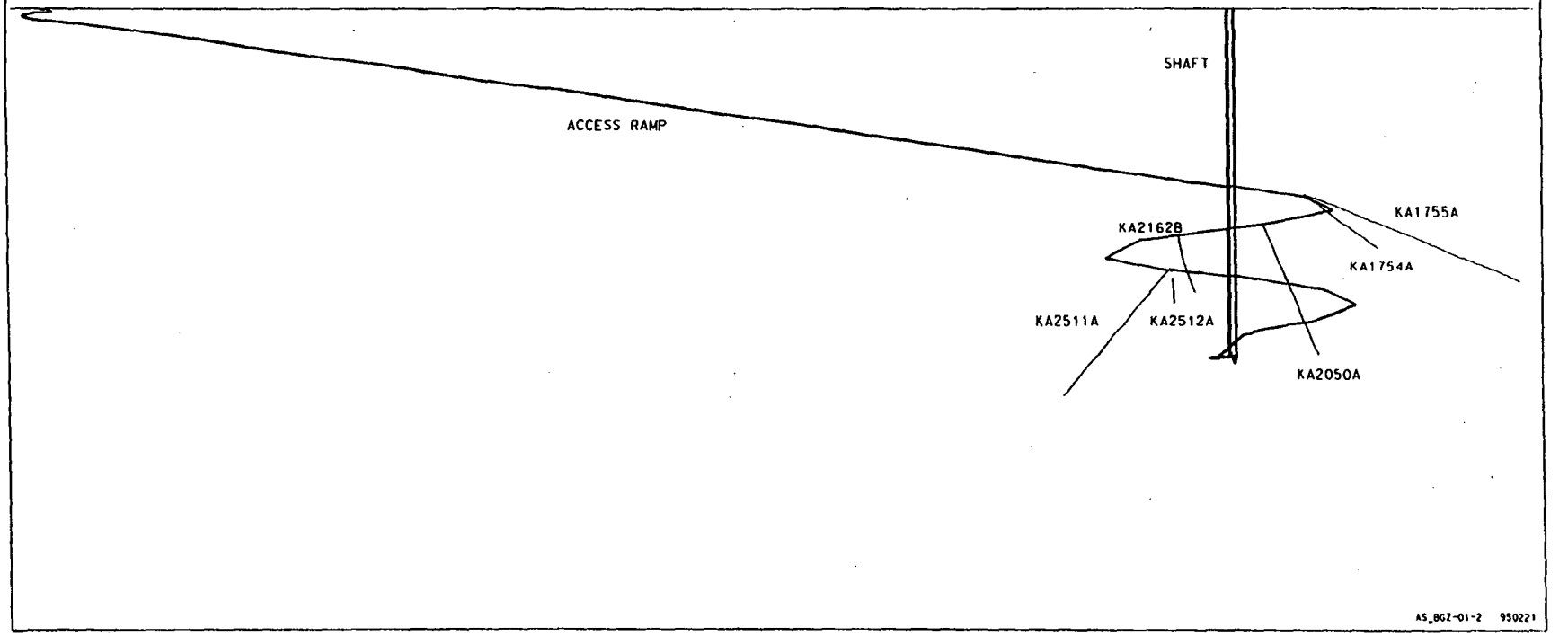

Fig 3-6b

Fig 3-6b.

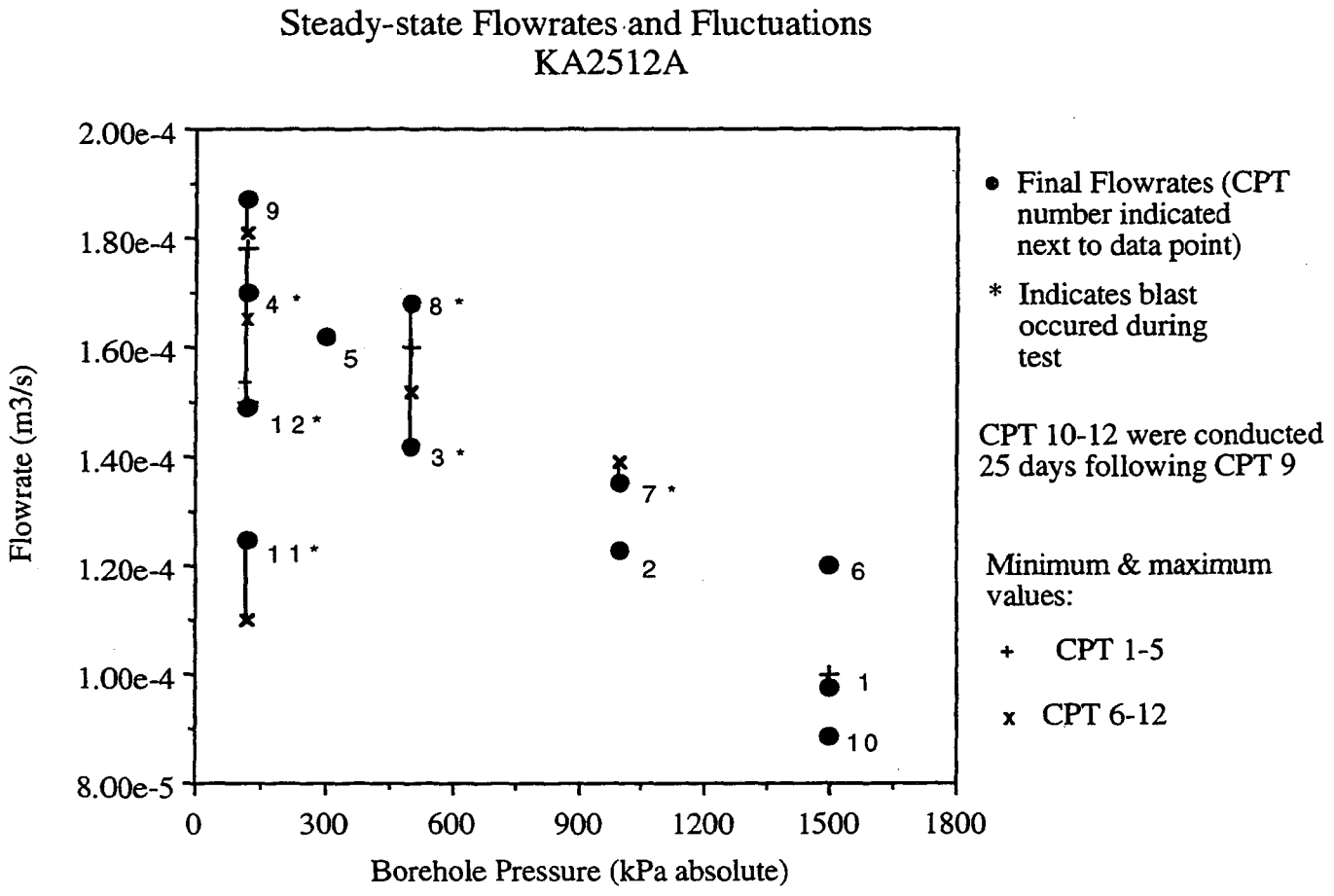
Steady-state Flowrates and Fluctuations
KA2512A
Flowrate (m3/s)
2.00e-4
1.80e-4
1.60e-4
1.40e-4
1.20e-4
1.00e-4
8.00e-5
0
300
600
900
1200
1500
1800
Borehole Pressure (kPa absolute)
9
4 *
5
8 *
1 2 *
3 *
7 *
1 1 *
2
6
1
1 0
• Final Flowrates (CPT number indicated next to data point)
* Indicates blast occured during test
CPT 10-12 were conducted 25 days following CPT 9
Minimum & maximum values:
+ CPT 1-5
x CPT 6-12

Figure 3-7

Fig 3-8

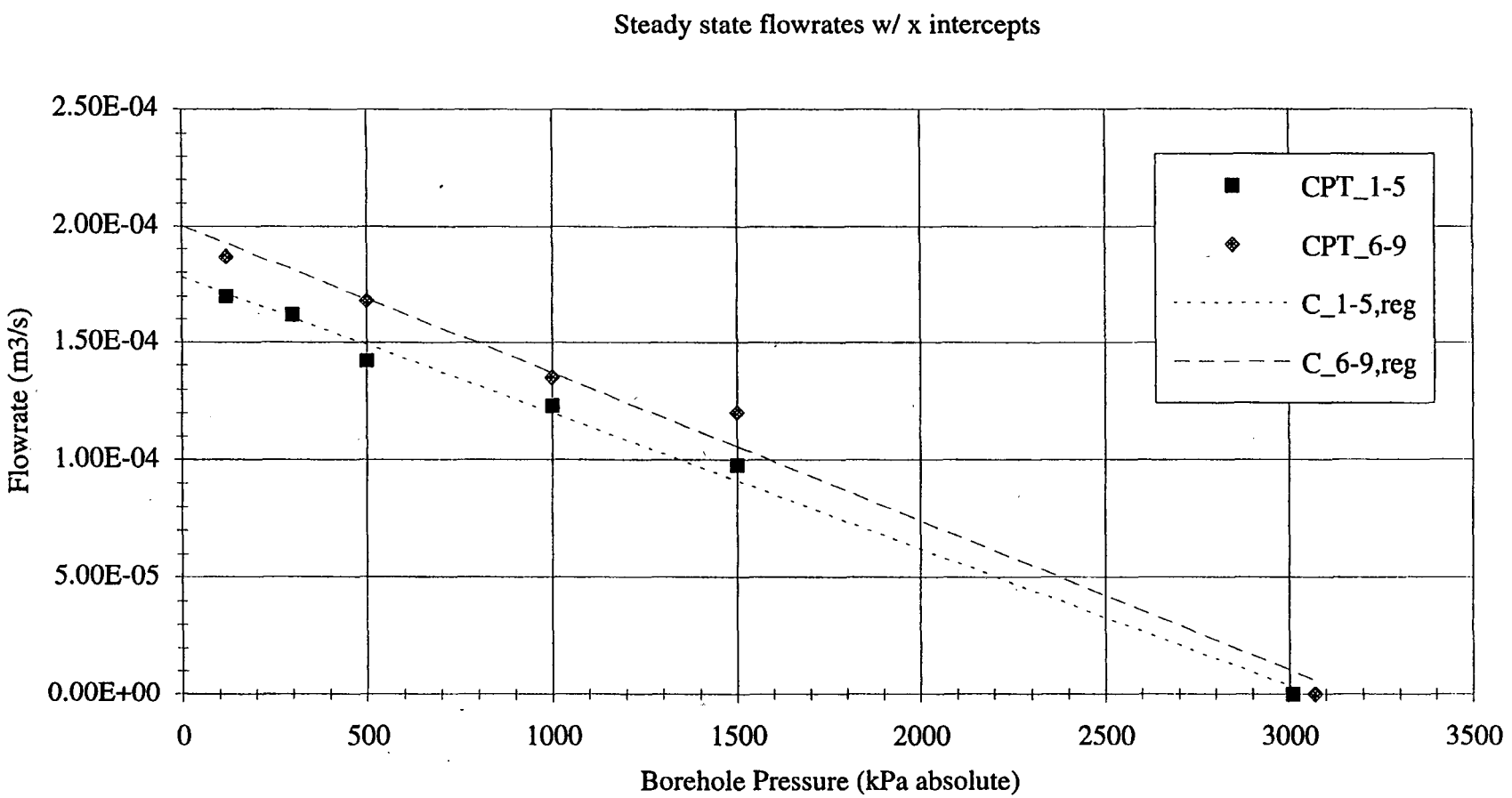

Figure 3-8

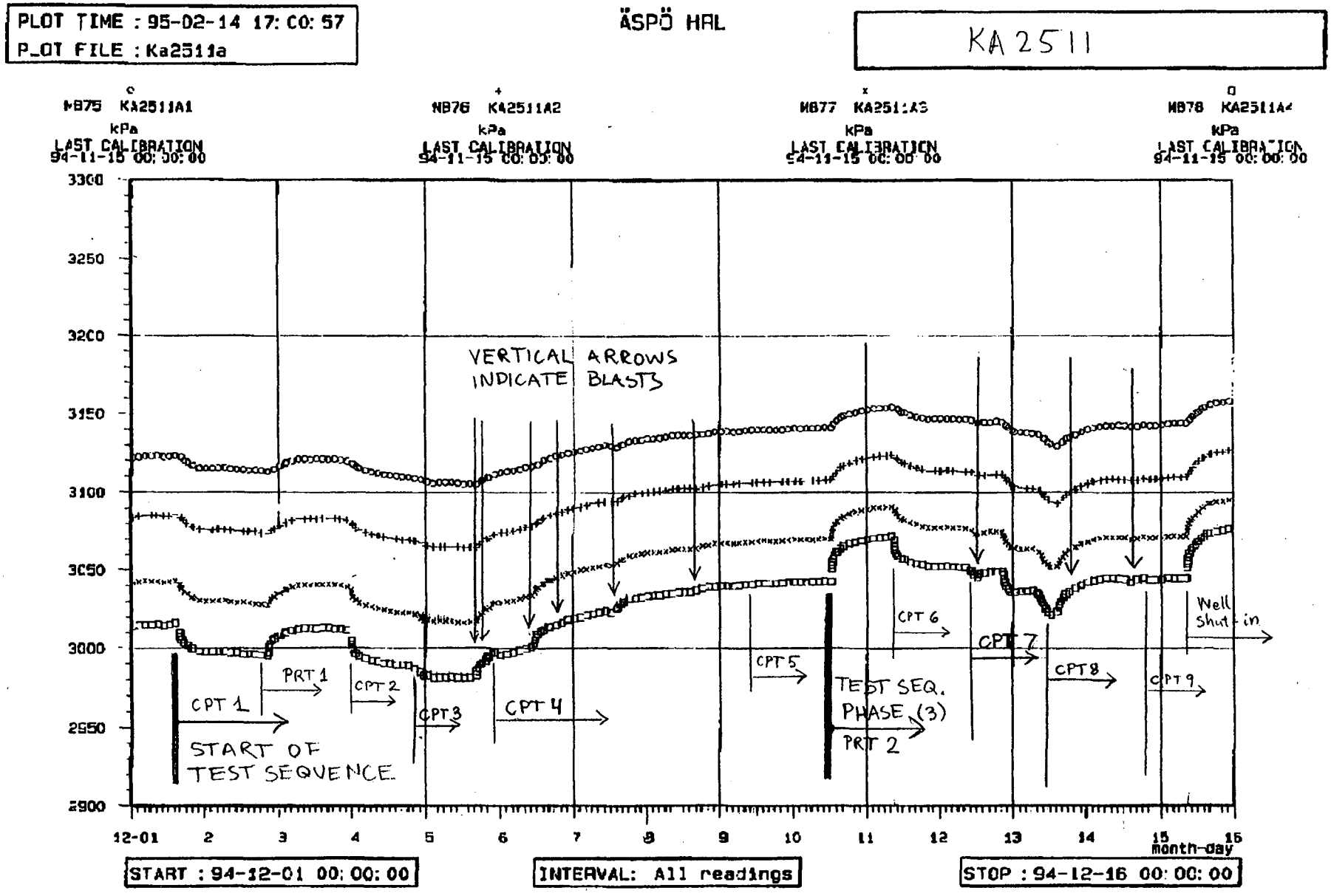

Fig 3-9

Figure 3-9

PLOT TIME : 95-02-14 17:03:33
PLOT FILE : Ka2162b

ÄSPÖ HRL

KA 2162B

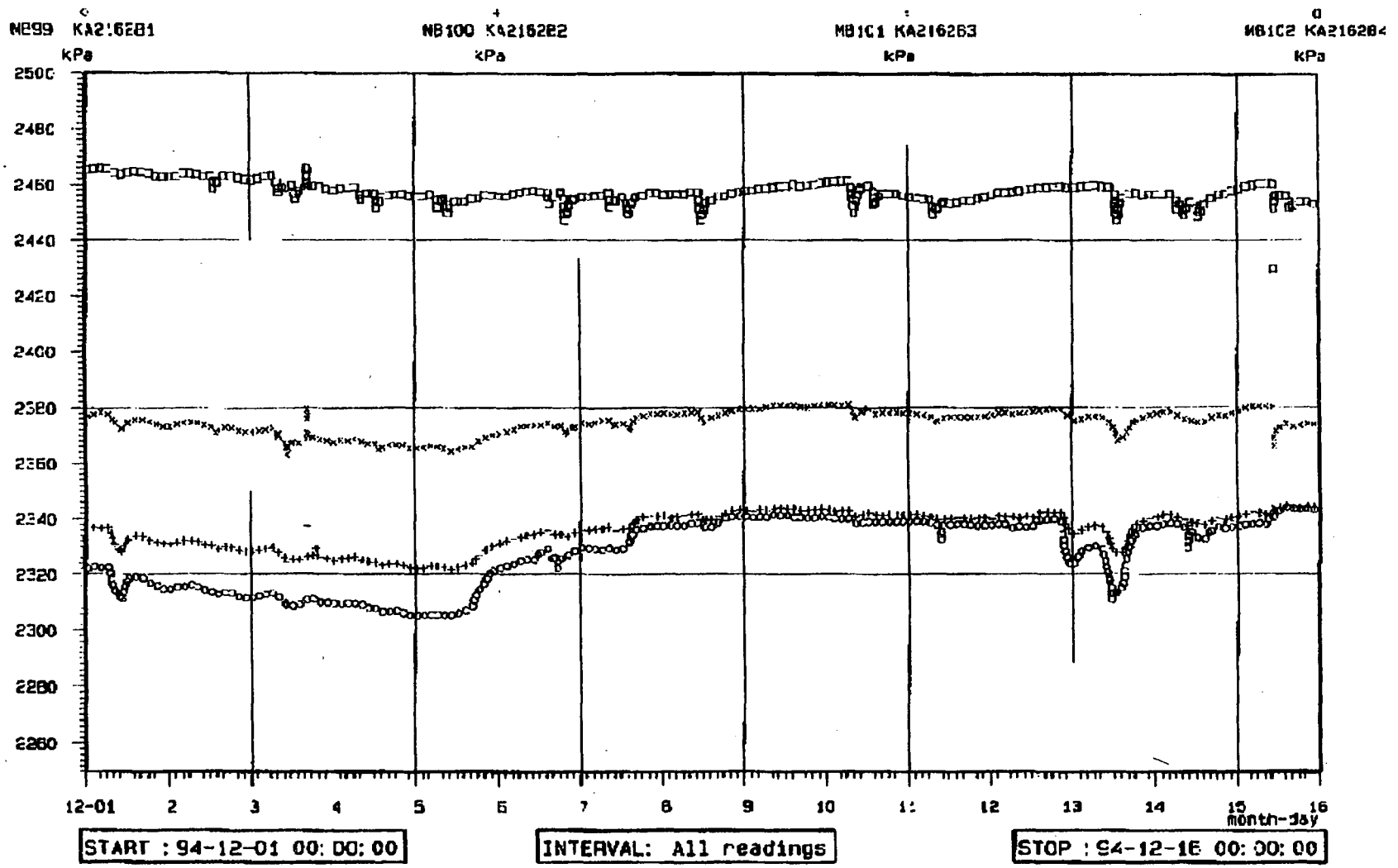

Fig 3-10

Figure 3-10

PLOT TIME : 95-02-14 17: 15: 41
PLOT FILE : Ka1754a

ÄSPÖ HRL

KA1754A

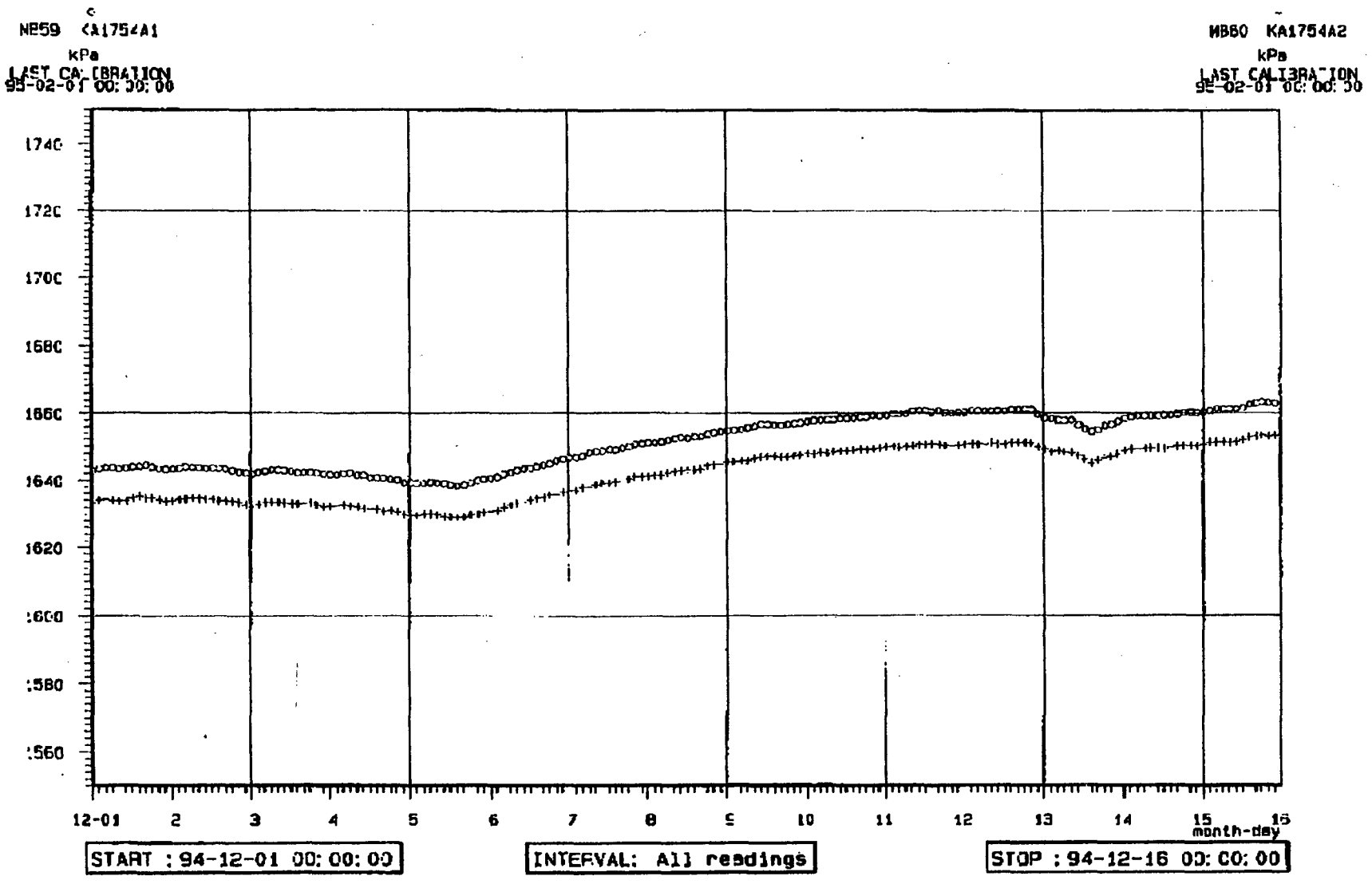

START : 94-12-01 00: 00: 00

INTERVAL: All readings

STOP : 94-12-16 00: 00: 00

Figure 3-11

Fig 3-11

PLOT TIME : 95-02-14 :7: 35: 33
PLOT FILE : Has13

ÄSPÖ HRL

Has 13

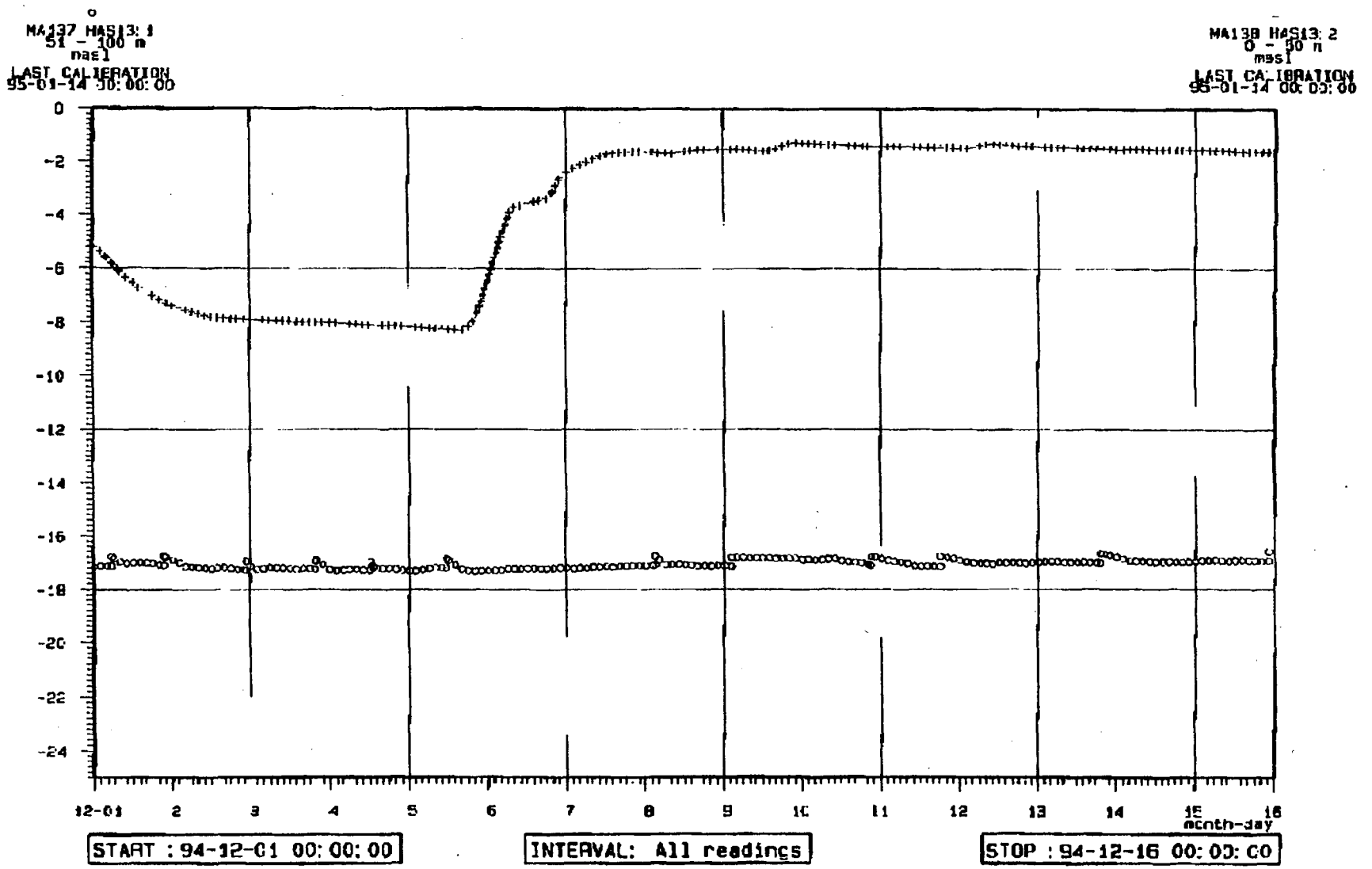

START : 94-12-01 00: 00: 00

INTERVAL: All readings

STOP : 94-12-16 00: 00: 00

Fig 3-12

Figure 3-12

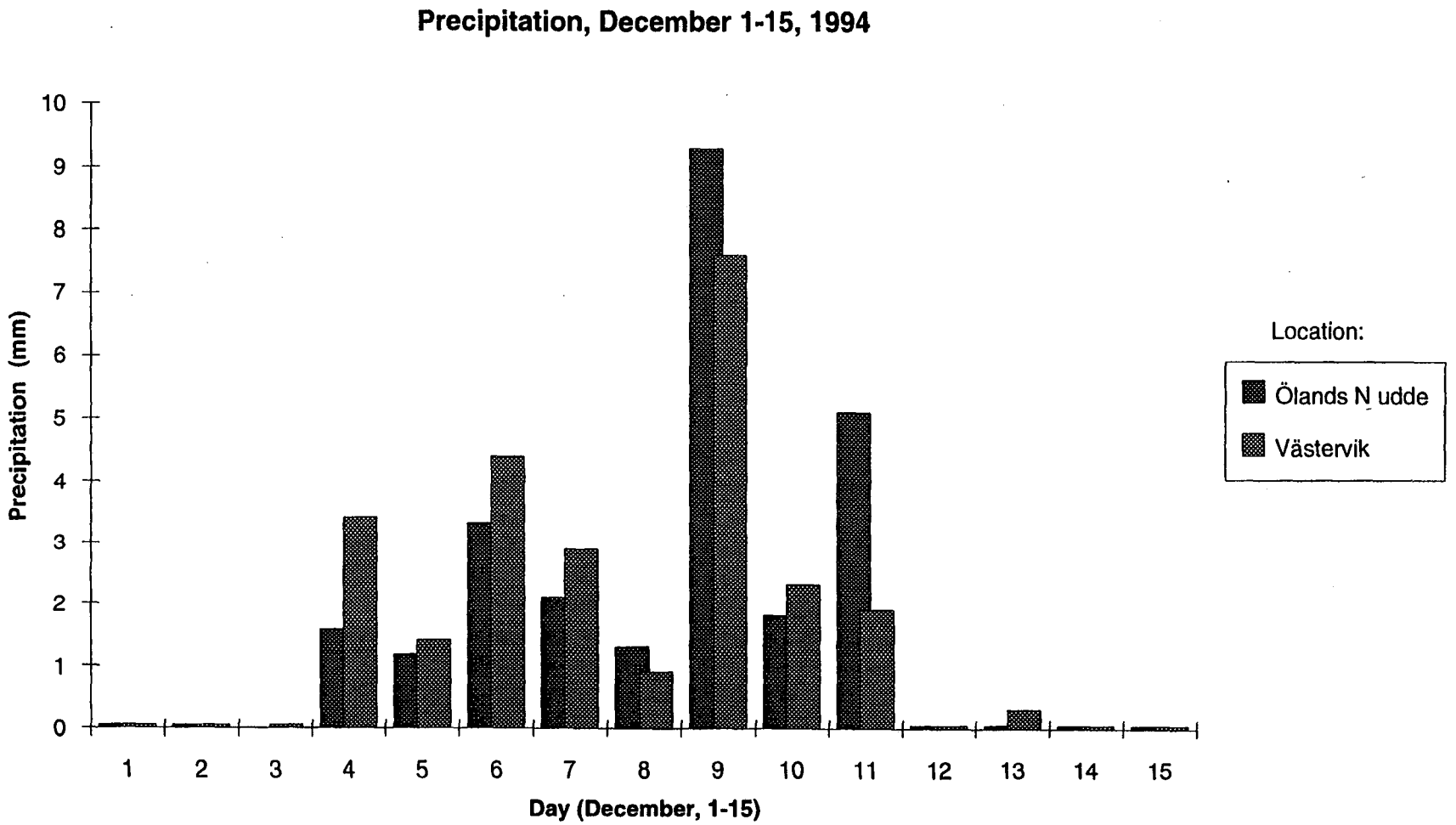
Precipitation, December 1-15, 1994
Precipitation (mm)
0
1
2
3
4
5
6
7
8
9
10
1
2
3
4
5
6
7
8
9
10
11
12
13
14
15
Day (December, 1-15)
Location:
Ölands N udde
Västervik

Fig 3:12a

Fig 3-13

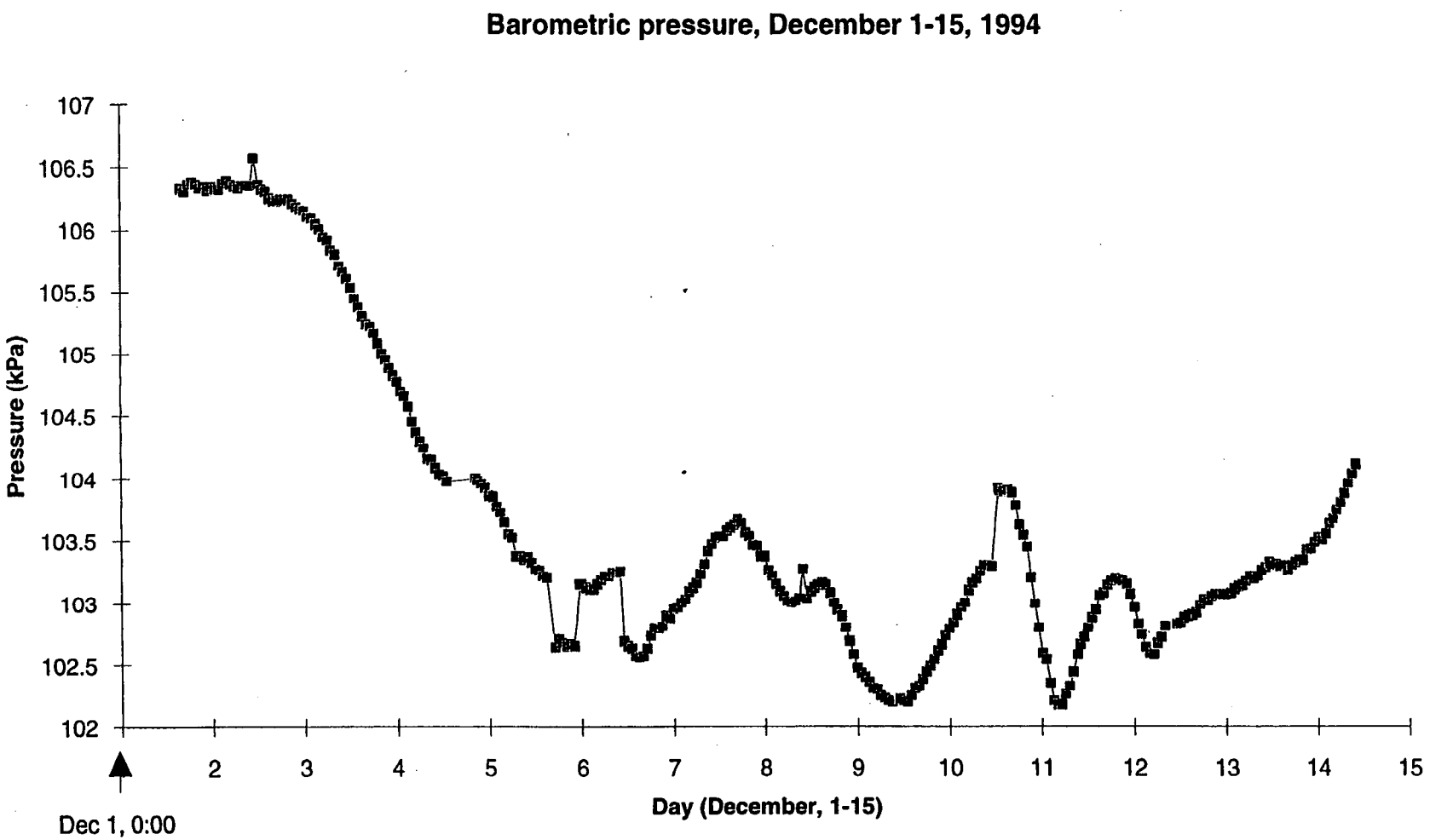

Fig 3-13

PLOT TIME : 95-02-14 17:44:31
PLOT FILE : Tun_tempinout

ÄSPÖ HRL

TEMPERATURE

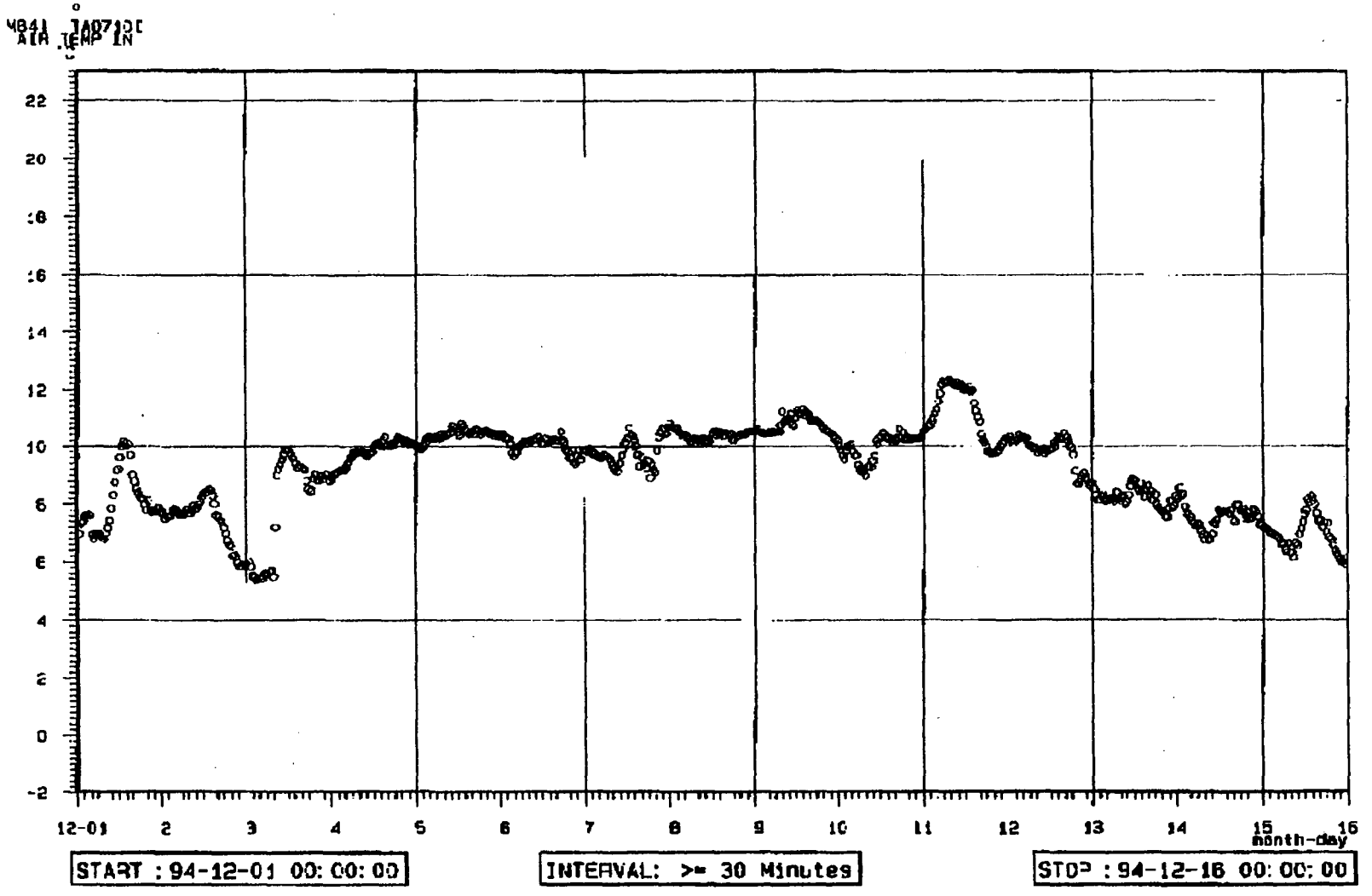

Figure 3-14

Fig 3-14

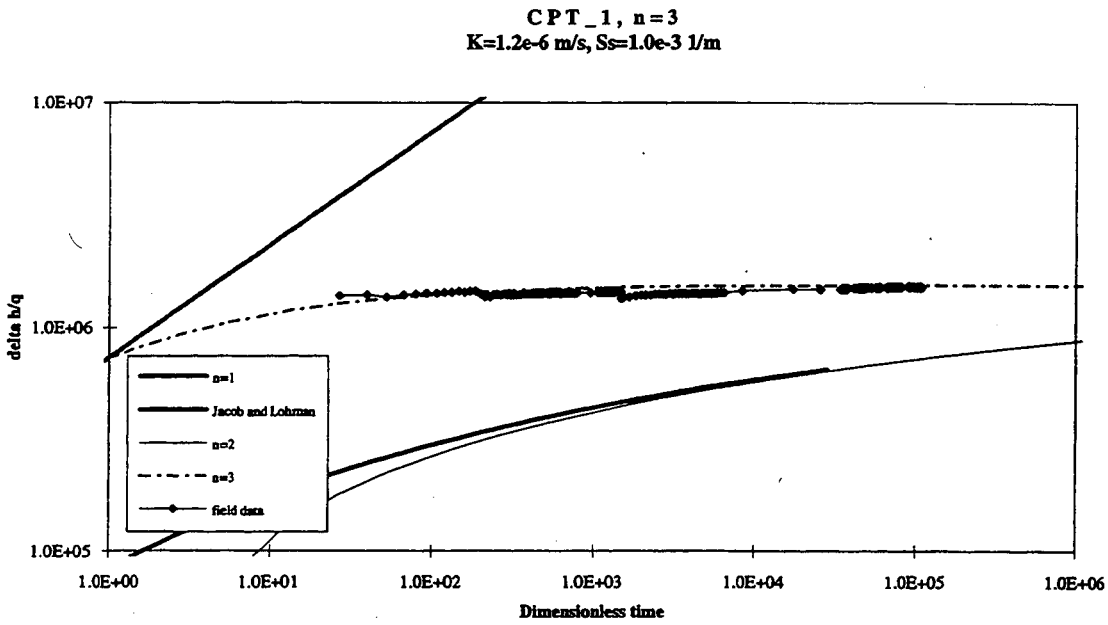
CPT_1, n=3
K=1.2e-6 m/s, Ss=1.0e-3 1/m
1.0E+07
1.0E+06
1.0E+05
delta h/q
1.0E+00
1.0E+01
1.0E+02
1.0E+03
1.0E+04
1.0E+05
1.0E+06
Dimensionless time
n=1
Jacob and Lohman
n=2
n=3
field data

Fig 3-15

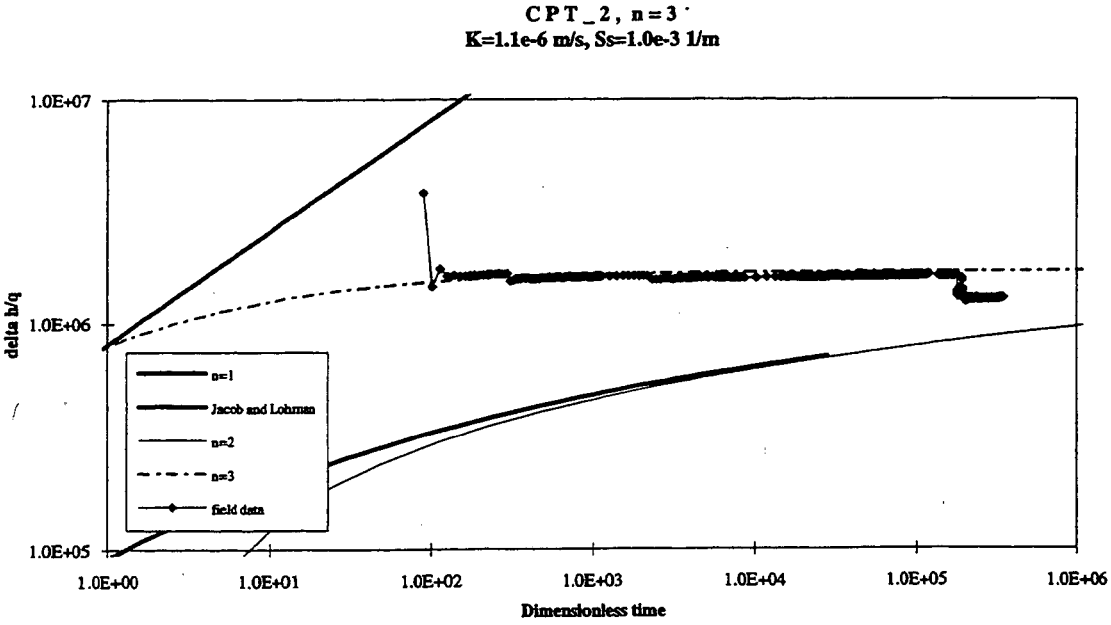
CPT_2, n=3
K=1.1e-6 m/s, Ss=1.0e-3 1/m
1.0E+07
1.0E+06
1.0E+05
delta h/q
1.0E+00
1.0E+01
1.0E+02
1.0E+03
1.0E+04
1.0E+05
1.0E+06
Dimensionless time
n=1
Jacob and Lohman
n=2
n=3
field data

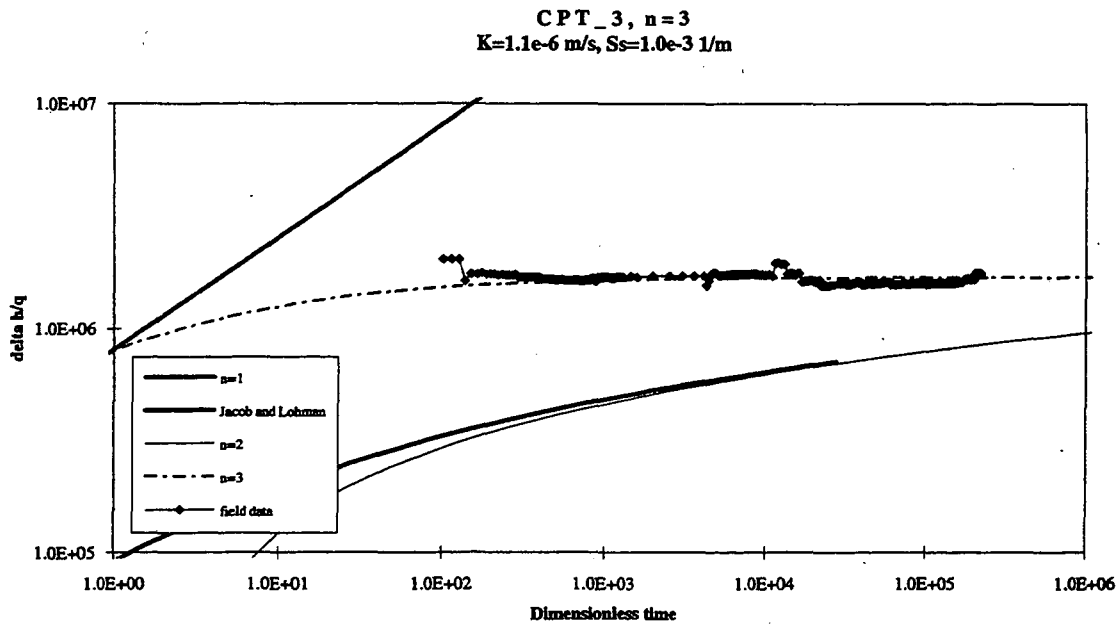

Fig 3-17

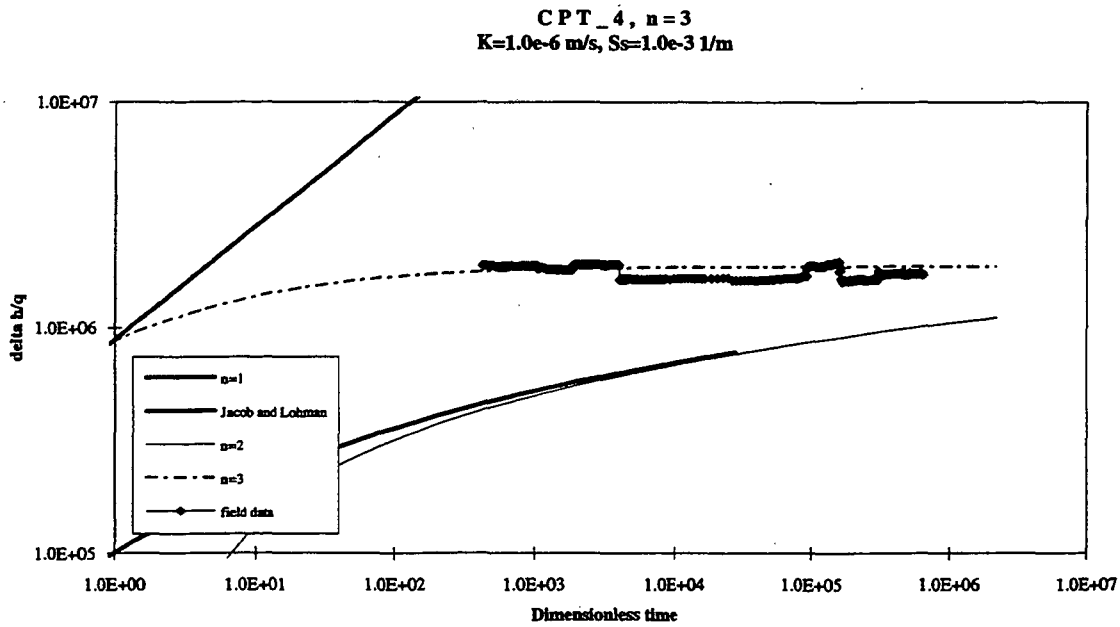

Fig 3-18

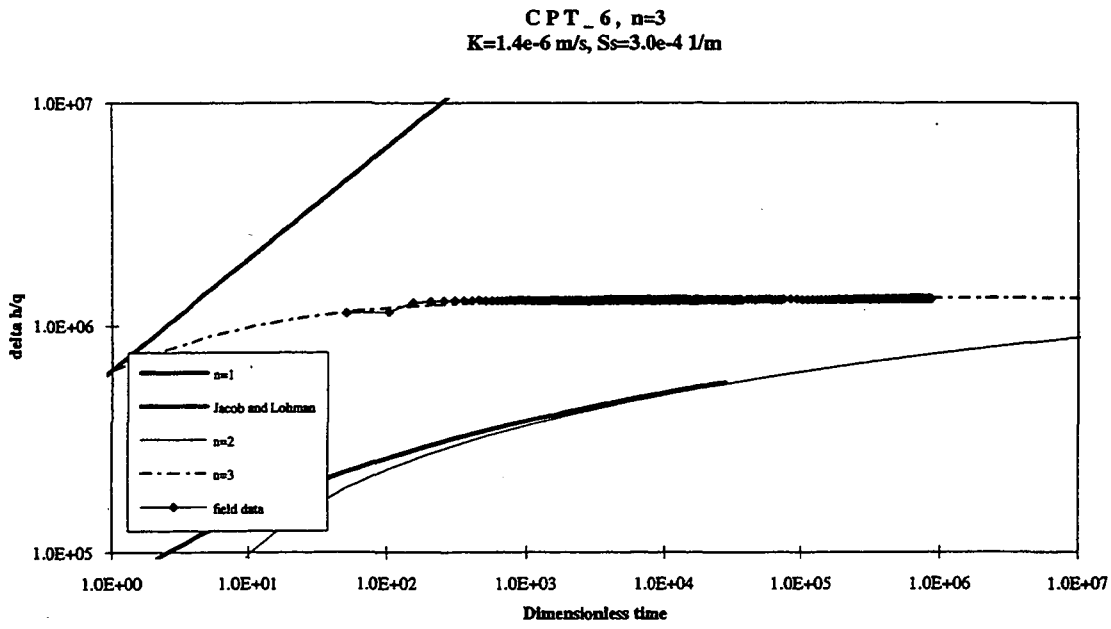

Fig 3-19

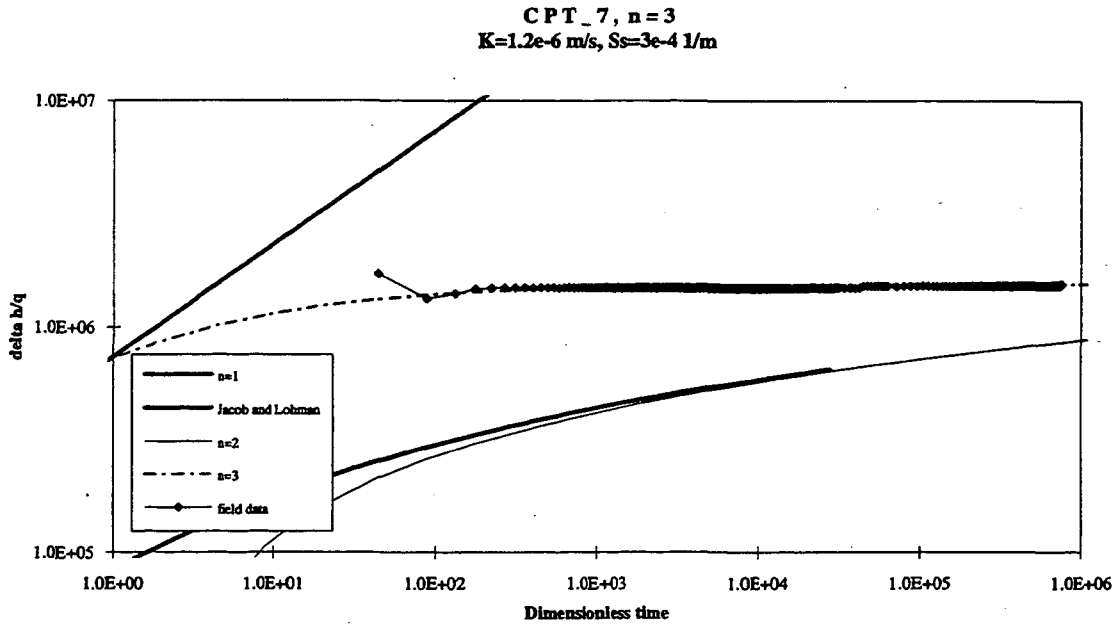

Fig 3-20

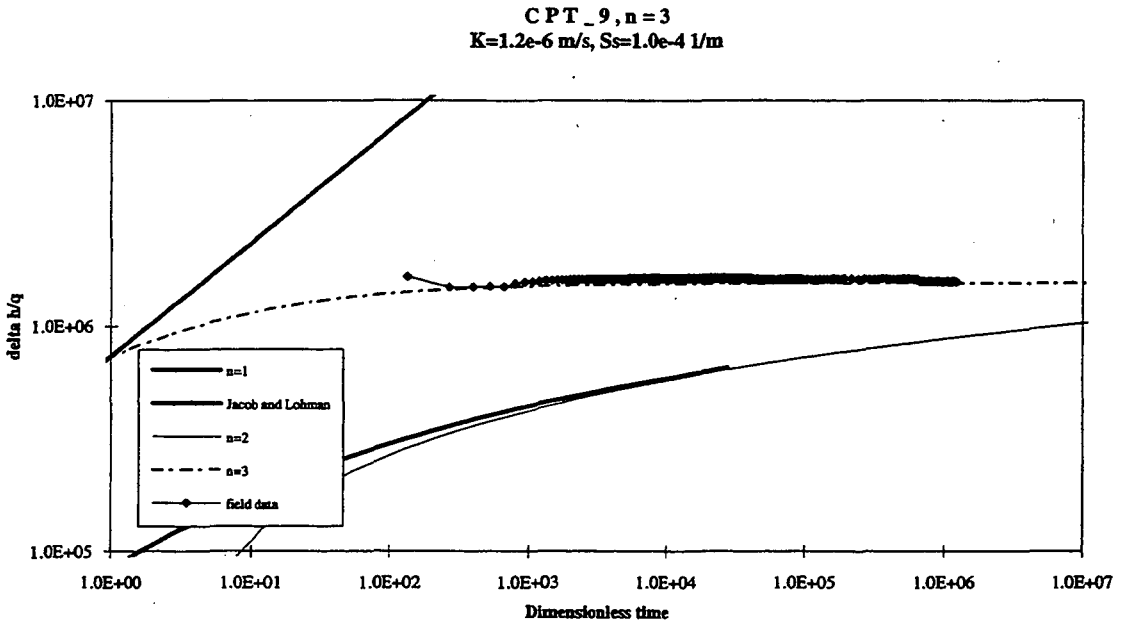

Fig 3-22

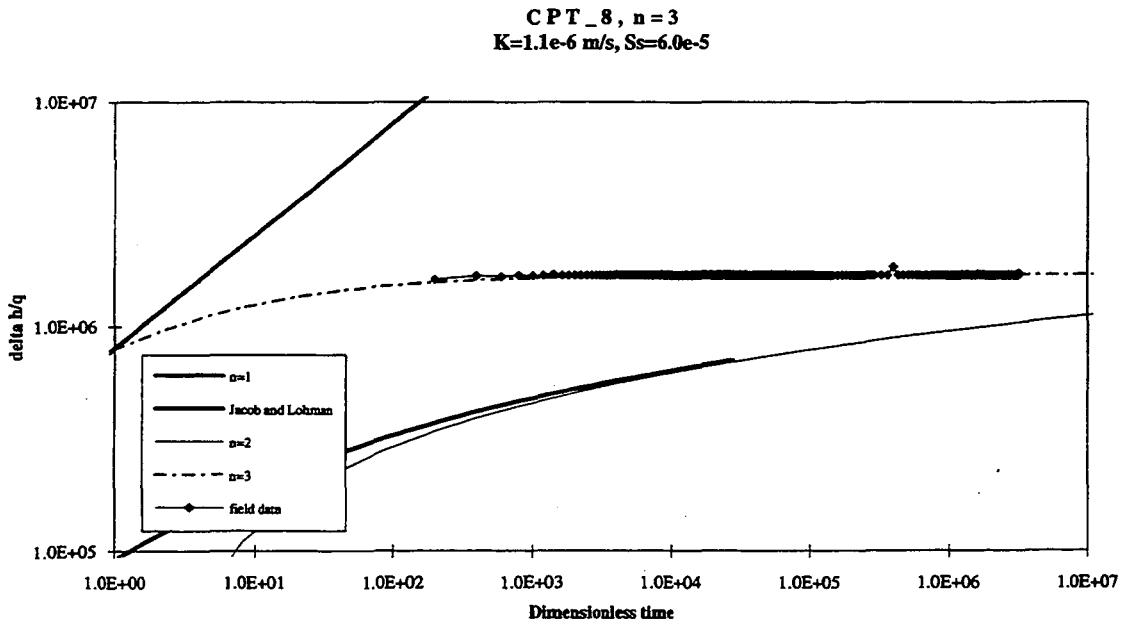

Fig 3-21

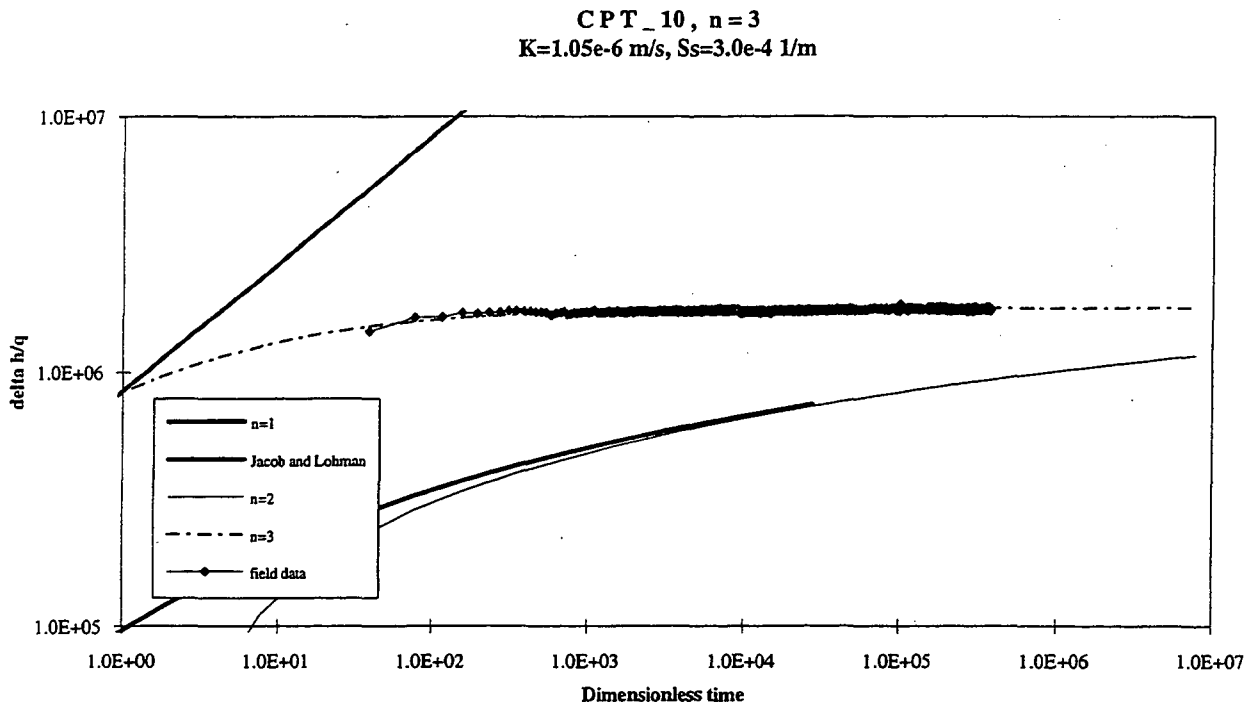

Fig 3-23

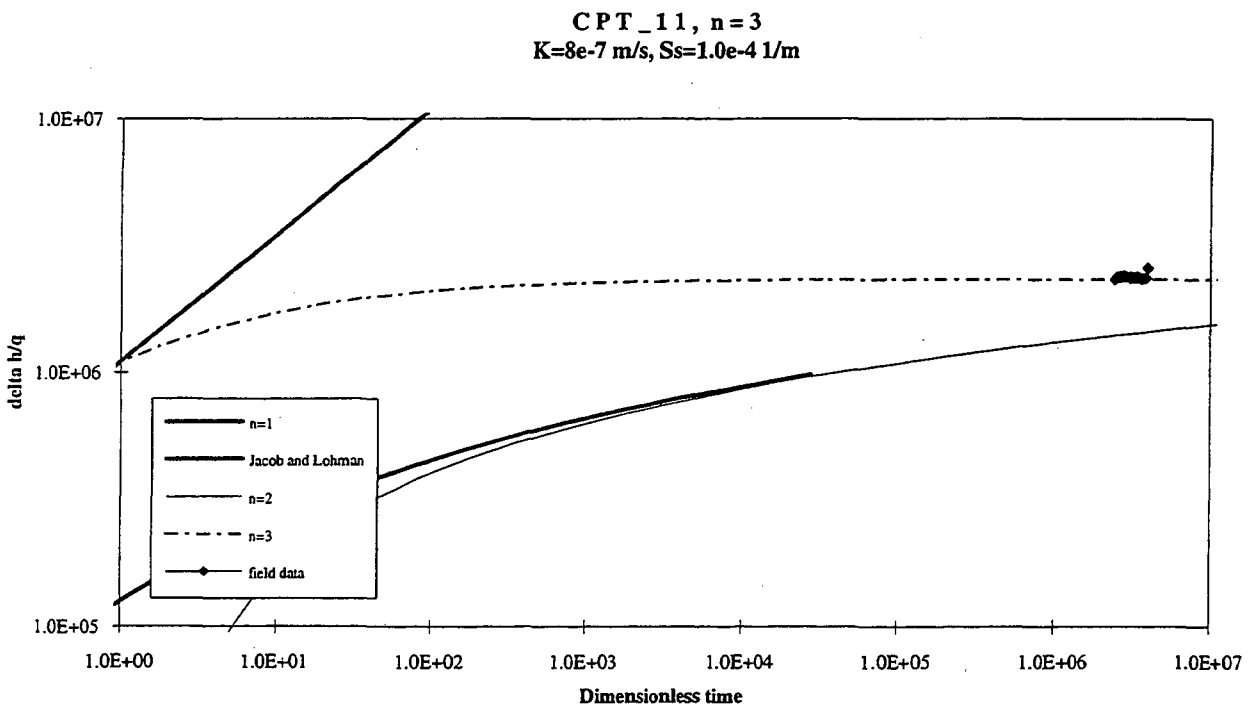

Fig 3-23a

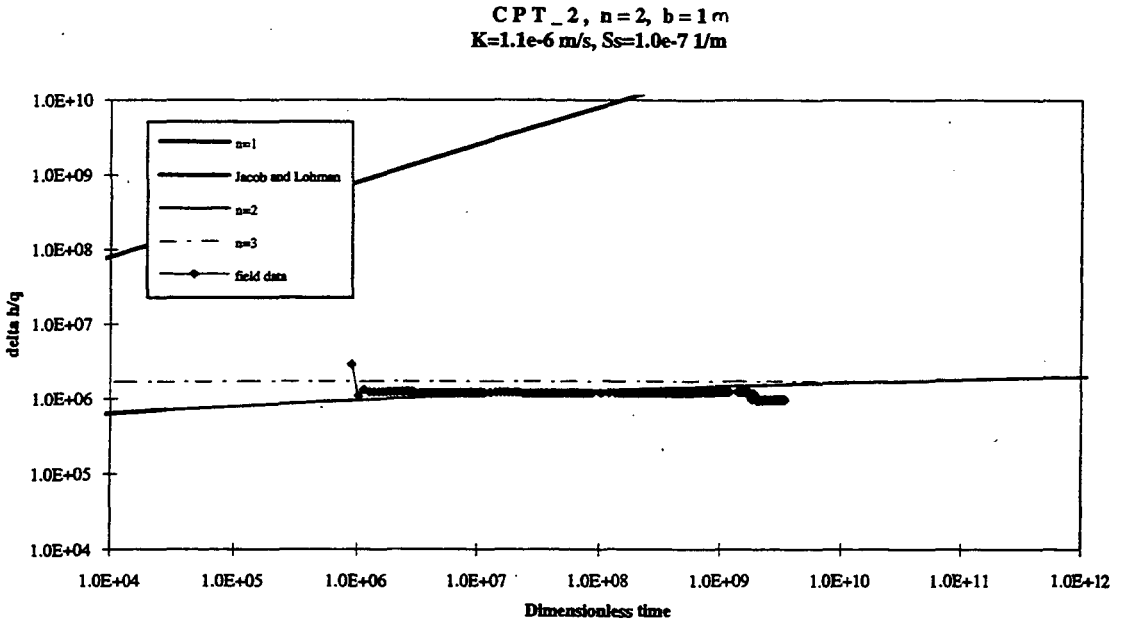

Fig 3-24

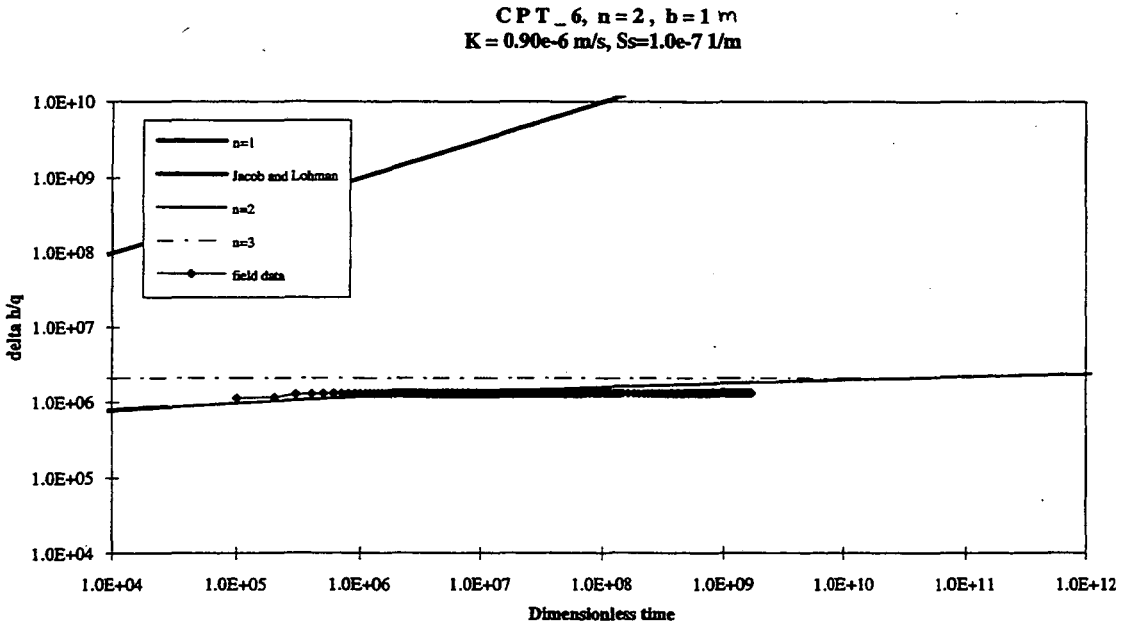

Fig 3-25

Fig 3-25a

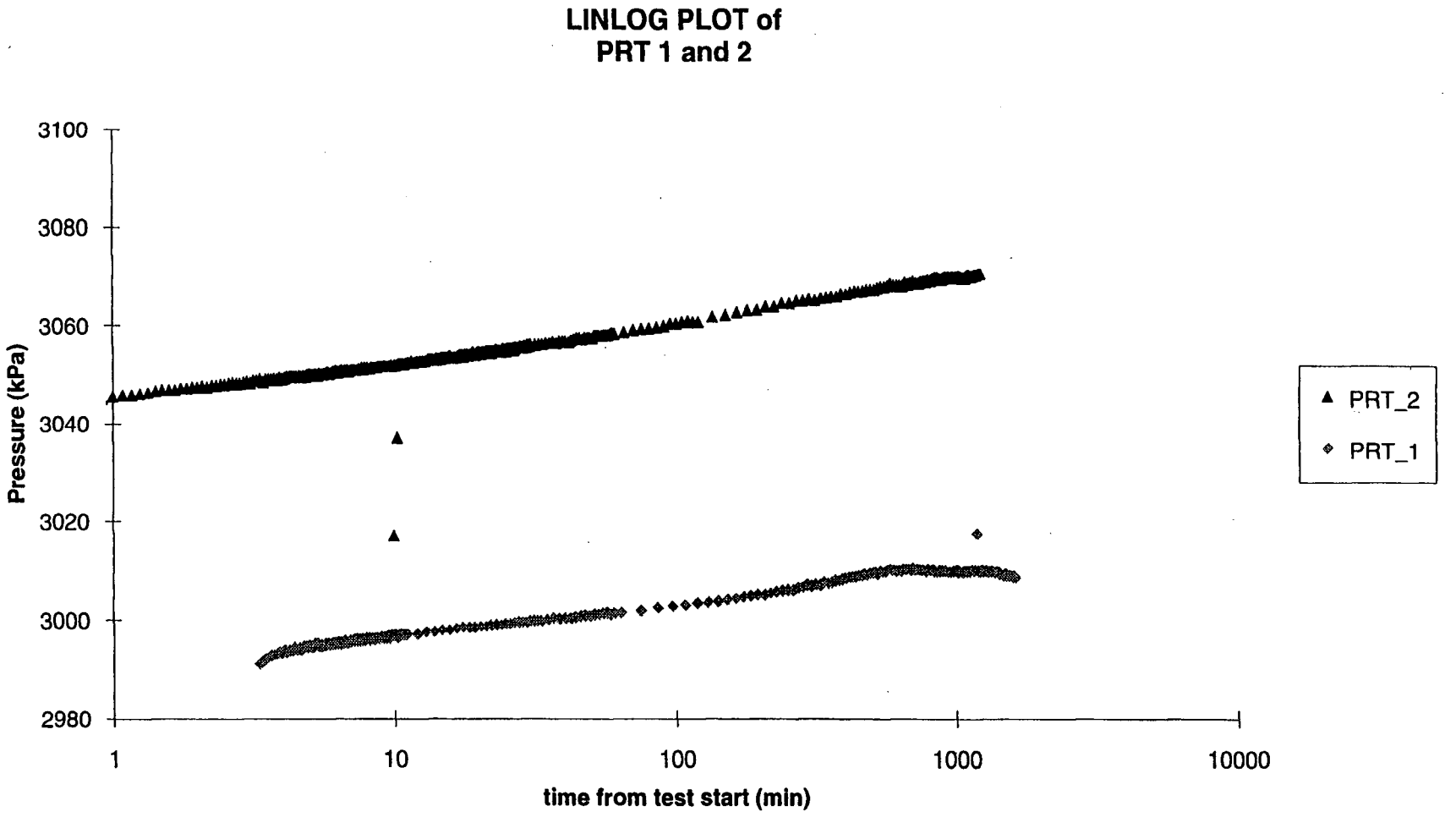

Fig 3-25a

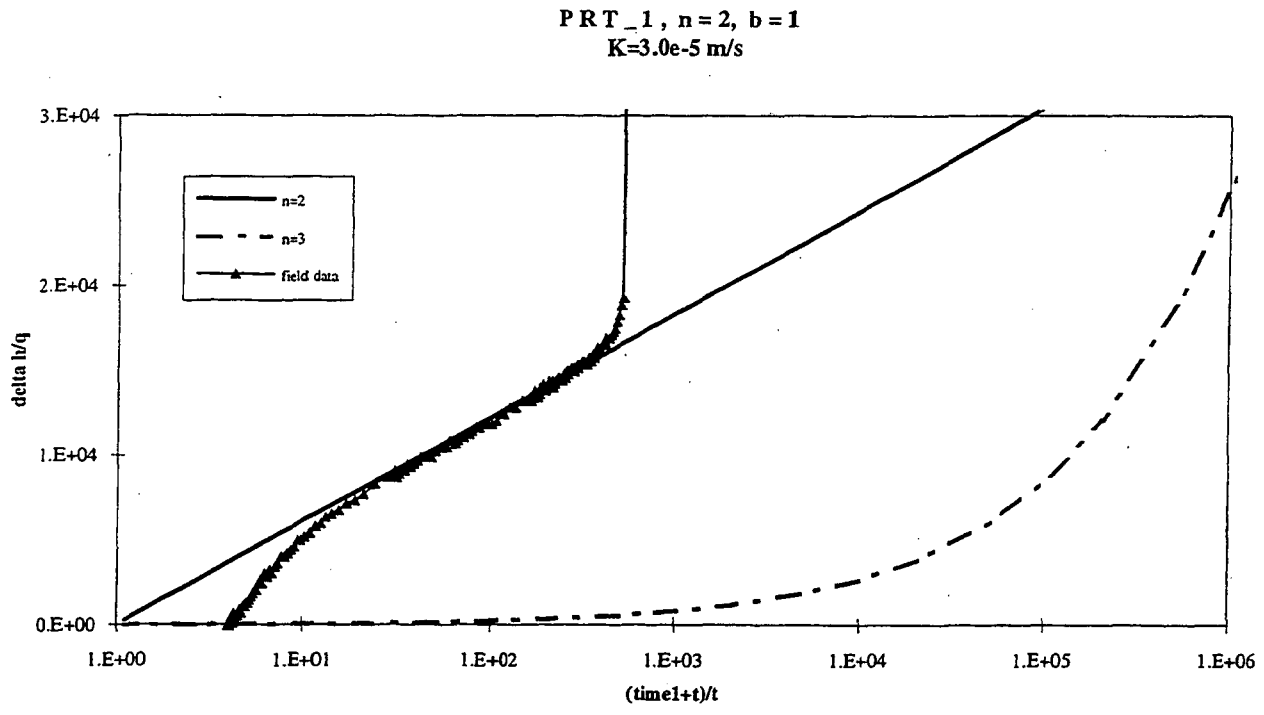

Fig 3-25b

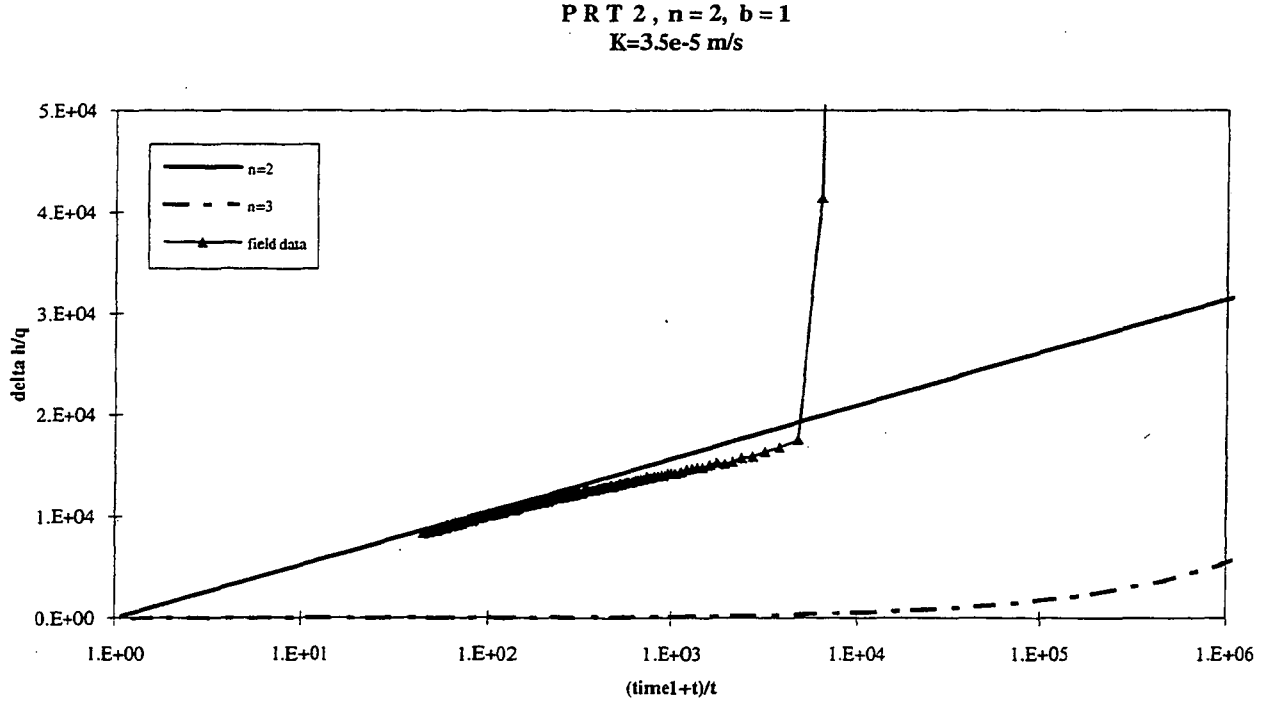

Fig 3-25c

PRT_1, n=3
K=1.2e-6 m/s, Ss=1e-3 1/m

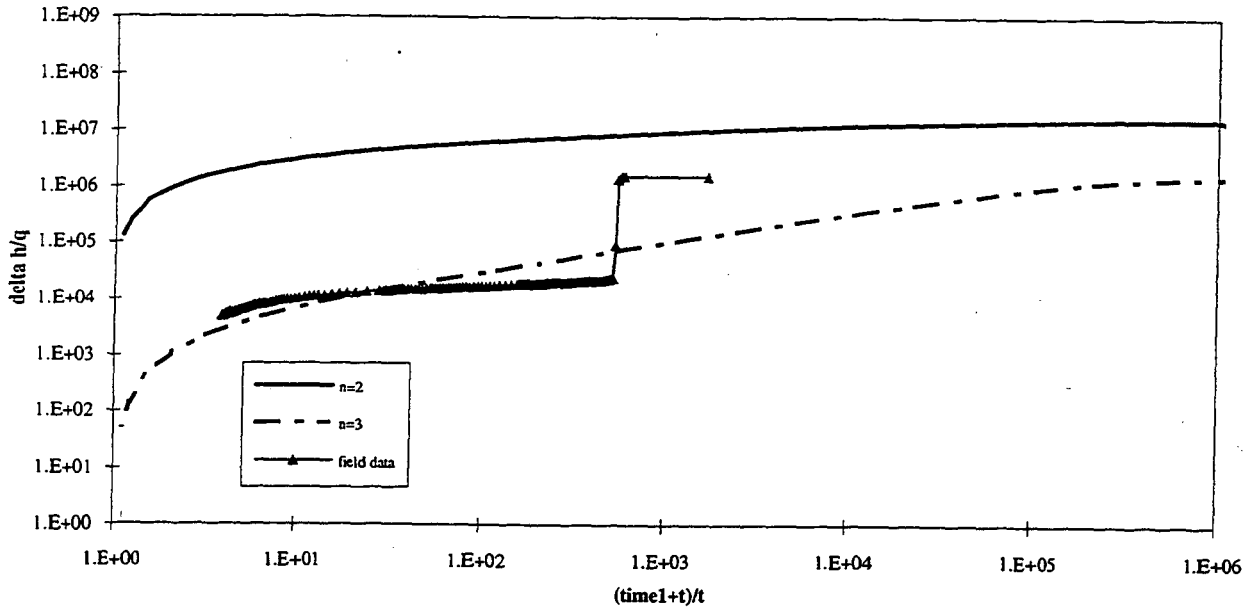

Fig 3-26

PRT 2, n=3
K=1.1e-6 m/s, Ss=6.0e-5 1/m (as best fit for CPT_8)

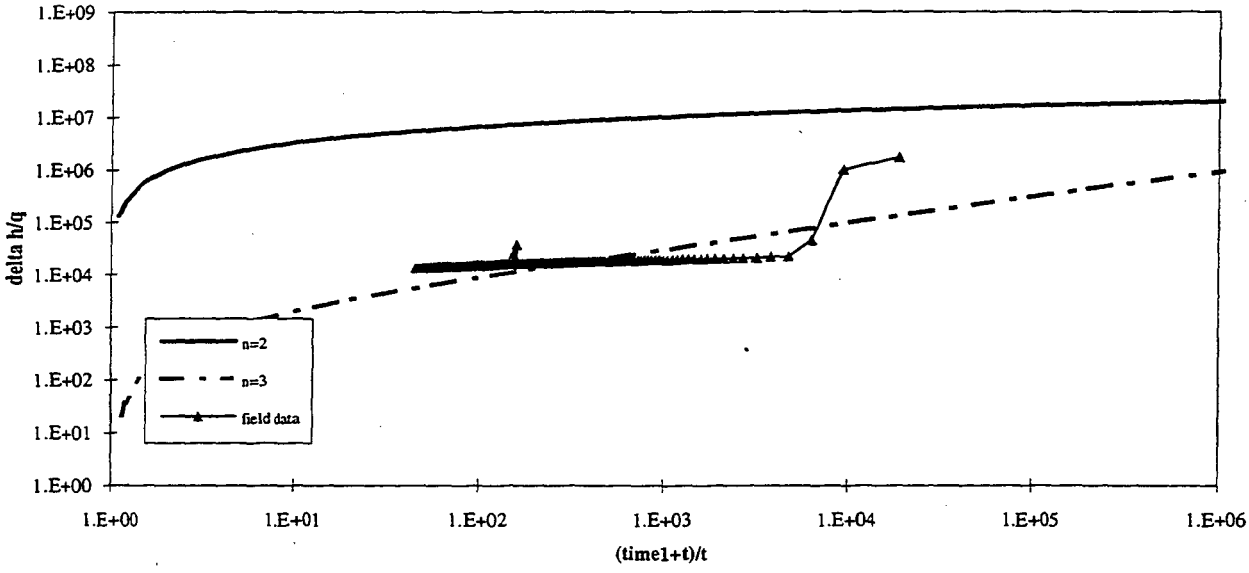

Fig 3-27

LAWRENCE BERKELEY LABORATORY
UNIVERSITY OF CALIFORNIA
TECHNICAL AND ELECTRONIC
INFORMATION DEPARTMENT
BERKELEY, CALIFORNIA 94720